DISSERTATION

submitted to the

Combined Faculties of the Natural Sciences and Mathematics

of the Ruperto-Carola-University of Heidelberg,

Germany

for the degree of

Doctor of Natural Sciences

Put forward by

M.Sc. Marc Hänsel

Born in Heidelberg

Oral Examination: 08.11.2017

Ultrafast Excited State Dynamics and Functional Interfaces Probed by Second Harmonic Generation

Referees: Prof. Dr. Annemarie Pucci
Prof. Dr. Albrecht Winnacker

Ultrafast Excited State Dynamics and Functional Interfaces Probed by Second Harmonic Generation

Understanding the ultrafast excited state dynamics in organic semiconductors after optical excitation is a key requisite on the road towards efficient organic solar cells. Additionally, the creation of functional interfaces built from organic molecular switches and the read-out of the photochromic state are essential for molecular electronics. In this thesis, static second harmonic generation (SHG) measurements were utilized to investigate the photochromism of different indolylfulgimide derivatives immobilized on silicon. During this, the influence of chemical modifications on the switching efficiencies (cross-sections) and the non-linear optical contrast between the switching states were investigated. In the second part of this thesis, femtosecond time-resolved second harmonic generation measurements were used to investigate the ultrafast decay mechanism of optically induced electronically excited states in organic semiconductors and donor/acceptor systems. These led to observations of relaxation into dimer induced states, charge trapping at native silicon oxide and ultrafast vibronic relaxation. For the donor/acceptor configurations, depending on the molecular orientation at the interface and the excitation energy, the creation of charge transfer states were investigated.

Ultraschnelle Dynamik von angeregten Zuständen und funktionalisierte Grenzflächen untersucht mittels Frequenzverdopplung

Die Gewinnung eines tieferen Verständnisses der ultraschnellen Dynamiken von angeregten Zuständen ist von größter Wichtigkeit in der Entwicklung von effizienten organischen Solarzellen. Des Weiteren ist der Aufbau von funktionalisierten Grenzflächen, bestehend aus organischen molekularen Schaltern, und das Auslesen des photochromen Zustands unverzichtbar für die molekulare Elektronik. In dieser Arbeit wurden statische Frequenzverdopplung (*engl. second harmonic generation (SHG)*) Experimente verwendet, um den Photochromism von verschiedenen Indolylfulgimidderivaten, die auf Silizium immobilisiert wurden, zu untersuchen. Dabei wurde der Einfluss von chemischen Veränderungen auf die Effizienz (Wirkungquerschnitte) der involvierten Prozesse und der nicht lineare optische Kontrast zwischen den Zuständen untersucht. Im zweiten Teil der Arbeit wurden SHG Messungen mit einer Femtosekunden Zeitauflösung verwendet, um die ultraschnellen Zerfallskanäle von optisch angeregten elektronischen Anregungen in organischen Halbleitern und Donor/Acceptor Systemen zu untersuchen. Hierbei wurden die Relaxation in von Dimeren erzeugten Zustände, das Einfangen von angeregten Ladungen durch natürliches Siliziumdioxid und ultraschnelle Schwingungsabregung beobachtet. In den Donor/Acceptor Systemen wurde die Bildung von Ladungstransferzuständen, abhängig von der Orientierung der Moleküle an der Grenzfläche und der Anregungsenergie, untersucht.

Contents

List of Figures

List of Tables

1 Introduction

The interaction of light with molecular systems is an important process and provides a broad variety of applications. It can be used to drive the photochromism of organic switches and thereby provide a switchable system on the size level of molecules [1–3], but also energy generation in organic photovoltaic devices [4–7] can be achieved, by absorption of light of organic molecules. To further improve the properties of such molecules, one needs a fundamental understanding of the involved elementary processes. Time-resolved second harmonic generation (SHG) can, on the one hand provide the time resolution to investigate the ultrafast sub-picosecond processes after the absorption of light in molecular layers [8–10]. On the other hand, SHG provides the sensitivity to resolve the photochromism of sub-monolayers of molecules immobilized on surfaces, with significant signal contrast [11–14]. Furthermore, processes at buried interfaces of stacks of functional materials can be observed [9, 10, 15]. The high surface/interface sensitivity of the SHG process is caused by the suppression of the SHG signal from centrosymmetric materials and thereby the creation of the signal mostly at symmetry breaks created by the surface/interface in the systems [11–14].

In the scope of today's increasing demand for data storage, the top-down approach of the conventional inorganic semiconductor devices reaches its limits in miniaturizing the basic building units [16, 17]. One possible approach to solve this problem could lie in the bottom-up approach of utilizing single molecules as fundamental data storage units [17–19]. In addition, by combining single molecular switches with other organic components, fully molecular electronics may become possible [3, 20, 21]. Combining molecular electronic devices with molecular storage could lead to novel photonic and optoelectronic devices. This makes completely new fields of applications available.
For these, an immobilization of organic molecules without hindrance of the photocromic properties of the molecules is essential. The photochromism of a variety of molecules has been well known since the 19th century [22, 23], but it is mostly investigated in solution, where the molecules can freely move around [24, 25]. So far, experiments based on immobilized organic switches have shown a large variety of challenges concerning the switching ability of immobilized molecules. The main approaches range from physisorption [26], Langmuir monolayers [27, 28], Langmuir-Blodgett-films [29], incorporation into polymer matrices [18] to chemical attachment via self-assembled monolayers [30]. Despite the large variety of approaches, there are usually two important challenges: The quenching of the excited state due to the electronic coupling to the substrate. This is a problem especially in physisorbed systems. In these, the surface can suppress the photochromism fully [31] or partly [32]. Furthermore, the thermal stability of different states can be influenced by the surface, and even reversed [33]. It has been shown that the strong

influence of the surface can be eliminated by the use of either bulky side groups [26, 34] or linker groups [30]. The second effect is steric hindrance by either the surface, the matrix or other functional molecules [35]. This can be overcome by carefully designing the used molecular structures.

In the framework of this thesis, the aim is to investigate the practicability of a new immobilization approach of different fulgimide molecules on a silicon surface. Especially the quality of the decoupling approach of the fulgimides from the surface used here and their switching efficiency are of great interest. Furthermore, the influence of chemical variations of the fulgimide and the linker group are under investigation. In addition to the investigations on the functionality of the switches, the second aim is to optimize the system in regard to the non-linear optical (NLO) contrast induced by the switching process.
For this, the photochromism of a sub-monolayer of 2- and 3-Indolylfulgimide molecules attached to an alkyne linker on a silicon(111) surface were investigated by SHG. The high interface-sensitivity of SHG has been utilized to observe the functionality of the fulgimides. Fulgimides are a photochromic molecular species, which undergoes a ring opening/closure reaction under illumination with UV and visible light respectively [36–38]. Additionally, a cis-/trans-isomerization can be driven by UV light in the open-form of the molecules [37, 38]. Based on the larger delocalized π-electron system of the closed-form compared to the open-form, a significant change in the SHG signal is expected for the switching process between the two forms [39]. Indeed NLO contrasts between the two forms of around 20 % were observed for all systems. For one sample a NLO contrast of over 30 % could even be observed for a well-chosen polarization combination of the incoming and the outgoing light. For the ring opening/closure reaction cross-sections in the order of 10^{-18} - $10^{-20}\,\mathrm{cm}^2$ were measured. Based on polarization-resolved measurements and calculations of the molecular first order hyperpolarizabilities with density functional theory the orientations of the fulgimide molecules on the surface have been determined. In addition to the expected switching process between the open- and closed-form a reversible signal change induced by the probe beam with up to five orders of magnitude lower cross-sections (around $10^{-23}\,\mathrm{cm}^2$) than the ring opening/closure reaction was observed. Furthermore the thermal stability of the closed-form was not given for all samples and the cross-sections of some sample systems were only in the regime of 10^{-19} - $10^{-20}\,\mathrm{cm}^2$ and not in the order of $10^{-18}\,\mathrm{cm}^2$ as expected for decoupled indolylfulgimides. All of these effects could be assigned to an interaction between a phenyl ring, which has been introduced between the fulgimid and the linker group, and the fulgimide. All three properties could be largely influenced by electronic decoupling of the phenyl ring from the fulgimides.

Organic photovoltaic devices have gained a lot of attention in the last decade [4–7]. The attention is due to the variety of possible applications of organic solar cells and the large increase in energy usage in today's society. Solar cells based on organic materials offer the possibility to create ultrathin, low-weight devices [6]. It has furthermore been proven that it is possible to build devices on flexible substrates, increasing the range of potential

applications [40]. The key functionality of such devices is provided by the interfacial interactions at the donor/acceptor interface [7]. This is where the high sensitivity of the SHG process to symmetry breaks and thus the interface between donor and acceptor material is used.
Two of the main challenges in the application of organic semiconductors in organic solar cells are the degradation due to environmental influences and the understanding of the ultrafast excited state dynamics directly after the optical excitation [7, 41]. The first one can be overcome by either encapsulation of the functional layers [42] or design of the molecules [6, 43, 44]. In the work of this thesis, two perylene derivatives, which are environmentally stable were used [45–47]. To increase the efficiency of solar cells the ultrafast processes on a femto- to picosecond timescale play a significant role [7, 41]. The key processes for an efficient solar cell operation are the creation of charge transfer (CT) states at the interface of the donor and acceptor material, and the following charge separation mediated by the interface [7]. Depending on the specific materials, the molecular orientation at the interface and the morphology of the films, different additional processes influence the CT generation [48]. For instance, the influence of the excess energy in hot excited states is currently under discussion [9, 49]. The fastest process is usually the vibronic relaxation of initial hot excitations on a femtosecond timescale [50]. Other processes like excimer formation can result in charge trapping [51, 52] and thus can suppress charge separation.

The main purpose of this thesis is to investigate the ultrafast dynamics of optically excited states and possible decay mechanisms to get a deeper understanding of the fundamental processes in organic photovoltaic devices. In order to do so, the main topics are the intrinsic decay mechanism of a single material layer, the influence of the substrate, and the interactions at a donor/acceptor interface. To resolve the influence of the excitation energy and especially for the donor/acceptor interface, the influence of the molecular orientation at the interface with regard to charge-transfer generation is of great importance in the scope of this thesis.
To investigate the aforementioned topics, a time-resolved SHG setup with a femtosecond time resolution was used to shine light on the ultrafast excited state processes in the two promising organic semiconductors diindenoperylene (DIP) and the perylene derivate n,n'-bis-(2-ethylhexyl)-1,7-dicyanoperylene-3,4:9,10-bis(dicarboximide) (PDIR-CN_2). Differently prepared bilayers made of the two materials were also investigated. In this context, the temporal resolution of better than 50 fs of the SHG setup is essential for studying such processes. Both materials form neat films and have high resistances against environmental influences [45–47]. For DIP an ultrafast relaxation into a dimer induced state, which acts as an energetic trap and possibly suppresses the CT generation, was identified. In PDIR-CN_2, the vibronic relaxation on a femtosecond timescale for different excitation energies were observed. Combining the two materials, a few new processes were identified. For the DIP/PDIR-CN_2 bilayer, no interaction of the excited states in either material with the interface could be detected. Changing the stacking order of the materials to PDIR-CN_2/DIP led to the observation of an energy transfer from the PDIR-CN_2 to an interfacial state. In the final step the molecular orientation

of the DIP layer was influenced, which led to similar results for the pure DIP film, but in interaction with the PDIR-CN_2 the generation of CT-states could be observed.

Outline

The thesis is composed of three main chapters. Chapter 2 poses an introduction to the principles of SHG and presents the setup used in this thesis is presented. It also gives a characterization of the setup is given and explains the measurement approaches. Chapter 3 discusses the results of the fulgimide functionalized surfaces. A brief introduction into the concept of photocromism and the recent research of different immobilization approaches are given. The sample preparation is addressed and a short investigation of the linker molecules is presented. The main part of chapter 3 is composed of the presentation of the SHG results of the fulgimide samples, and finished by a comparison with results based on DFT-simulations and a discussion of the observed features and processes. In chapter 4, the TR-SHG measurements of organic semiconductors are evaluated. The chapter begins with a brief introduction of optically excited states and their dynamics in organic molecules. Afterwards the results of the different investigated systems (DIP and PDIR-CN_2) and their bilayers are presented. The chapter closes with a discussion of all observed properties of the different systems. Finally, the results of the thesis are summarized in chapter 5.

2 Second Harmonic Generation

With second harmonic generation (SHG) the second-order susceptibility tensor $\chi^{(2)}$, which describes the second-order non-linear optical properties of a medium, is used to probe a variety of processes in different materials and material systems. The SHG concept was first proven shortly after the invention of the ruby laser in 1960 [53]. In 1961, the first results from experiments in the Weinrich group at the University of Michigan were published showing generation of light at the doubled frequency by a focused ruby laser in a quartz crystal [54]. In 1967, the electric field enhanced second harmonic generation (EFISH) was discovered [55]. Starting with the discovery of surface-enhanced SHG by Shen *et al.*, SHG became a versatile method to investigate surface properties [11–14]. Nowadays, it has been used to investigate nearly all properties of surfaces, buried layers, and sub-surface layers, like for example their charge [56–58], roughness [59, 60], electronic state density [61, 62], adsorption [63–65], initial band bending [66, 67], orientation and symmetry [68–70]. Because of the high interface/surface sensitivity [13–15] SHG got attention as a probe technique for ultrafast processes, like for example excited state dynamics in organic semiconducting single layers, as well as in organic bilayers, where the focus lies on the dynamics of the charge transfer (CT) [8–10]. Furthermore, it is possible to investigate changes of $\chi^{(2)}$ even in sub-monolayers of photochromic molecules [12].

In the thesis at hand a femtosecond pulsed laser setup has been used to probe the nonlinear optical properties of two completely different material systems. Accordingly, two different approaches have been used: (1) Quasi static experiments on fulgimide functionalized silicon surfaces have been conducted, probing the change in the second order susceptibility due to a ring opening/closure reaction driven by an external stimulus such as light. (2) Ultrafast time resolved pump/probe experiments have been done using the femtosecond resolution of the laser setup on organic semiconductors, probing the dynamics of optically induced excitations in organic layers. Additionally the influence of various interfaces between two organic semiconductors (e.g. donor/acceptor interfaces) as well as the influence of the substrate to the dynamics were investigated.

In this chapter, an introduction into SHG and its realization as a versatile surface/interface-sensitive probing method is given. In section 2.1, the basic principles of SHG are explained. The realization of the SHG setup with a pulsed laser source used for this thesis and its application to investigate the different samples is described in section 2.2.

2.1 Second-order non-linear optics

When an electromagnetic wave travels through a dielectric medium, it invokes a displacement of electrons with respect to the atomic cores. The displaced electrons become the source of the ongoing electromagnetic field, which leads to an induced dielectric polarization $\mathbf{P}(\mathbf{E})$. For weak electric fields $\mathbf{E}$ the polarization behaves linearly in $\mathbf{E}$:

$$\mathbf{P} = \epsilon_0 \chi \mathbf{E} \tag{2.1}$$

where ϵ_0 is the vacuum permittivity and χ is the susceptibility of the medium. In general, $\mathbf{E}$ and $\mathbf{P}$ are three component vectors and χ is a 3×3 tensor. For high intensities of the electric field, where the electric field strength is not negligible in comparison to the the atomic Coulomb field, the displacement of the electrons becomes anharmonic and the assumption of a linear behavior between the polarization and the electric field is not longer valid. In this case, the polarization can be described by a power series expansion of χ, which leads to:

$$\begin{aligned} \mathbf{P} &= \epsilon_0 \chi \mathbf{E} \\ &= \epsilon_0 (\chi^{(1)}\mathbf{E} + \chi^{(2)}\mathbf{E}^2 + \chi^{(3)}\mathbf{E}^3 + ...) \\ &= \mathbf{P}^{(1)} + \mathbf{P}^{(2)} + \mathbf{P}^{(3)} + ... \end{aligned} \tag{2.2}$$

where $\chi^{(2)}$ and $\chi^{(3)}$ denote the second- and third-order susceptibilities. This expansion is only valid as long as $\chi^{(i)} \ll \chi^{(j)}$for $j > i$. The second-order susceptibility in its generalized form is a three-dimensional $3 \times 3 \times 3$ tensor corresponding to the three wave mixing. To calculate the effect of this expansion to the involved light, the simplest approach is to take into account two different electric fields modeled by plain waves, described as follows:

$$\mathbf{E} = \mathbf{E}_1 * \mathrm{e}^{-i\omega_1 t} + \mathbf{E}_2 * \mathrm{e}^{-i\omega_2 t} + c.c. \tag{2.3}$$

with the frequencies ω_1 and ω_2. c.c. stands for the complex conjugated. Calculating the second order term of equation (2.2) for the plain waves of equation (2.3), the second order term becomes:

$$\begin{aligned} \mathbf{P}^{(2)}/\epsilon_0\chi^{(2)} = &(\mathbf{E}_1^2 \mathrm{e}^{-i2\omega_1 t} + \mathbf{E}_2^2 \mathrm{e}^{-i2\omega_2 t} + c.c.) \\ &+ 2(\mathbf{E}_1\mathbf{E}_2 \mathrm{e}^{-i(\omega_1+\omega_2)t} + c.c.) \\ &+ 2(\mathbf{E}_1\mathbf{E}_2 \mathrm{e}^{-i(\omega_1-\omega_2)t} + c.c.) \\ &+ 2(\mathbf{E}_1^2 + \mathbf{E}_2^2) \end{aligned} \tag{2.4}$$

All four terms describe the second-order non-linear response of the medium. The first term depends only on the doubled frequencies of the incoming electric fields and therefore

describes the SHG process. The other three processes in the order of the terms are: sum frequency generation (SFG), difference frequency generation (DFG) and electro-optical rectification (EOR). For $\omega_1 = \omega_2$ these terms are reduced to the SHG process. The SFG is normally used in SFG-spectroscopy by tuning the wavelength of one of the beams involved in the SFG process. The DFG process is usually used in optical parametric amplifiers (OPA) to tune the wavelength of a laser beam [71, 72].
The SHG process has two important properties. First of all it is highly surface/interface-sensitive, which is due to the fact that the SHG vanishes for centrosymmetric systems like the bulk of most materials [13–15]. This becomes clear when looking at the second order dielectric polarization:

$$\mathbf{P}^{(2)} = \epsilon_0 \chi^{(2)} \mathbf{E}\mathbf{E} \tag{2.5}$$

For systems with inversion symmetry the electric field and the polarization vectors have to be invariant under the inversion of the coordinate systems. This means for a simultaneous change from $\mathbf{E}$ to $-\mathbf{E}$ and $\mathbf{P}^{(2)}$ to $-\mathbf{P}^{(2)}$ the relationship equation (2.5) still has to be valid. For non-vanishing electric fields, this is only possible for a vanishing $\chi^{(2)}$. In consequence, the SHG is highly sensitive to symmetry breaks like surfaces and interfaces, which can be used to investigate very thin layers of materials or even single molecules on a surface.
Secondly, for $I(2\omega) \ll I(\omega)$ the intensity of the SHG beam depends quadratically on the intensity of the incoming beam ($\mathrm{I}(\omega)$):

$$\begin{aligned} \mathrm{I}_{\mathrm{SHG}}(2\omega) &\propto |\mathbf{P}^{(2)}(2\omega)|^2 \\ &\propto |\chi^{(2)} \mathrm{E}^2(\omega)|^2 \\ &= |\chi^{(2)}|^2 \mathrm{I}^2(\omega) \end{aligned} \tag{2.6}$$

Additionally, light of the doubled frequency can also be created via the third order susceptibility. In the presence of a static electric field ($\mathbf{E}^{DC}$) the four-wave-mixing effect called electric field enhanced second harmonic generation (EFISH) takes place [55]. It can be described as follows:

$$\mathbf{P}^{\mathrm{NL}}(2\omega) = \mathbf{P}^{(2)}(2\omega) + \mathbf{P}^{\mathrm{EFISH}}(2\omega) \tag{2.7}$$

which generates the second harmonic field:

$$\begin{aligned} \mathbf{E}(2\omega) &= \mathbf{E}^{(2)} + \mathbf{E}^{\mathrm{EFISH}}(2\omega) \\ &\propto \chi^{(2)} \mathbf{E}^2(\omega) + \chi^{(3)} \mathbf{E}^2(\omega) \mathbf{E}^{\mathrm{DC}}(0) \end{aligned} \tag{2.8}$$

The intensity then becomes:

$$\begin{aligned} \mathrm{I}(2\omega) &= |\mathbf{E}^{(2)}(2\omega) + \mathbf{E}^{\mathrm{EFISH}}(2\omega)|^2 \\ &\approx \mathrm{I}(2\omega, \mathbf{E}^{\mathrm{DC}} = 0) + \alpha[\chi^{(2)*}\chi^{(3)} + \chi^{(2)}\chi^{(3)*}]\mathrm{I}^2(\omega)\mathbf{E}^{\mathrm{DC}} \end{aligned} \tag{2.9}$$

where α is a constant, $\chi^{(i)*}$ denotes the complex conjugated to $\chi^{(i)}$ and the quadratic term in $\chi^{(3)}$ is neglected due to $\chi^{(3)} << \chi^{(2)}$. equation (2.9) directly points to a linear dependence of the SHG generated by EFISH from the static electric field. Normally, the third-order effects are negligible compared to the second-order process, but for either high static electric field intensities or a symmetry break due to the static electric field, the third-order effect can reach the same order of magnitude as the second-order effect. For charge transfer (CT) between molecules very high static electric fields are created locally between molecules and therefore the EFISH process can be used as a very sensitive probe for CT and decay processes even at buried interfaces [8–10].

Another important property for high conversion rates of light with the SHG process is the so-called phase matching [71, 72]. It is of high importance for the process of generating tunable pump light for pump/probe experiments. In the discussion above the phase information of the waves was completely omitted. Introducing a phase in the plain wave description leads to:

$$\mathbf{E}_\alpha = \mathbf{E}_\alpha \cdot e^{-i(\mathbf{k}_\alpha \mathbf{x} + \omega_\alpha t)} + c.c. \tag{2.10}$$

with the wave vector $||\mathbf{k}_\alpha|| = \omega_\alpha(\omega_\alpha)/c$, where n is the refractive index and c is the speed of light. In a non-linear and non-centrosymmetric medium the wave generates waves with $\mathbf{k}_\gamma = \mathbf{k}_\alpha + \mathbf{k}_\beta$ at each point advancing through the medium. Most of the light is annihilated due to the dispersion relation $n = n(\omega_\alpha)$. By using a birefringent crystal, like β-phase barium borate (BBO), it is possible to avoid the destructive interference by orienting the crystals in a way that the different polarized fundamental and the generated second harmonic light experience the same velocities. As a result, high intensities of second harmonic light can be generated.

2.2 Experimental setup

The following section gives a brief introduction into the laser setup and the data acquisition. For an extended description of the setup and the measurement chamber refer to the PhD thesis of Michael Schulze [73]. Additionally, this chapter holds a characterization of the current state of the setup, as well as a description of the extension of the setup and of the software used for automating the measurements of molecular switches.

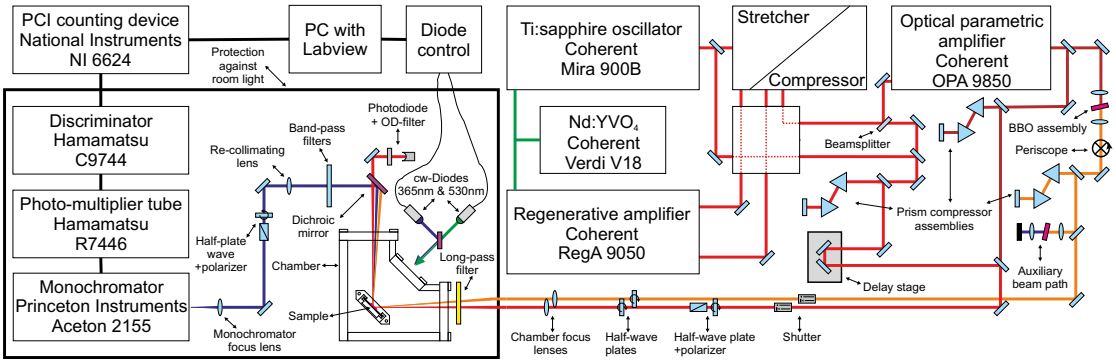

Figure 2.1: The right side shows a schematic of the the laser setup generating the probe (red) and pump (orange) pulsed beam. On the left side, the beam path in the measurement compartment and signal detection is visualized. For experiments on the molecular switching processes two additional diodes were used inside the measurement compartment for illumination of the samples.

2.2.1 Laser setup

This section presents the laser setup. A schematic overview is shown in figure 2.1. The setup can be roughly divided into three parts: (1) Light generation and light tuning, (2) SHG generation and sample compartment, and (3) signal detection and data acquisition.

(1) Light generation and light tuning
The initial light is generated by a frequency-doubled Nd:YVO_4 cw-laser (Coherent Verdi V18), which is split up into two beam lines to pump a mode-locked Ti:sapphire oscillator (Coherent Mira 900B) and a femtosecond regenerative amplifier (Coherent RegA 9050, 300 kHz, $\lambda = 800$nm), which is seeded by the Ti:sapphire oscillator. The RegA output is split into two beam paths. The first one is used as the probe beam. For the time-resolved pump probe experiments a variable temporal delay is introduced by a piezo driven automatic stage (PI M-505.4DG). The probe beam line is then compressed by a pair of highly dispersive prisms (Thorlabs AFS-SF10) which are calibrated by the SHG signal from a GaAs sample. A variable power control is introduced by an Glan Thomson polarizer (Thorlabs GTH10M-B) combined with an achromatic half-wave plate (Thorlabs AHWP10M-980). The polarization of the probe beam can be varied with a second achromatic half-wave plate (Thorlabs AHWP10M-980). The second beam path is used in the time resolved measurements as pump beam. It pumps a tunable optical parametric amplifier (Coherent OPA 9850) whose output beam is frequency-doubled by a BBO crystal creating visible light in the regime between 650 nm and 550 nm. The bandwidth of the visible beam is approximately 25 nm. A compression of the visible beam is also done by a prism pair, which is calibrated by an auxiliary beam path by driving a SHG process of the visible light. The polarization of the visible beam is controlled by a half-wave plate and the power is controlled by the beam focus in the BBO crystal behind the optical parametric amplifier. The two beams are focused by lenses and can be blocked by shutters, both of which are mounted in front of the sample compartment.

(2) SHG generation and sample compartment
The sample compartment shields the entire sample chamber and the beam path behind the sample from external light sources. In the sample compartment, both beams are focused under an incident angle of 45° onto the sample. The spatial and temporal overlap is optimized by maximizing the SFG signal of the superposition of the two beam paths. The resulting cross correlation is in the order of 70 fs, corresponding to a single laser pulse below 50 fs. Environmental UV light is filtered by a longpass colored glass filter (Thorlabs FGL495S) in front of the sample. Behind the sample the light of the fundamental beam and generated SHG beam are separated by a beamsplitter (Thorlabs DMLP567). The SHG beam is further filtered by an array of three bandpass filters (Thorlabs FGB37S, FGB25S and FGS900S) and then focused on a monochromator (Princeton Instruments Aceton 2155). Two diodes (Thorlabs M530L2 and M365L2) are mounted in the sample compartment in order to illuminate the whole sample equally with light of a wavelength of either 530 nm or 365 nm. The diodes can be controlled either manually or with the newly implemented expansion of the measurement software described in section 2.2.4. The sample itself is mounted on a copper plate in the sample chamber, which is kept under an inert gas atmosphere (nitrogen, purity '5.0'). The light is coupled in via CaF_2 windows, which are transparent in the complete visible regime and can withstand high laser intensities.

(3) Signal detection and data acquisition
The SHG photons are converted into an electric signal by an photomultiplier tube directly after the monochromator. The photomultiplier tube works linearly for count of rates up to 20.000 counts/s. For higher count rates the response does not keep up and the system leaves the linear dynamic counting rate. After the photomultiplier the electronic signal is transferred through a discriminator to reduce background noise, and then to a counting unit (Hamamatsu C9744), where the signal is converted to a digital signal level. The converted signal is acquired by a PCI data acquisition card (National Instruments NI 6624) and further handled by a personal computer.

2.2.2 Characterization of the experimental setup

The laser setup can be used for quasi static and for femtosecond time-resolved pump/probe measurements. For both measurements, the destruction of the sample by high laser intensities, and the linear dynamic regime of the photomultiplier limit possible count rates. As discussed before, the SHG signal scales quadratically with the incoming light intensity. A power dependent static SHG measurement to verify this behavior was done on GaAs. The result is shown in figure 2.2a. As it can be clearly seen the SHG signal scales perfectly quadratically for count rates below 20.000 counts/s and differs from this behavior for higher count rates due to the non-linearity of the photomultiplier tube. This limit did not pose a limit for the measurements in this thesis, because for non-damaging laser intensities only count rates below 2000 counts/s were reached.
The temporal trace of the pulses were measured via the SFG signal of the pump and

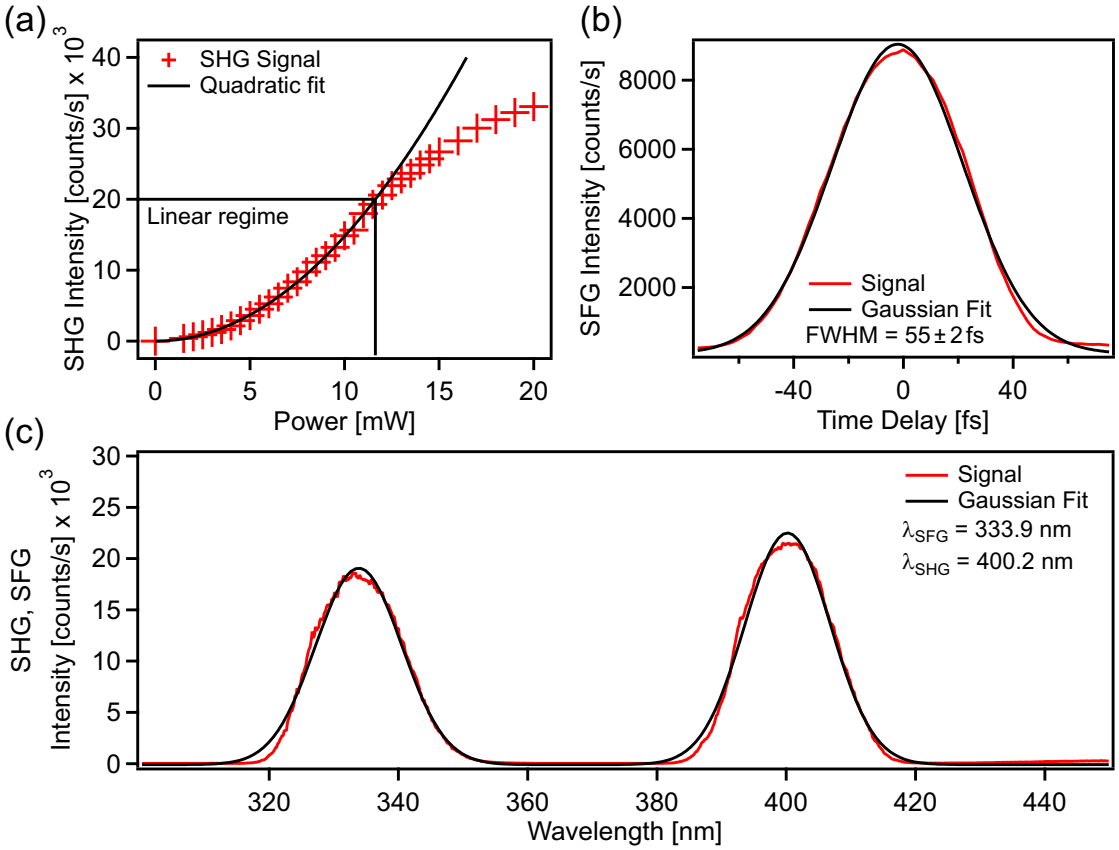

Figure 2.2: (a) Up to 20.000 counts/s the SHG signal scales quadratically with the incoming light as theoretically expected, which means that the signal processing behaves linearly (linear regime). For higher count rates the linear behavior of the signal processing stops. (b) SFG cross-correlation of the pump and probe beam. The FWHM of 55 fs means that the single beams have a width of 39 fs. (c) Wavelength scan done with the monochromator to resolve the spectral behavior of the SFG and SHG signal.

probe pulse. A typical cross correlation is shown in figure 2.2b. The cross correlation can be perfectly modeled by a Gaussian distribution with full width half maximum (FWHM) of 55±2 fs, which leads to single pulses below 50 fs.

By turning the monochromator, the wavelength of the SFG and SHG signal can be scanned. The result is shown in figure 2.2c. The scan can be well-modeled by two independent Gaussian distributions describing the SHG and SFG signal. Both features are noticeable symmetric and the peaks lie at the expected wavelengths.

A time-resolved single scan on the organic samples has a low signal-to-noise ratio, which is mainly due to the low SHG intensity. The ratio can be significantly improved by measuring up to ten scans at the same spot (depending on a possible beam damage) and then moving to a nearby spot and doing another up to ten measurements. By repeating this approach, the quality of the data can be systematically improved and inhomogeneities in the sample are mediated. The results are visualized in figure 2.3.

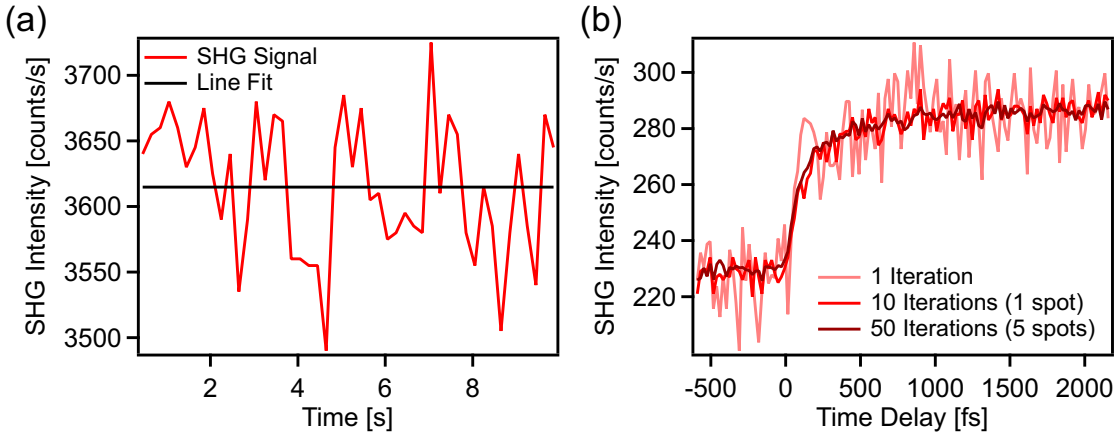

Figure 2.3: (a) For static SHG, a scan with at least a 10 s measurement time corresponding to 50 data points were taken to determine one signal level. (b) Signal to noise ratio increases due to 10 iterations at one spot and usage of multiple spots on one sample.

2.2.3 Measuring methods

The SHG signal changes were created either by changing the static second-order susceptibility of the sample by switching photochromic molecules by light (illumination experiment), or by introducing an optical excitation in a thin organic film by a pump beam and measuring the dynamical changes in the second-order susceptibility (pump/probe experiment). In both cases the relative changes of the SHG signal were detected.

Illumination experiments

In the case of the photochromic fulgimide molecules, the SHG signal changes are induced by the ring-opening/ring-closure reaction, because only the closed-form has a delocalized π-electron system, while the open-form does not. Thus a significant change of the electronic structure is created by the switching process. The switching is triggered by illumination with light at different wavelengths. In the experiment, the illumination is realized via two diodes ($\lambda = 530\,\text{nm}$ and $\lambda = 365\,\text{nm}$), which are mounted outside of the sample chamber, but still inside of the sample compartment. From the laser setup, only the fundamental beam for the SHG process is used. If needed, the full power from the setup can be used to drive the SHG process at the sample. The light of the diodes is coupled into the sample chamber perpendicular to the sample, using lenses directly attached to the diodes in a way that the whole samples are homogeneously illuminated. SHG measurements during illumination are not possible due to the high amount of scattered light from the diodes. The polarization of the probe beam can be controlled in front of and behind the sample. The general measurement scheme has been illumination with small amounts of light by one diode, followed by a short SHG measurement and has been repeated until a saturation of the SHG signal is reached. By this procedure, the effective cross-section for the switching process for this kind of treatment can be extracted, as long as there is no fast thermal relaxation and no changing of the sample induced

by the probe beam. Thermal stability of both photocromic states and no influence by the probe beam were expected for the samples investigated in this thesis, but this did not prove to be true. Especially a saturating signal change due to the probe beam was detected. Therefore, the procedure was changed: (1) The samples were illuminated for a fixed amount of time, to induce a change in a part of the molecules. (2) Directly after the illumination, to avoid thermal relaxation, the SHG signal was measured until the saturation of the changes introduced by the probe beam. (3) By illuminating the samples with light corresponding to the opposite switching process of that in step 1, the molecules were brought back into their initial state. (4) This procedure was repeated with increasing illumination times in step 1 until no further change by the illumination could be detected. Through this procedure the initial values of all measurements done in step 2 trace the amount of switched molecules depending on the illumination time. The initial signal amplitudes were determined by a single exponential fit of the measurements done in step 2. By plotting the resulting data points against the illumination time, the cross-sections of the switching process were determined. Another important property for applications of the photochromic molecules is their thermal stability and the reversibility of the switching process. For the thermal stability measurements the samples were illuminated until saturation and then stored for at least 12 hours, after which the SHG signal level was measured again. The switching stability was determined by fully switching the samples between the two states at least 10 times and always checking the SHG signal level for both states in each cycle. A brief description of an automation for all experiments described here can be found in section 2.2.4. It has been written in LabView as part of the experimental work.

Polarization-resolved experiments

To determine the orientation of the photochromic molecules and the orientation of excited states in the organic semiconductors, polarization-resolved measurements were conducted. In the experimental setup the polarization of the pump and probe beam can be continuously controlled by $\lambda/2$-waveplates, which are normally set to p-polarization. A polarization-resolved measurement of the SHG signal can be realized, too. In this case a $\lambda/2$-waveplate in combination with a polarization filter is used to filter the polarization of the outgoing light. The p-polarized light has one component perpendicular and one parallel component to the surface, whereas the s-polarized light only has a parallel component. A sketch of the beam and polarization geometries is shown in figure 2.4.

Power-dependent experiments

The intensity of the SHG light depends quadratically on the incoming beam intensity as shown theoretically in section 2.1 and proven experimentally in section 2.2.2. Increases in the amount of switched molecules or of excited states in a molecular layer scales linearly. To differentiate between different effects, to find a balance between sample destruction and high signal amplitudes, and to identify non-linear effects a power variation of the pump and the probe beam was done.

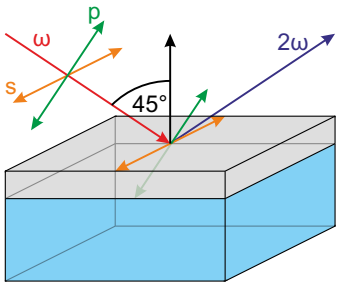

Figure 2.4: Geometry of the different beam polarizations with respect to the sample.

Energy-dependent experiments
In the case of the time-resolved pump/probe experiments spectroscopic investigations are possible. With the OPA it is possible to change the wavelength of the pump beam, which can be used to investigate different excitations in the organic thin films. Especially the influence of excess energy above the initially needed energy and the influence of excitation into higher lying excited states (e.g. S_2) are of great interest.

2.2.4 Automation of the illumination experiments

An automation of the measurements of the illumination experiments was developed, and the measurement program (written in LabView) was expanded. For a detailed description of the basic measurement program refer to the PhD thesis of Michael Schulze [73]. The current section of the thesis at hand explains the additional options that come with the expansion.
The illumination experiments are usually done by illuminating the sample for a given time and then measuring the change in the SHG signal level, both done repeatedly until the signal saturates. This is performed to measure the amount of light needed to switch the complete sample. Afterwards the effective cross section for this switching process can be calculated. Another common procedure is to illuminate until saturation, measure, illuminate with the other wavelength until saturation, measure, and repeat a few times in order to investigate the stability and reversibility of the switching process. Both kinds of measurements can be very time-consuming. The automation gives the user the possibility to easily program the setup to do a full illumination series with varying illumination times and both light sources. In figure 2.5 the user interface of LabView is shown. In (1), up to two treatments can be chosen. The upper field defines the general behavior (illumination or dark (no illumination)) and the lower one decides the kind of illumination (UV or VIS) in case of illumination. The three available options therefore are: no illumination, UV or VIS illumination. Other illuminations are possible by exchanging the corresponding diodes. In (2) the times for treatment one can be set individually for every iteration for up to 20 iterations. In each iteration, treatment one is done for the time set in (2) for that iteration and then treatment two is done for the time set in (3). A time of zero in (2) or (3) means that treatment is skipped. In (4) the measurement time after treatment one and two is set. The measurement time is set for

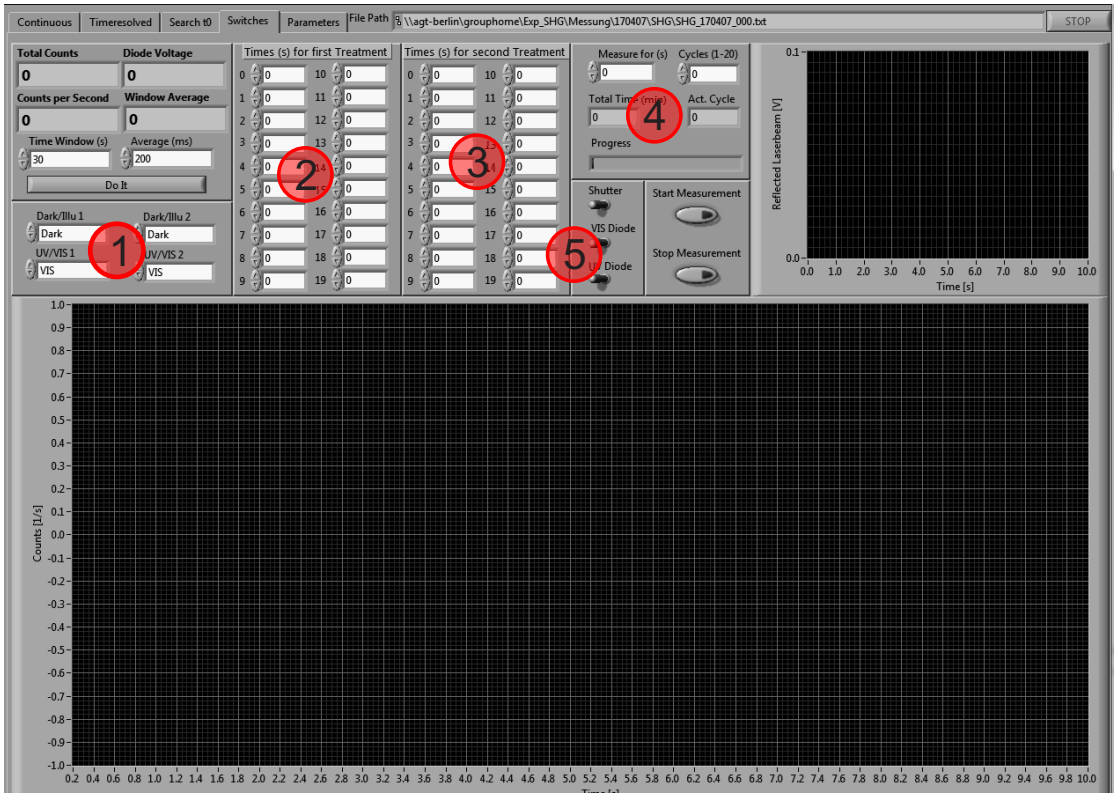

Figure 2.5: The user interface shown here of the expansion enables fully automated measurements of illumination experiments. The marked areas are described in the text.

all iterations. For all times except the measurement time the laser beam is blocked by a shutter in front of the measurement compartment. The cycle window in (4) is only needed for calculating the approximated time for the full measurement and the progress bar. The progress bar is for the full measurement and not the individual iterations. When no cycle is set the measurement is done, but no progress is shown. In (5), the shutter and the two diodes can be controlled manually. Using the manual controls during a automated measurement can lead to errors. The intensity of the illumination has to be set manually once, before the measurements starts. To use the automation the diode control has to be set from cw to trigger, so it can be switched on and off by the computer. For an efficient use of the automation a new arrangement of the diodes was built. In the setup used before, only one diode could be mounted at the same time. By the inclusion of a beam splitter (Thorlabs DMLP505) in front of the sample chamber, both diodes can be used at the same time. With the beam splitter in place, the VIS diode is mounted as before and the light passes through the beam splitter. The UV diode is mounted perpendicular to the setup and the light is reflected by the beam splitter. With this setup the samples can be illuminated by both light sources without changing the illumination source, and the measurement time is only limited by the laser stability, which lies in the range of several hours.

3 Functional Interfaces

In this chapter the results of SHG investigations on the switching behavior of fulgimide derivatives immobilized by an alkyne linker on a Si(111) surface are presented. Three aspects are investigated by SHG generation measurements: (1) the thermal stability of the different molecular states, (2) the switching ability and reversibility, and (3) the cross-sections of the switching processes. Furthermore, the NLO contrast between the different molecular states for various laser beam polarization combinations is combined with the results of simulations to get information about the molecular alignment of the molecules with respect to the surface. Based on a modification of the linker group and on previous experiments by Michael Schulze [73, 74], the rise of a new molecular state and the influence of a phenyl ring on the switching properties and thermal stabilities of the different photochromic states of the fulgimides in the configuration used here are discussed. This chapter begins with an introduction to the molecular class of fulgimides and their photochromism (section 3.1), followed by a short description of the sample preparation (section 3.2). Subsequently, the results of the three systems investigated in this thesis are presented (section 3.3) and compared to results based on calculations by Clemens Rietze of Prof. Peter Saalfrank's group at the Institut für Chemie at the Universität Potsdam (section 3.4). Finally, the results are discussed with a focus on the newly discovered IR-state (section 3.5).

3.1 Introduction

The key property of fulgimides are their photochromic properties. Photochromism is defined as the "reversible transformation of a chemical species induced in one or both directions by absorption of electromagnetic radiation between two forms, A and B, having different absorption spectra" [75]. Thereby, the molecular form A is thermally stable and can be transformed into form B by irradiation with electromagnetic waves. The back transfer from form B to form A can be driven thermally or photochemically. In figure 3.1a the general concept of photochromism is visualized. Prominent examples of photochromism are the ring-opening/ring-closure reaction of fulgides [76–78] and fulgimides [30, 36, 37, 78], furthermore spiropyrans [79] and diarylethenes [80, 81], as well as the conformational trans/cis isomerization of azobenzene [23, 82, 83] and its derivatives [84, 85].
Fulgimides are the imide derivative of the fulgides. Fulgides were synthesized, investigated and named at the beginning of the 20th century by Stobbe [22, 76]. Based on the fulgides, in 1957 the first imide derivatives named fulgimides were reported [36]. A highly efficient synthesis developed by Liang *et al.* opened the way for large-scale production of indolylfulgimides [37, 38]. In solution the indolylfulgimides show a strong

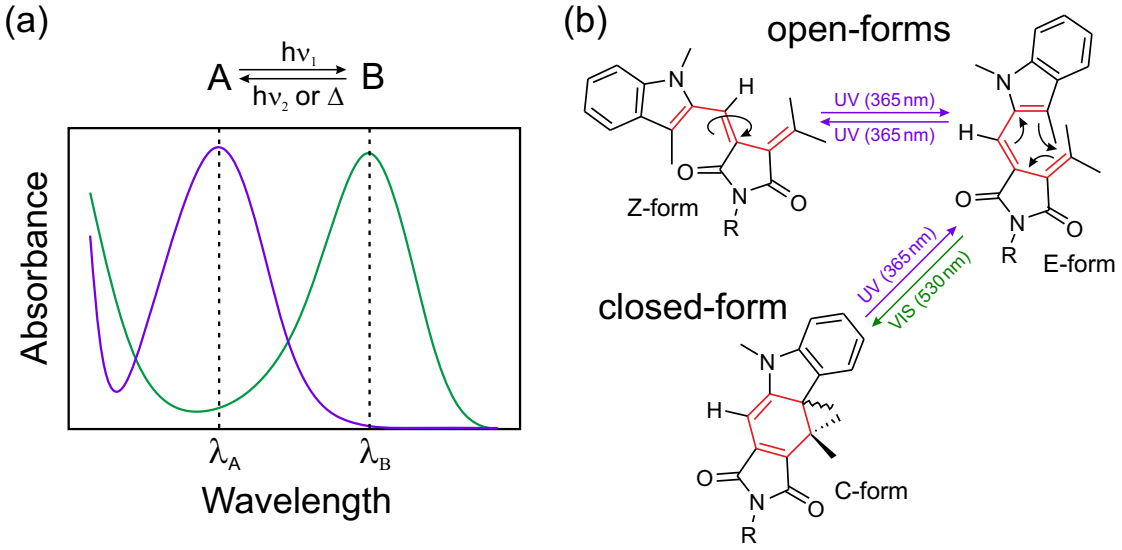

Figure 3.1: (a) Visualization of the general definition of photochromism. (b) Photochromism of the 2-indolylfulgimide.

thermal stability of both switching states at room temperature and a very high fatigue resistance of the switching process [38]. In general, fulgides and fulgimides in solution show various properties facilitating commercial applications: (1) As mentioned before, complete thermal stability. (2) High conversation between the open- and closed-form. (3) High quantum efficiencies in both directions. (4) A good fatigue resistance. (5) Suitable for large-scale synthesis [78]. Furthermore, the switching processes between the open- and closed-form takes place on the timescale of a picosecond and without formation of intermediate meta-stable states [24, 77, 86, 87]. Thus the Woodward-Hoffmann rules can be applied to the ring-opening/ring-closure reaction of this molecules [88–90]. Based on the these rules the photochemical process of the ring-closure reaction is a conrotatory electrocyclization of the central hexatriene moiety, as highlighted in figure 3.1b. The ring-closure reaction is optically symmetry allowed and can therefore be driven by UV light. Due to the almost planar four-ring conjugated π-electron system formed in the closed-form (C-form) the absorbance is shifted to higher wavelengths, the molecules become colored and the ring-opening reaction is driven by visible light [38]. Apart from of the ring-opening/ring-closure reaction the molecules can undergo a cis-/trans-isomerization in the open-form. Here both directions of the process are driven by UV light. The ring-closure reaction can only be accomplished coming from the trans-form (E-form), while for the cis-form (Z-form) the ring-closure reaction is not possible, due to the large distance between the indole and the methylene groups. In general the cis-/trans-isomerization is regarded as an undesired process leading to a waste of energy [91]. Under UV illumination a photostationary state forms between the E- and the Z-form. Due to the one-way ring-closure process under UV illumination the E-form is depleted into the C-form and thereby the Z-form is depleted, too. For the illumination with visible light the C-form is switched back into the E-form, a further transfer to the

Z-form does not take place here. The combination of both processes leads to a small amount of molecules in the Z-form. With substituents, which are not involved in the electrocyclization, the ratio between the Z- and the E-form can be tuned [92, 93]. For the 3-indolylfulgimide in benzoic solution, ratios of (Z/E/C) = 6/15/79 and 6/94/0 in the photostationary state for UV- and visible illumination have been reported [30]. As shown for the photostationary state under UV illumination for a similar indolylfulgimide the ratio in solution also depends on the solvent used [94].
A large variety of applications of fulgide and fulgimide molecules have been demonstrated. First of all the possibility of using the open- and closed-form as binary data storage with a read-out in the IR-regime has been realized [95]. Liang *et al.* achieved a full non-destructible readout molecular memory by attaching a molecular dye to the fulgimide unit, thus making the fluorescence of the dye molecule dependent on the photochromatic state of the fulgimide. A proof of concept device was built by immobilizing the dye-driver units in an PMMA matrix [18]. Furthermore, a 3-D data storage system with full read, write, and erase capability based on fulgimides was achieved [19]. Apart from the application in storage systems fulgides were used for re-writable holographic films [96] and switchable energy transfer [20]. Regarding molecular opto-electronics full molecular all-optical logic units based on fulgimide-porphyrin-dithienylethen [21] and molecular transistors based on the switching state of a fulgimide [3] were realized.
For most of the applications mentioned above immobilization of the fulgimides is needed. For example for data storage the same molecules have to be addressed in the read and write cycles. The immobilization of organic switches, while conserving the functionality, has proven to be challenging. Different approaches have been applied. One of the early approaches used a fully controlled environment by evaporating molecular switches in UHV onto noble metals. In many of these systems the interaction between the metal and the molecular switch led to changes in the switching behavior ranging from fully losing the functionality of the molecules (e.g. azobenzene on gold [31]) to one-way processes (e.g. thienylcyclopentenes between gold contacts [32]) and to inversing the thermal stability (e.g. nitrospiropyran [33]). Besides the reduction of functionality by the coupling between molecules and metal surfaces the interaction can also increase functionality by enabling effective switching due to a reduction of the transformation barrier (e.g. in alkene derivatives on Cu(110) [97]).
Different coupling processes between the surface and the molecules have been discussed. The most prominent are: (1) Steric hindrance of conformational changes induced by the presence of the surface [35]. (2) The presence of ultrafast de-excitation channels introduced by the surface [98]. (3) Strong reductions of the thermal barrier of physisorbed molecules on surfaces [31]. To overcome and manage the interaction between the surface and the photochromic molecules various strategies have been developed. One example is the introduction of bulky side groups decoupling the functional parts of the molecules from the surface [26, 34]. Another approach is to use a passivation layer [99]. For the samples investigated in this work another approach has been used. The functional molecules are attached to the surface by an SAM layer. Thereby, the adsorbate-substrate as well as the adsorbate-adsorbate interaction can be tuned by the SAM molecules. This can be achieved by varying the lengths of the anchoring group or by introducing spacer

units [30, 100]. Usually thiole SAMs are used to connect functionalized molecules with gold surfaces [101], or molecules are grafted directly on a silicon surface [30]. One major problem for immobilized molecular switches can be steric hindrance either due to the surface (including the SAMs) or due to other molecular switches in the molecular layer [100, 102]. Beside steric hindrance also excitonic coupling between molecular switches can play a role [103].
Investigating the switching behavior of sub-monolayers of photochromatic molecules is rather difficult, especially in regard of the application as data storage, where a significant and reproducible change is needed. Furthermore, the state of the molecules should not be changed nor the molecules degraded by the measurement of the system. Probing the second order NLO properties is a promising option. The SHG signal generation is limited to symmetry breaking interfaces and therefore leads to a high ratio of the signal from the molecular layer compared to the substrate [11–14]. Furthermore, in the case of fulgimides the ring-closure reaction introduces a large closed π-electron system [37], which is known to influence significantly the second order susceptibility and thereby the SHG signal [39]. For the SHG generation a light source with a low photon energy outside of the optical absorbance of any of the molecular states can be chosen and thus an influence of the measurement to the molecular state can be avoided. With a focused beam a spatial resolution of the measurement could be achieved. In summary SHG measurements of a fulgimide system fulfill a necessary requirements for a method to investigate such a system with high signal to noise ratios and high contrast between the different molecular states. For the system of 3-indolylfulgimides attached with an amide linker a second order NLO contrast of 20 % has been reported [104]. In this work the resulting systems of the immobilization approach of two indolylfulgimide derivatives via a alkyne linker have been investigated with SHG.

3.2 Sample preparation

All fulgimide samples were prepared by Christoph Barta in the group of Prof. Karola Rück-Braun at the Institut für Chemie at the Technische Universität Berlin. In the first step the Si(111) surfaces were cleaned for 30 min at 100 °C with piranha solution (H_2SO_4/H_2O_2) and etched afterwards with 40 % ammoniafluoride solution for 15 min at room temperature, leading to a fully H-terminated Si(111) surface. In the next step the alkyne monolayer was grafted by the thermal reaction of the Si(111) surface with 1,8-Nonadiyne at 170 °C for 3 h under protective gas atmosphere (N_2). The fulgimides functionalized with a phenyl ring at the nitrogen of the succinimid part were attached to the alkyne monolayer by a Sonogashira-reaction (5 mM fulgimide, 10 mol% $Pd(PPh_3)_4$ and 10 mol% CuI in toulene, DMF, Et_3N solution for 18 h at room temperature). Afterwards the samples were cleaned and stored under argon until the transfer into the sample chamber, where they were stored and measured under nitrogen. X-ray reflectivity (XRR) studies of the samples done by Christopher Weber in the group of Prof. Stefan Kowarik at the Institut für Physik at the Humboldt-Universität zu Berlin revealed a surface coverage of 68±5 % coverage with alkyne linker molecules and a fulgimide coverage

of every 7th alkyne chain with a fulgimide molecule. This results were confirmed by XPS studies of Daniel Przyrembel in the group of Prof. Martin Weinelt at the Department of Physics at the Freie Universität Berlin.

3.3 Experimental results

In this chapter the experimental results of SHG measurements on submonolayer of indolylfulgimides immobilized on a silicon surface are presented. In section 3.3.1 the preliminary experiments on the linker molecules without the fulgimide switch are briefly shown. Starting with section 3.3.2 the results on three different indolylfulgimide systems are presented. In section 3.3.2 the results from 2-indolylfulgimide are presented. Based on the results of the 2-indolylfulgimide in section 3.3.3 the same fulgimide decoupled from the phenyl ring by an CH_2-spacer are shown. For direct comparison with published results the investigations on a sample with a 3-indolylfulgimide immobilized in the same way as the 2-indolylfulgimide are presented in section 3.3.4. A summary of all systems investigated here is given in figure 3.2, in which sample (a) is only used as a reference system, which has been investigated by Schulze *et al.* [74]. Samples (b) to (d) are the samples presented and discussed in this thesis.

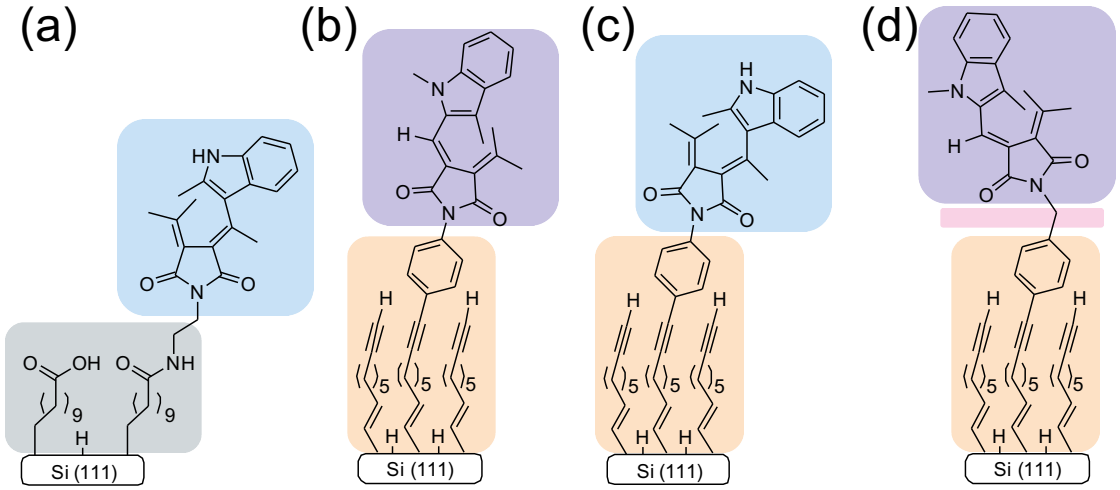

Figure 3.2: Basic structures of the different fulgimide samples. Sample (a) is used as a reference and discussed in ref. [74]. The results of samples (b) to (d) are discussed in this thesis. The systems are: (a) 3-indolylfulgimide with an amide linker, (b) 2-indolylfulgimide with an alkyne linker, (c) 3-indolylfulgimide with an alkyne linker and (d) 2-indolylfulgimide with an alkyne linker and CH_2 spacer group.

3.3.1 Linker molecules immobilized on Si(111)

Before investigating the behavior of the fulgimides attached to the silicon surface, the influence of the linker molecules onto the SHG signal has been measured. The results

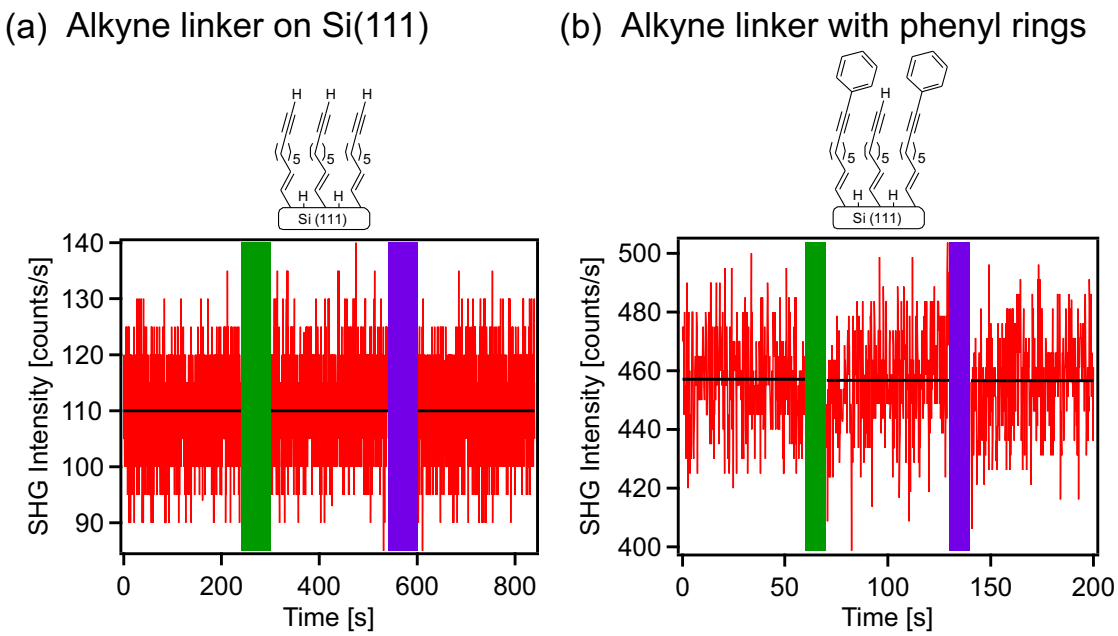

Figure 3.3: SHG signal and influence of illumination (colored bars) to the linker immobilized at Si(111). (a) SHG signal of a monolayer of alkyne. (b) SHG signal of a monolayer of alkyne with phenyl rings attached.

for an alkyne monolayer on H-terminated silicon and for a layer with some phenyl rings attached to the alkyne monolayer are shown in figure 3.3.
Both samples were measured with SHG before any treatment with light, after illumination with green (530 nm) and with UV (365 nm) light, which were used to change the photochromic state of the fulgimide molecules. As shown in figure 3.3, no change in SHG signal could be invoked by the illuminations, and the SHG measurement with a high intensity probe beam (800 nm) has no influence on the signal level. Due to the high sensitivity of the SHG signal to symmetry breaks the signal origin is mostly assigned to the molecular monolayer and the significantly higher signal level with phenyl rings is due to the delocalized electron system. From the static signal it is concluded that no destruction and no excited state of the sample were invoked by neither the illumination nor the probe beam. All signal changes are therefore attributed to the fulgimides in the following sections.

3.3.2 2-Indolylfulgimide

In figure 3.4a the results of the SHG measurements after illumination with visible light (530 nm) and with UV light (365 nm) are shown. After both illuminations the SHG signal shows a significant rise with measurement time, saturating independently of the preceding illumination treatment, after approximately 150 s. A clear difference can be seen in the SHG amplitudes at the beginning of the measurements. The signal after illumination with visible light starts at a lower signal level than the signal after illumi-

nation with UV light. Measuring for longer times as shown here does not change the signal further. Waiting after the SHG measurement without any illumination leads to a reduction of the SHG signal with a decay constant of 424±30 s back to the level measured after illumination with visible light (see figure 3.4b). This process is independent of the illumination of the sample before and can be repeated for at least 100 times without any significant change. Based on these measurements it is assumed that the system can be brought into three different states and that it is possible to switch between the three states reversibly by illumination with visible light, UV light, and high intensity IR-light. At least the state invoked by the illumination with IR-light is not thermally stable and decays back into the state created by the visible light. Due to the photochromism of the fulgimides (see section 3.1) the state created by visible light is assigned to the E/Z-form (open-forms) and the state created by the UV light is assigned to the C-form (closed-form). For now the IR-state is not assigned to a specific process. A detailed discussion of the IR-state is given in section 3.5.

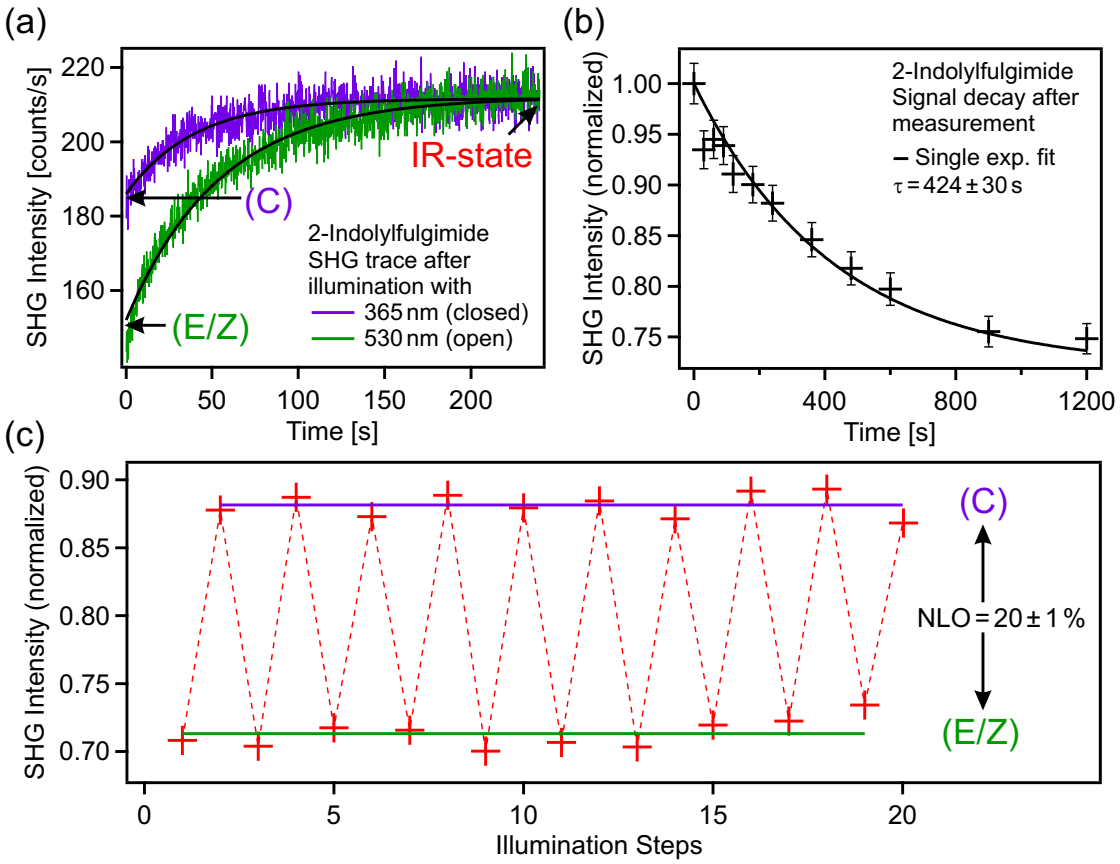

Figure 3.4: Switching of 2-indolylfulgimide. (a) Dependence of the SHG signal on illumination and measurement time. (b) Thermal decay after a measurement with the probing beam. (c) Reversible switching of the 2-indolylfulgimide layer for 10 cycles.

First the reversibility of the switching process open ↔ closed and the stability of the molecules during the switching cycles were tested by switching the molecules 10 times between the two states. The signal level corresponding to the open- and the closed-form have been calculated by fitting the SHG measurements by single exponential functions and extracting the initial signal level. The result is shown in figure 3.4c. All measurements have been normalized on the signal level of the IR-state. Based on the normalization of the IR-level the closed-form has a signal level of 88±1 % and the open-form has a signal level of 71±1 %. This leads to a NLO contrast of 20±1 % between the open- and the closed-form using the signal level of the closed-form as reference. No significant NLO reduction has been detected for at least 10 switching cycles. During the course of the deeper investigations discussed below the molecules have been switched for at least 100 times and even then no significant change in the signal levels of the three states or in the reversibility was detected. Thus a reversible switching of the molecules has been proven.
In the next step the thermal stability of all three states were investigated. As shown before, the IR-state is not thermally stable and decays back into the open-form. To verify the thermal stability of the open-form the sample was illuminated with visible light and then stored for different times without illumination. As shown in figure 3.5a no signal change could be detected for at least 20 min. The same procedure was done with the closed state (UV illumination). As it can be clearly seen in figure 3.5b the closed-form is not thermally stable at room temperature and the signal level decays with a decay time of 302±30 s into the level of the open-form. Furthermore, the level of the open-form has always been measured in the first measurement after a night of storage. The instability of the closed-form is highly unexpected for a fulgimide [38, 94, 105, 106]. In general both forms are thermally stable at room temperature in fulgimides and no reaction between the two states is observed [38]. Nevertheless the open-form is the global minimum in fulgimides [24, 77]. Therefore a possible explanation could be a lowering of the barrier between the two photochromic states. It is well-known for various systems that an electrically conductive surface can act as a quencher and thereby influence the switching process [31, 33, 98]. This possibility can be most likely excluded here, because the fulgimide molecules are decoupled by the isolating alkyne linker from the substrate. Another possibility could be an interaction between the fulgimide and the phenyl ring, which is directly attached to the fulgimide. This could explain the reduction of the thermal stability of the closed-form. For a detailed discussion of the effect of the phenyl ring on the fulgimide see section 3.5.
To shortly summarize the results so far: (1) The signal level of the 2-indolylfulgimide shows three distinct levels and a reversible switching between the three levels is possible by illumination with visible, UV, and IR-light. (2) The two states invoked by the illumination with visible and UV light are assigned to the open- and closed-form of the fulgimide. (3) A clear attribution to the IR-state is not possible up to now. (4) Only the open form is stable and both other forms decay into the open-form.
To get a better understanding of the processes involved the cross-sections of all six switching processes between the three states were measured. This was done by illuminating the sample with the respective light to create the initial state and directly

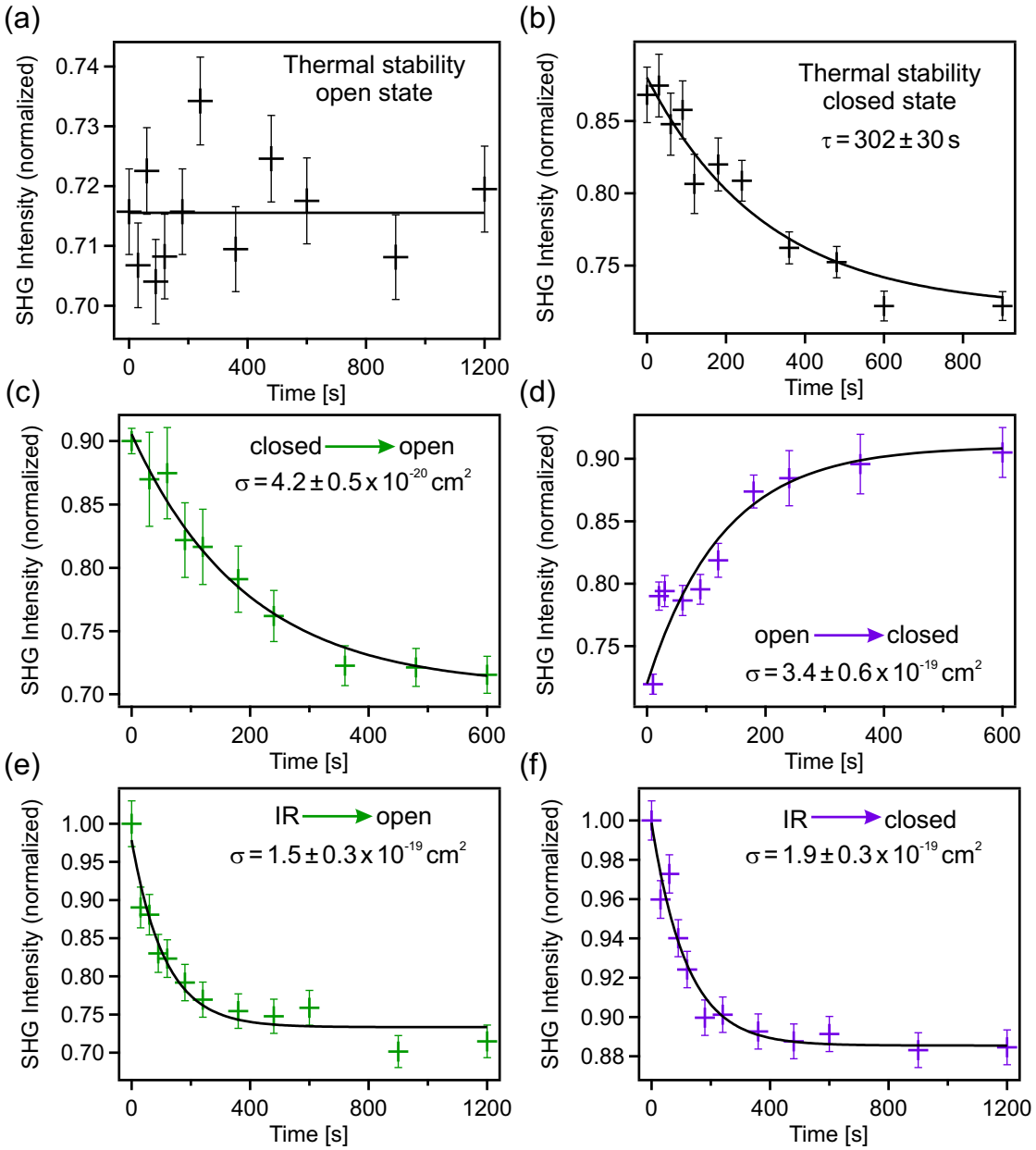

Figure 3.5: Thermal stability and cross-section measurements of the three different states of a 2-indolylfulgimide layer. (a) Thermal stability of the E/Z-state (open). (b) Thermal stability of the C-state (closed). (c)-(f) Determination of the cross-section of (c) the ring opening reaction, (d) the ring closure reaction, (e) the ring opening reaction coming from the IR-state and (f) the ring closure reaction coming from the IR-state.

afterwards illuminating the sample for increasing times with the light corresponding to the switching process into the final state. To determine the signal level the resulting SHG curves were fitted by a single exponential function and based on the fits the initial signal levels were extracted. These initial signal levels were plotted over the illumination time and modeled by a single exponential fit. The resulting SHG signal curves for the processes closed → open, open → closed, IR → open, and IR → closed are shown in figure 3.5c-f. The times for the processes open → IR and closed → IR have been taken from the measurements shown before in figure 3.4. Due to the thermal instability of the IR-state and the closed-form the thermal decay has to be considered in the calculation of the cross-sections. In the first step the measurement curves have been modeled by single exponential fits and the decay times of the various processes have been taken from the single exponential fits. In the second step the measured decay times have been corrected by the thermal decay times by calculating the effective decay times by solving the corresponding rate equations. For the case of two competing processes (thermal and illumination) the cumulative time (measured under illumination) becomes:

$$\frac{1}{\tau_\mathrm{c}} = \frac{1}{\tau_\mathrm{i}} \pm \frac{1}{\tau_\mathrm{t}} \tag{3.1}$$

where τ_c denotes the cumulative decay under illumination, τ_t the thermal decay, and τ_i the part introduced by the illumination. The "+" is used for processes, in which the thermal and the light-induced part drive the same process, and "−" for the opposite case. Solved for the illumination part, equation (3.1) becomes:

$$\tau_\mathrm{i} = \frac{\tau_\mathrm{c} \cdot \tau_\mathrm{t}}{\tau_\mathrm{t} \mp \tau_\mathrm{c}} \tag{3.2}$$

Based on the effective decay times τ and the photon dose n_p on the sample surface per time interval the cross-sections for all six processes have been calculated by:

$$\sigma = \frac{1}{\tau \cdot n_p} \tag{3.3}$$

In the here discussed experiments a photon flux of $f_{UV} = 2.07 \cdot 10^{16}$ photons/s cm^2 has been used during the illumination with UV light, a photon flux of $f_{VIS} = 2.79 \cdot 10^{16}$ photons/s cm^2 during the illumination with visible light and a photon flux of $f_{IR} = 8.68 \cdot 10^{21}$ photons/s cm^2 during the measurements induced by the probe beam. The resulting cross-sections are: $\sigma_{o\to c} = 3.4 \pm 0.6 \cdot 10^{-19}\,\mathrm{cm}^2$ for open-form → closed-form, $\sigma_{c\to o} = 4.2 \pm 0.5 \cdot 10^{-20}\,\mathrm{cm}^2$ for closed-form → open-form, $\sigma_{o\to IR} = 3.0 \pm 0.3 \cdot 10^{-23}\,\mathrm{cm}^2$ for open-form → IR-state, $\sigma_{c\to IR} = 5.6 \pm 0.8 \cdot 10^{-23}\,\mathrm{cm}^2$ for closed-form → IR-state, $\sigma_{IR\to o} = 1.5 \pm 0.3 \cdot 10^{-19}\,\mathrm{cm}^2$ for IR-state → open-form, and $\sigma_{IR\to c} = 1.9 \pm 0.3 \cdot 10^{-19}\,\mathrm{cm}^2$ for IR-state → closed-form. A summary of all the processes, their cross-sections, and their thermal properties is given in figure 3.6. Compared to published results for similar fulgimides immobilized on silicon with cross-sections of $\sigma_{o\to c} = 2.3 \pm$

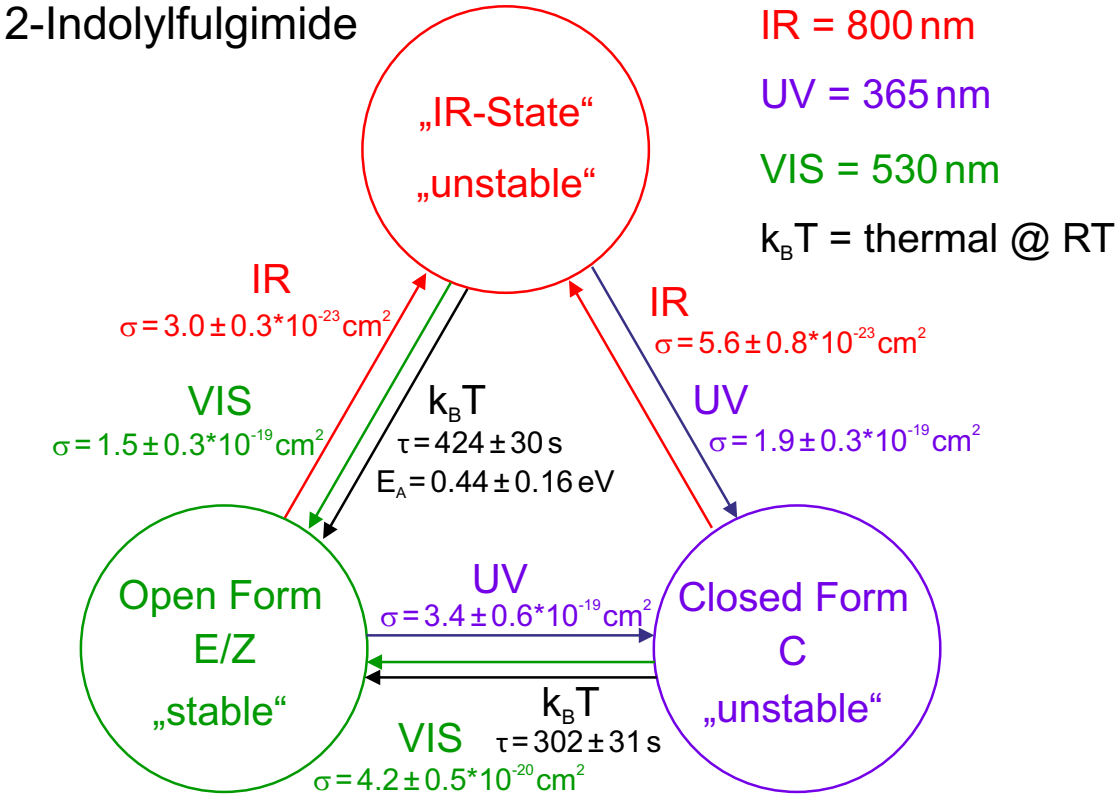

Figure 3.6: Summary of all cross-sections and thermal decays of the system 2-indolylfulgimide on silicon.

$0.3 \cdot 10^{-18}\,\mathrm{cm}^2$ and $\sigma_{c\to o} = 1.2 \pm 0.3 \cdot 10^{-18}\,\mathrm{cm}^2$ the cross-sections for the switching between the closed- and open-form are lowered by an order of magnitude [74]. Compared to other systems the decoupling from the substrate can still be seen as a success. For azobenzene physisorbed on Au(111) cross-sections for the cis/trans isomerie three orders of magnitude lower have been reported [34]. By decoupling the azobenzene from the gold surface a increase of the cross-sections to the range 10^{-18} - $10^{-19}\,\mathrm{cm}^2$ could be achieved [107]. Another example for coupled molecules is spiropyran on bismuth with cross-sections in the range of $10^{-22}\,\mathrm{cm}^2$ [108]. The here found cross-sections for the ring opening/closure reaction are slightly lower than the cross-sections for the decoupled azobenzene [107] and one order of magnitude lower than reported for a different linker group [74], but still significantly larger than the cross-sections for molecules coupled to a conductive substrates [34, 108]. Based on measurements of fulgimides in solution a cross-section range of 10^{-17} - $10^{-18}\,\mathrm{cm}^2$ would be expected for the non-influenced fulgimide molecules [37]. Thus the results can be interpreted as successful decoupling of the fulgimides from the surface, but there is a hindrance invoked by the here used immobilization approach by the alkyne linker in comparison to the amide linker [74]. Interesting for the further interpretation is that the cross-sections for switching into the IR-state are four orders of magnitude lower than the cross-sections for switching into

the open- or closed-form.
To get a better understanding of the thermal decay one of the samples has been heated during the thermal decay of the IR-state. The same procedure has been planned for the thermal decay of closed state, but unfortunately all other samples on which the heating procedure has been tried were destroyed during the heating and only results for the thermal decay of the IR-state could be measured. The resulting decay curves are shown in figure 3.7a and the corresponding Arrhenius plot to calculate the activation energy of the process is shown in figure 3.7. Based on the linear fit in the Arrhenius plot a activation energy of 440±160 meV has been determined.

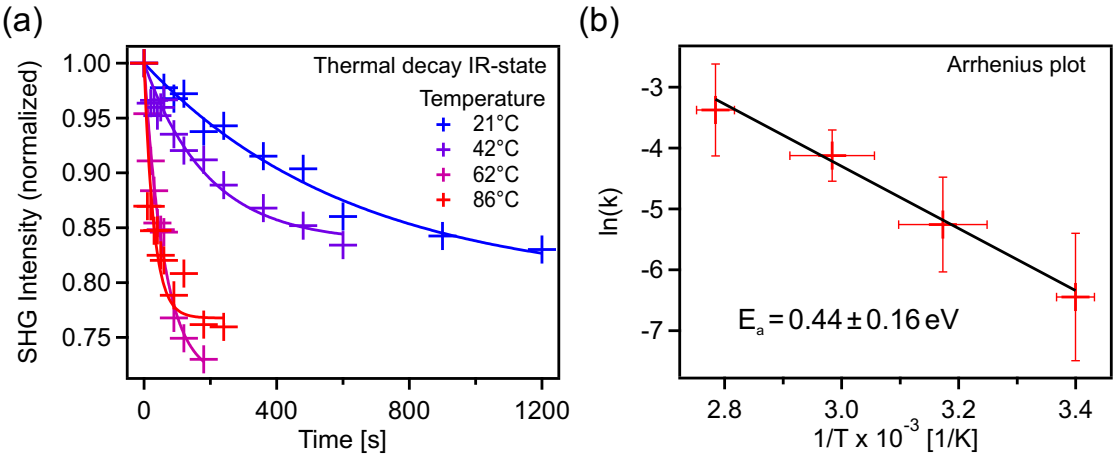

Figure 3.7: Determination of the activation energy for the energy barrier of the thermal decay of the IR-state. (a) Decay curves for different temperatures. (b) Corresponding Arrhenius plot.

Additionally, polarization-resolved measurements have been done to investigate the molecular alignment at the interface. Hereby the incoming and the outgoing polarization of the probe-beam has been changed to probe the different elements of the second order susceptibility tensor. The results are shown in figure 3.8. All signal level are referenced to the level of the IR-state for p-in/p-out polarization.
Five important observations can be made from the polarization-resolved measurements: (1) All three signal level could be detected for all polarization combinations and they are always in a similar NLO signal range. (2) For all polarization combinations the IR-state has the highest NLO signal and can be clearly separated from the other two forms. (3) The highest signal levels are not reached for the p-in/p-out combination, but for p-in/s-out and for none of the polarization combinations the signals are largely suppressed. (4) For the combination s-in/p-out the signal level of the closed- and the open-form switched their order. (5) The smallest difference in the NLO contrast between the open- and the closed-form is 5.2 % and has been measured for s-in/s-out.
In general the polarization-resolved NLO signal depends on the orientation of the second order susceptibility, which is coupled to the orientation and state of the molecule. Especially the delocalized π-system in the closed-form of the 2-indolylfulgimide gives a large contribution to the NLO signal [39] and therefore the highest NLO signal is expected

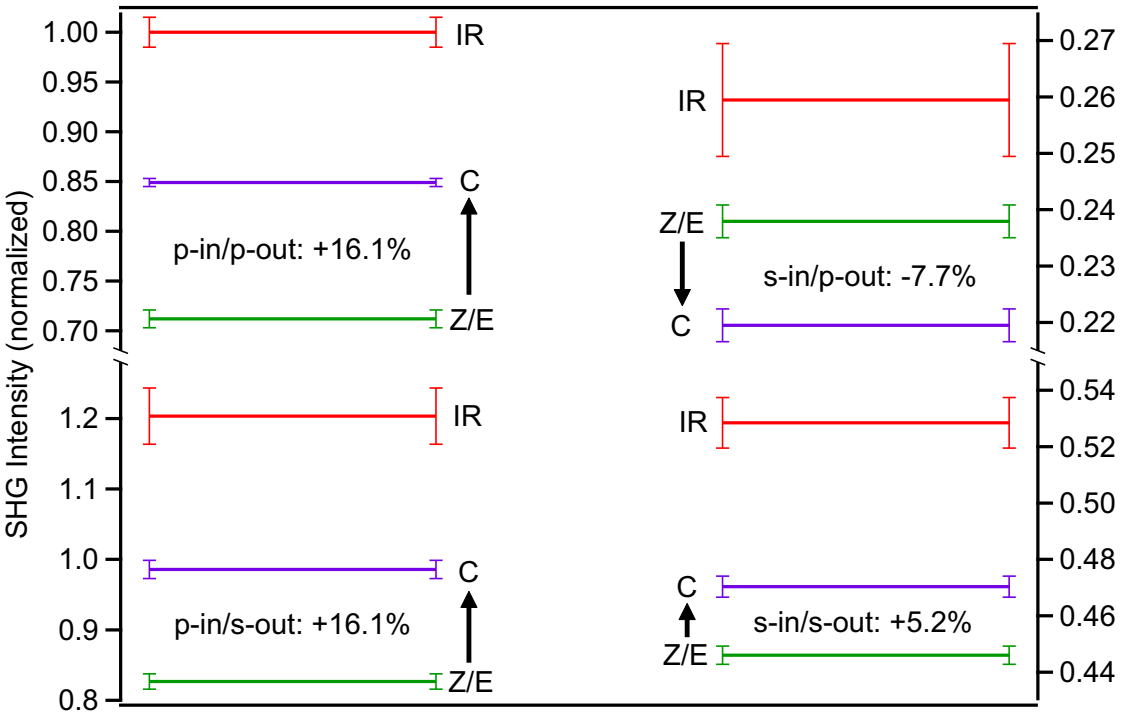

Figure 3.8: SHG signal level of the three states for different polarization combinations. All signal levels are referenced to the IR-level for p-in/p-out polarization.

parallel to the long molecular axis, at least for the closed-form. Only with the p-in/p-out combination the tensor component perpendicular to the surface is probed. The NLO level of the closed-form is highest for the combination p-in/s-out and not for p-in/p-out, which would be expected for a fully standing up configuration. Therefore a tilt of the molecules towards the surface can be assumed. A lying configuration is excluded by the fact that the s-in/s-out component is by a factor of two lower compared to the p-in/p-out component. Furthermore, the NLO contrast between the open- and the closed-form is the lowest for the s-in/s-out configuration, which means that the influence of the closed π-system is negligible compared to the signal of the other parts of the molecules. This is the case for measuring perpendicular to the π-system. In summary, the orientation of the molecules is assumed to be mostly perpendicular to the surface with a slight tilt towards the surface, which is reasonable for the molecular configuration used here.

Based on the similarity of the polarization-resolved behavior of the IR-state and the behavior of the open- and closed-form it is assumed that the signal of the IR-state is generated in the fulgimide or at the interface between the fulgimide and the phenyl ring. This is supported by the observation that the signal from the linker (including the phenyl ring) does not change during the measurements or illumination.

In summary three molecular states have been observed. Only two of the molecular states have been expected and can be assigned to the closed- and the open-form of the 2-indolylfulgimide. The origin of the third state (labeled as IR-state) remains unclear

for now and will be discussed in detail in section 3.5. It is possible to switch between all three states leading to six different switching processes. Only the open-form of the molecules is stable and both the IR-state and the closed-form decay into it at room temperature. The instability of the closed-form is unexpected and could be due to an influence of the phenyl linker. A deeper investigation of the influence of the phenyl ring is given in the next section. From the polarization-resolved measurements a rough determination of the orientation of the fulgimides on the surface has been made and the origin of the IR-state has been attributed to the fulgimide or fulgimide/phenyl interface.

3.3.3 2-Indolylfulgimide + CH_2 spacer

To investigate the influence of the phenyl ring on the stability of the 2-indolylfulgimide a CH_2 spacer was introduced (see figure 3.2d). Thereby, the influence of the π-electron system on the fulgimide should be lowered and a change in the molecular orientation of the molecules with respect to the surface is possibly introduced, too.
In figure 3.9a the influence of illumination with visible light (530 nm), UV light (365 nm), and of the SHG measurements themselves is presented. A similar behavior as for the 2-indolylfulgimide (compare figure 3.4a) was measured for the 2-indolylfulgimide with CH_2 spacer unit. The SHG signal still increases during the measurement, while the starting level depends on the before used illumination with visible or UV light (open- or closed-form). Waiting after the measurement without illumination leads to a reduction of the signal back to the signal level of the open-form on a mean timescale of 199±67 s. Despite the slightly different decay times no significant difference between the decay times dependent on the illumination used before the measurement could be detected and the process is thereby assumed to be independent of the before used illumination (see figure 3.9b). Again the process is fully reversible for at least 100 cycles. In the next step the reproducibility of the switching between the open- and the closed-form was measured. The results for switching between the open- and the closed-form 10 cycles with the signal level referenced to the IR-state are presented in figure 3.9c. For the closed-form a signal level of 79±1 % and for the open-form a signal level of 62±1 % of the level of the IR-state were measured. A NLO contrast of 22±3 % between the open- and the closed-form referenced to the closed-form, which does not significantly change for at least 10 cycles, was detected. Thus the NLO contrast between the open- and the closed-form is not strongly influenced by the CH_2 spacer unit, but the NLO contrast of the signal of IR-state in comparison to both the signal of the open- and the closed-form is increased by a factor of 1.5.
In the next step the thermal stability of the open- and closed-form was checked. Therefore the samples were brought in a defined state (open or closed), were stored for at least 16 h without illumination at room temperature and then a measurement of the resulting state was done. For both states, open and closed, no change could be detected, thus both the open- and the closed-form are stable. So reducing the influence of the phenyl ring to the fulgimide brought back the expected stability of both the open- and the closed-form [25, 38].
Based on the results on the thermal stability the cross-sections for all six photoinduced

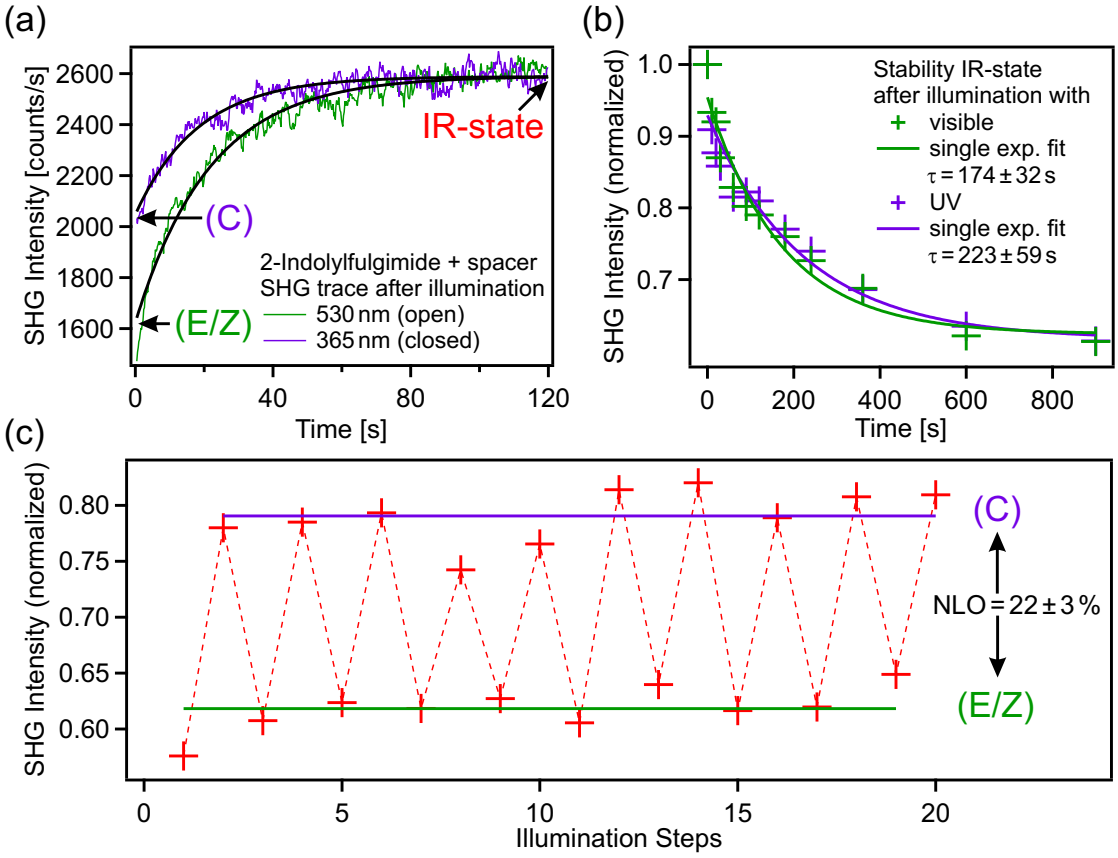

Figure 3.9: Switching of the 2-indolylfulgimide with CH_2 spacer unit. (a) Dependence of the SHG signal on illumination and SHG measurement time. (b) Thermal decay after a measurement in dependence of the before used illumination. (c) Reversible switching of the 2-indolylfulgimide layer with spacer for 10 cycles.

processes between the three states were measured. The resulting curves for the processes closed → open, open → closed, IR → open, and IR → open are presented in figure 3.10. The cross-sections for open → IR and closed → IR were calculated from the measurements shown in figure 3.9. Based on the used light intensities, the measured decay times and including the thermal decay for the switching processes including the IR-state, as discussed before in section 3.3.2, and the photon fluxes of $f_{UV} = 2.48 \cdot 10^{16}$ photons/s cm^2, $f_{VIS} = 3.97 \cdot 10^{16}$ photons/s cm^2 and $f_{IR} = 4.34 \cdot 10^{22}$ photons/s cm^2 for the corresponding illumination experiments. The following cross-sections have been calculated: $\sigma_{o\to c} = 2.0 \pm 0.7 \cdot 10^{-18}$ cm^2 for open-form → closed-form, $\sigma_{c\to o} = 1.2 \pm 0.5 \cdot 10^{-19}$ cm^2 for closed-form → open-form, $\sigma_{o\to IR} = 1.0 \pm 0.3 \cdot 10^{-24}$ cm^2 for open-form → IR-state, $\sigma_{c\to IR} = 8.9 \pm 3.2 \cdot 10^{-25}$ cm^2 for closed-form → IR-state, $\sigma_{IR\to o} = 4.0 \pm 0.5 \cdot 10^{-19}$ cm^2 for IR-state → open-form, and $\sigma_{IR\to c} = 1.4 \pm 0.2 \cdot 10^{-18}$ cm^2 for IR-state → closed-form. A summary of the discussed processes including the measured cross-sections is given in figure 3.11. In comparison to the cross-sections of the 2-indolylfulgimide without CH_2

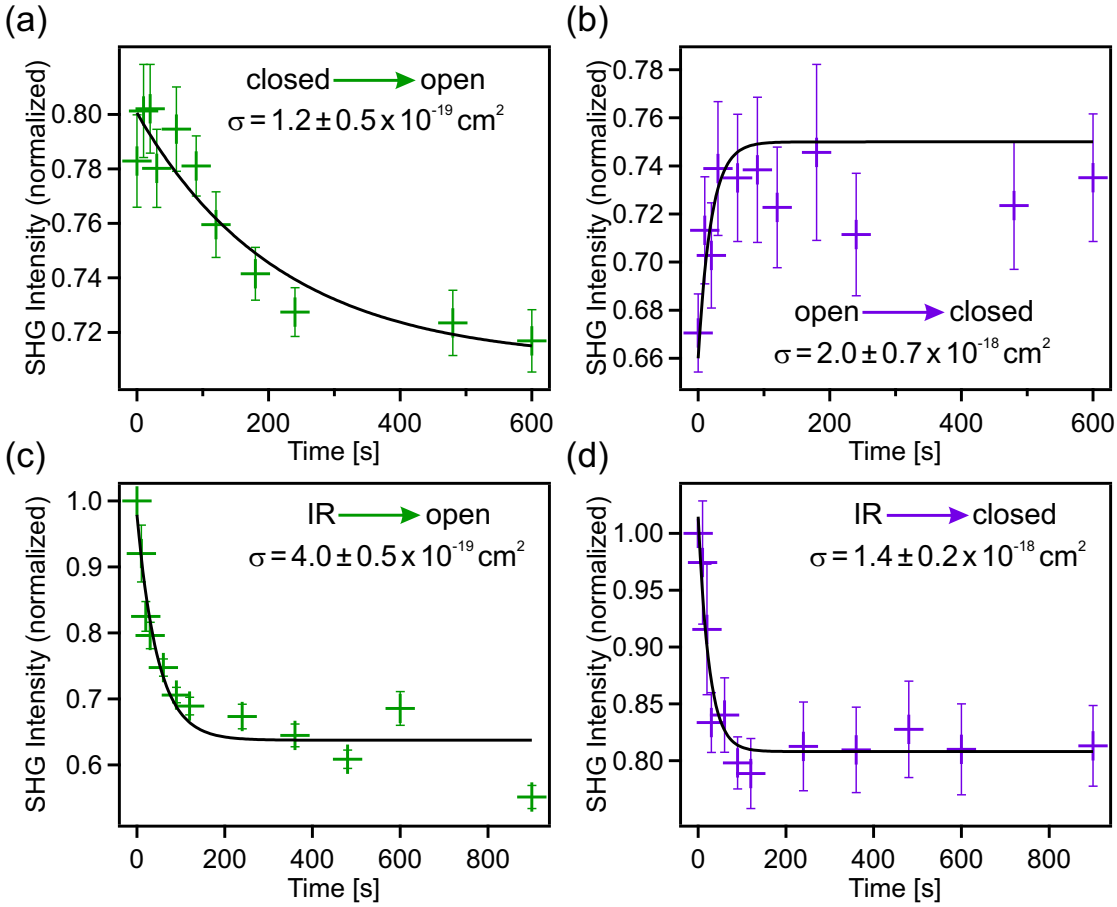

Figure 3.10: Thermal stability and cross-section measurements of the three different states of a 2-indolylfulgimide layer. (a)-(d) Determination of the cross-section of (a) the ring opening reaction, (b) the ring closure reaction, (c) the ring opening reaction coming from the IR-state, and (d) the ring closure reaction coming from the IR-state.

spacer the cross-sections with CH_2 spacer changed significantly. The cross-sections of the switching process into the open- and the closed-form increased by nearly an order of magnitude and are thereby at the same order of magnitude as expected for decoupled fulgimide molecules [37, 74], as discussed before in section 3.3.2. Thus the introduction of the CH_2 spacer led to a proper decoupling of the fulgimides. Furthermore, the cross-sections for the switching into the IR-state were reduced by nearly two orders of magnitude. Combined with the faster thermal decay (half of the thermal decay time without spacer) this can be interpreted as suppression of the process leading to the IR-state by the spacer.

In figure 3.12 the results of the polarization-resolved measurements are presented. All measured level intensities are again referenced to the IR-state for the p-in/p-out configuration. A few interesting observations can be made: (1) The IR-state has the highest signal level for all polarization combinations and the NLO contrast to the next signal

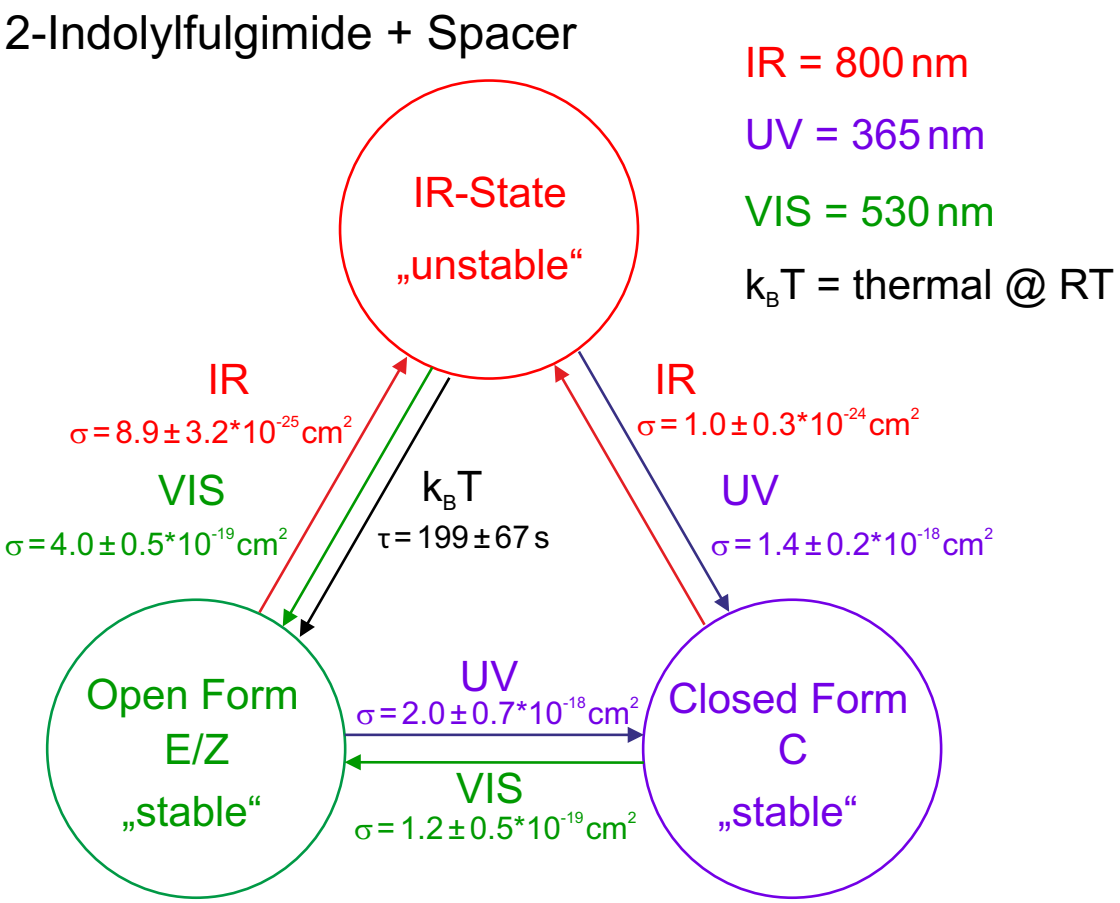

Figure 3.11: Summary of all cross-sections and thermal decays of the system 2-indolylfulgimide with spacer on silicon.

level is always rather large. (2) The highest NLO contrast between the signal level of the open- and the closed-form has been measured for the p-in/p-out combination probing the perpendicular component of the molecules. (3) For the s-in/p-out combination no significant NLO contrast between the signal of the closed- and open-form could be measured, while the signal of the IR-state can still be separated from the others. (4) Despite the highest NLO contrast the highest signal levels have not been measured for the p-in/p-out combination, but for the p-in/s-out combination and with the s-in/s-out as second largest.

Combining these observations with the results for the 2-indolylfulgimide without CH_2 spacer a clear change in the orientation of the molecules has to be considered. Especially considering the high signals for the s-in/s-out configuration do not support any standing up configuration of the molecular core of the fulgimide. This is even more supported by the low signal level of the p-in/p-out configuration compared to the p-in/s-out and the s-in/s-out configuration. Under the assumption that these changes come from the changed geometry of the fulgimide relative to the surface by the spacer unit, the position

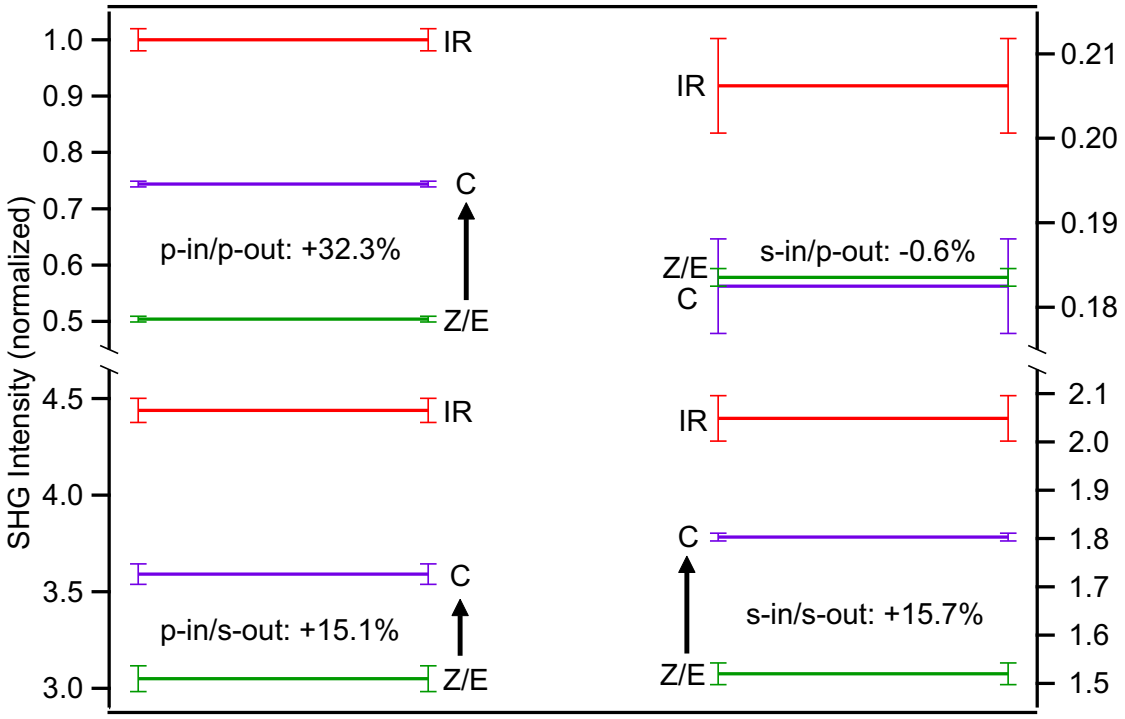

Figure 3.12: SHG signal level of the three states for different polarization combinations. All signal levels are referenced to the IR-level for p-in/p-out polarization.

of the phenyl ring compared to the surface is still the same. Based on the observation that the signal of the IR-state shifts in intensity like the open- and closed-form, the origin of the IR-state has to be located at the fulgimide and not on the phenyl part.

Summarizing the results from the 2-indolylfulgimide with CH_2 spacer the introduction of the spacer unit has led to a suppression of the IR-state leading to cross-sections of up to two orders of magnitude lower than without spacer and at the same time increasing the cross-sections for the ring opening and closure reactions. Furthermore, the closed-form became thermally stable, which is attributed to the decoupling of the fulgimide from the phenyl ring. Despite the suppression the IR-state still influences the photochromism of the fulgimides. It can still be measured, is thermally unstable, and interacts with the switching state of the fulgimides. The IR-state seems to be an additional excitation, which decays independent of the previous photochromic state of the fulgimide always into the open-form. From the polarization-resolved measurements follows a change of the orientation of the fulgimides with respect to the surface and the interpretation that the IR-state is located at the fulgimide and not the phenyl ring or alkyne linker is further proven. Additionally, a NLO contrast between the signal level of the open- and the closed-form of above 30 % could be achieved coming from only a submonolayer of fulgimide molecules, showing the strength of SHG measurements to detect ring opening/closure reactions.

3.3.4 3-Indolylfulgimide

3-indolylfulgimide samples using the alkyne linker and the phenyl ring for attachment to the linker were made (see figure 3.2c). The 3-indolylfulgimide immobilized with an amide linker on a similar prepared silicon surface (see figure 3.2a) was already investigated with SHG by Schulze *et al* [74]. For the 3-indolylfulgimide only the open- and the closed-form were detected and it was proven that both forms are thermally stable for at least 24 h. The aim of the investigations on the 3-indolylfulgimide with alkyne linker is two-fold: (1) It is possible to check if the IR-state is a 2-indolylfulgimide specific feature, and (2) the influence of the linker to the thermal stability, cross-sections and orientation of the fulgimide can be directly compared.

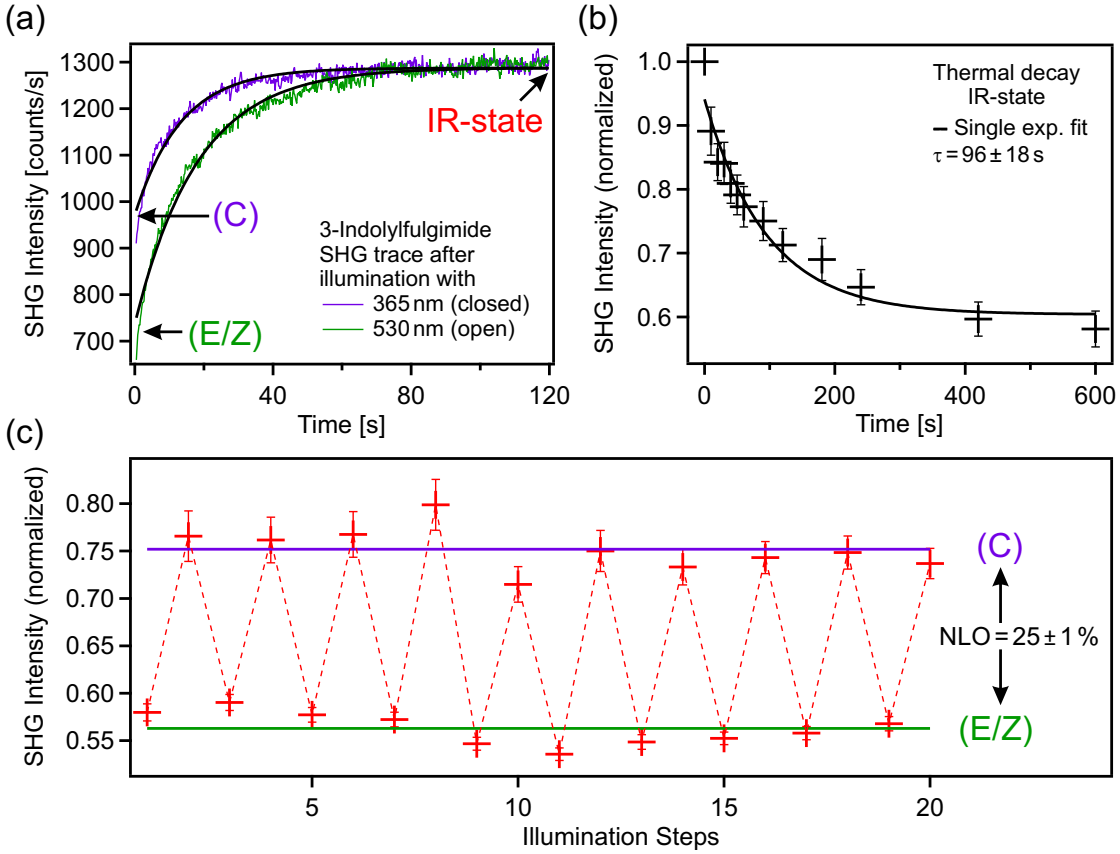

Figure 3.13: Switching of 3-indolylfulgimide. (a) Dependence of the SHG signal on illumination and measurement time. (b) Thermal decay after a measurement. (c) Reversible switching of the 3-indolylfulgimide layer for 10 cycles.

The results of SHG measurements directly after illumination with visible light (530 nm) and UV light (365 nm) are shown in figure 3.13a. As before for the 2-indolylfulgimide a change of the SHG signal with SHG measurement time and an illumination-dependent level at the beginning of the measurements was detected. Thus the 3-indolylfulgimide with alkyne linker behaves more like the 2-indolylfulgimide with alkyne linker and not

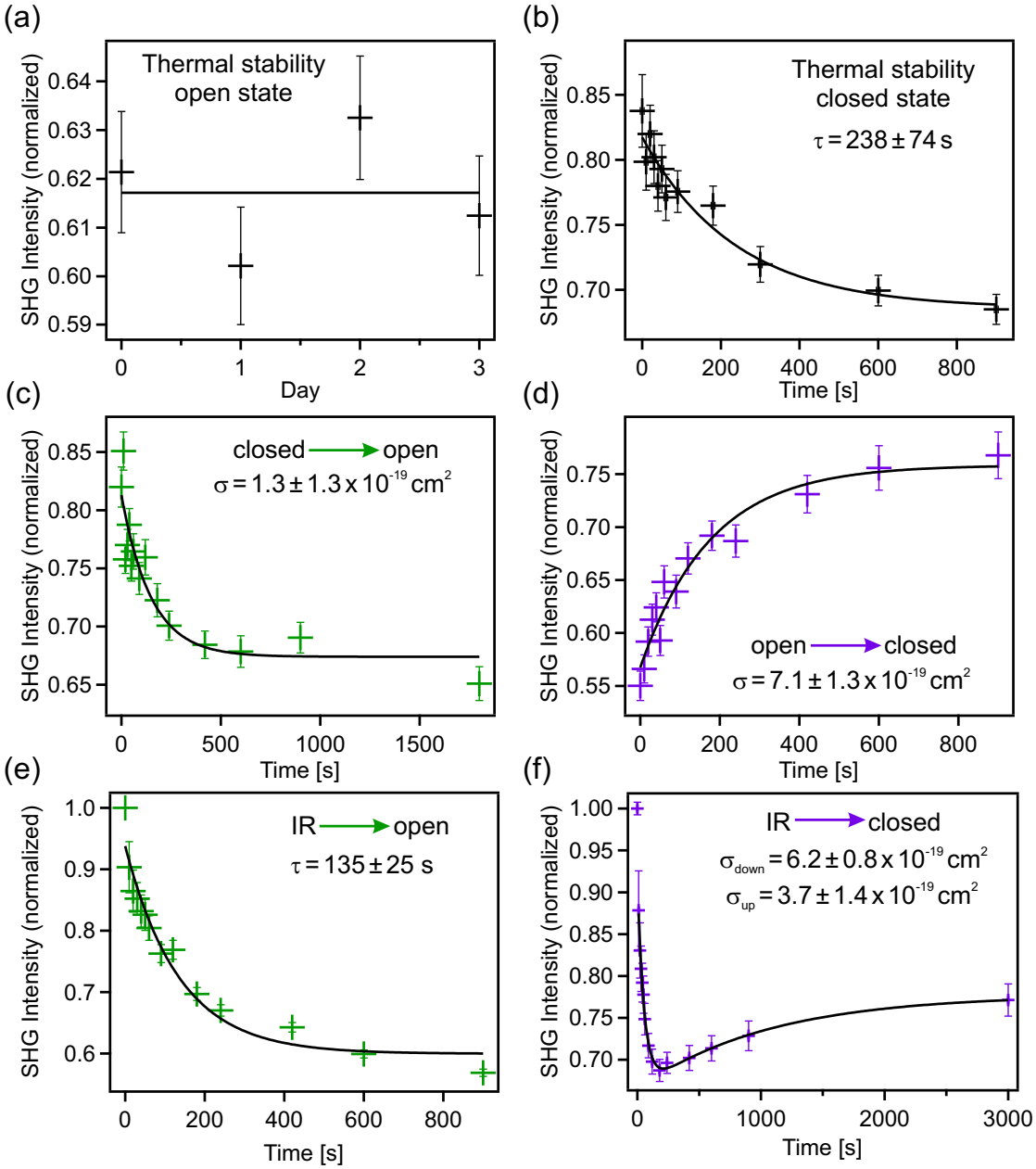

Figure 3.14: Thermal stability and cross-section measurements of the three different states of a 3-indolylfulgimide layer. (a) Thermal stability of the E/Z-state (open). Each of the data points has been measured after waiting for one day. (b) Thermal stability of the C-state (closed). (c)-(f) Determination of the cross-section of (c) the ring opening reaction, (d) the ring closure reaction, (e) the ring opening reaction coming from the IR-state, and (f) the ring closure reaction coming from the IR-state.

like the 3-indolylfulgimide with amide linker. In the next step the thermal stability of the IR-state was checked (figure 3.13b). As before the IR-state is not thermally stable and the signal decays back to the level of the open-form with a decay time of 96±18 s. This decay is four times faster than for the 2-indolylfulgimide and the IR-state seems to be less thermally stable. Again the reproducibility and NLO contrast of the switching between the open- and the closed-form were measured. The result for 10 cycles is presented in figure 3.13c. In the course of the switching a NLO contrast of 25±1 % referenced to the closed-form and no significant decay of the NLO contrast was observed. As expected a reversible and non-destructive switching of the molecules is possible.
Again the thermal stability of the open- and closed-form was investigated. For the open-form at four measurement days the sample was stored over night in the open-form and the state of the sample was checked in the morning (see figure 3.14a). All four measurements showed the signal level of the open-form. It is therefore assumed that the open-form is thermally stable. For the closed-form a decay of the signal to the signal level of the open-form on a timescale of 238±74 s was measured (see figure 3.14b), which means that the closed-form is not thermally stable. The decay time is a little shorter than for the 2-indolylfulgimide (302±31 s). Based on this observation it can be assumed that the thermal instability of the closed-form is introduced by the different linker group and not by the different fulgimide derivative.
To get a deeper understanding of the influence of the linker group and the IR-state on the switching efficiency the cross-sections of the six switching processes between the three states were measured. In figure 3.14c-f the results of these measurements are presented. For the switching between the open- and the closed-form and into the IR-state the cross-sections were calculated as in section 3.3.2 including the thermal decay of the closed-form into the open-from and based on the photon fluxes of $f_{UV} = 2.50 \cdot 10^{16}$ photons/s cm^2, $f_{VIS} = 3.23 \cdot 10^{16}$ photons/s cm^2, $f_{IR} = 1.52 \cdot 10^{23}$ photons/s cm^2. The cross-sections are $\sigma_{o\rightarrow c} = 7.1 \pm 1.3 \cdot 10^{-19}$ cm^2 for switching process open-form $\rightarrow$ closed-form, $\sigma_{c\rightarrow o} = 1.3 \pm 1.3 \cdot 10^{-19}$ cm^2 for the switching process closed-form $\rightarrow$ open-form, $\sigma_{o\rightarrow IR} = 5.9 \pm 0.2 \cdot 10^{-23}$ cm^2 for the process open-form $\rightarrow$ IR-state, and $\sigma_{c\rightarrow IR} = 7.7 \pm 0.2 \cdot 10^{-23}$ cm^2 for the process closed-form $\rightarrow$ IR-state. These cross-sections are at the same order of magnitude as for the 2-indolylfulgimide, but one order of magnitude lower than for the 3-indolylfulgimide with the amide linker ($\sigma_{o\rightarrow c} = 2.3 \pm 0.3 \cdot 10^{-18}$ cm^2 open $\rightarrow$ closed and $\sigma_{c\rightarrow o} = 1.2 \pm 0.3 \cdot 10^{-18}$ cm^2 closed $\rightarrow$ open) [74]. Thus the IR-effect could be coupled to lowering of the cross-sections of the switching between the open- and the closed-form independent of the fulgimide derivative. A detailed comparison and discussion of the cross-sections for the different systems is given in section 3.5.
For the processes IR $\rightarrow$ open and IR $\rightarrow$ closed the determination of the cross-sections under illumination was complicated. From figure 3.14e a decay time under illumination with visible light for the IR-state into the open-form of 135±25 s was measured. In comparison to the 96±18 s, which were measured without illumination, no lowering of the transfer time due to the illumination could be detected. The measured transfer time under illumination is even higher than for no illumination, but not significantly. Thus no influence of the illumination on the decay process is assumed and an influence

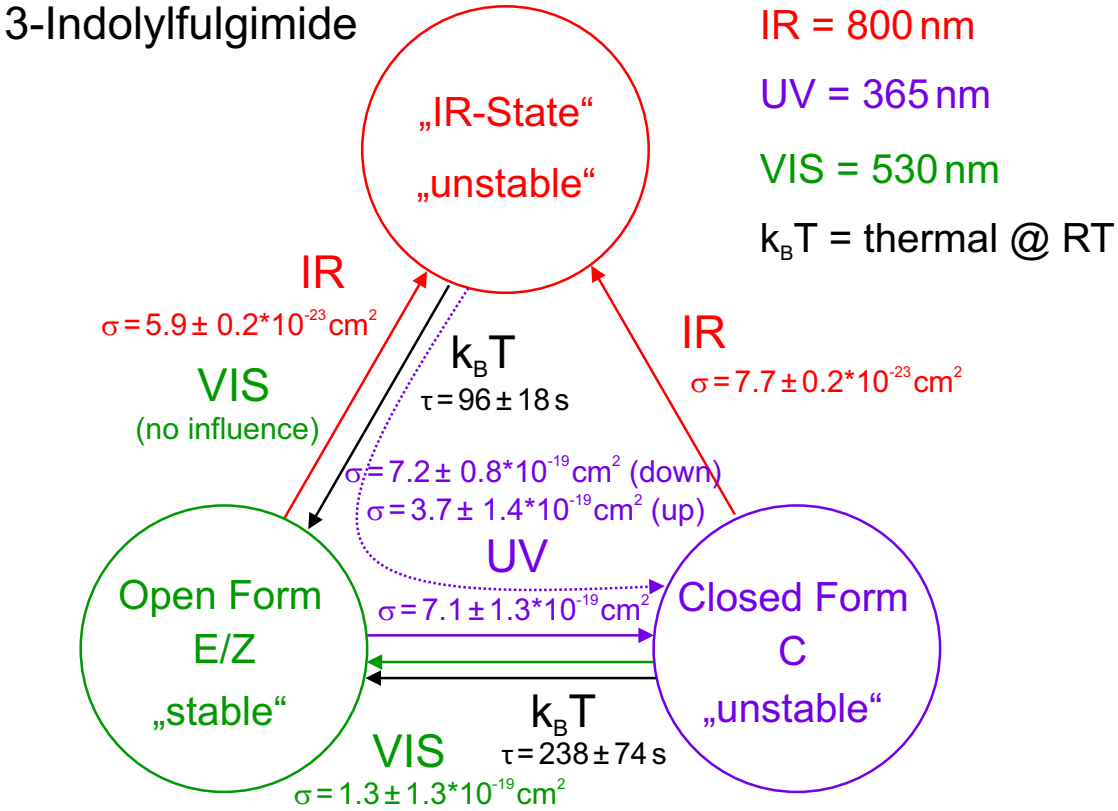

Figure 3.15: Summary of all cross-sections and thermal decays of the system 3-indolylfulgimide on silicon.

of the illumination is neglected. Therefore no cross-section for the process IR → open could be determined. For the process IR → closed the behavior becomes more complex. The result is presented in figure 3.14f. Here a decay of the signal to a level below the closed-form followed by a rise of the signal to the signal level of the closed-form was detected. In contrast to both 2-indolylfulgimide systems it does not seem possible to switch directly into the closed-form coming from the IR-state with UV light. To model such a two-step process the signal trace was modeled with a two-step first-order kinetic model assuming a transfer from the IR-state into the open-form followed by an switching from the open-from into the closed-form. In contrast to the illumination with visible light the illumination with UV light has an influence on the initial decay of the signal describing the decay of the IR-state into the open-form. A decay time of 53±5 s, which is significantly smaller than the 96±18 s for the thermal decay, was extracted by the model. Based on the time measured under illumination and the thermal decay time a cross-section of $\sigma_{down} = 6.2 \pm 0.8 \cdot 10^{-19}\,\mathrm{cm}^2$ for the signal lowering was determined. For the signal increase a cross-section of $\sigma_{up} = 3.7 \pm 1.4 \cdot 10^{-19}\,\mathrm{cm}^2$ was calculated including the thermal decay of the closed-form into the open-form. This cross-sections is lower compared to the cross-section of $\sigma_{o\to c} = 7.1 \pm 1.3 \cdot 10^{-19}\,\mathrm{cm}^2$ measured for the pure

switching process between the open- and the closed-form. Based on this observations it is assumed that there is a difference between the IR-state of the 3-indolylfulgimide compared to the IR-state in the 2-indolylfulgimide. A discussion of the phenomenon will be given in section 3.5. The results presented above are summarized in figure 3.15.
In the last step polarization-dependent SHG measurements of the level of the three molecular states were done. The results of these measurements are presented in figure 3.16. For the 3-indolylfulgimide the following observations were made: (1) The signal level of the IR-state scales with the signal levels of the open- and closed-form. (2) The closed-form signal level is above the open-form signal level for all polarization combinations. (3) The NLO contrast between all levels is similar for all polarizations. (4) The signal is the highest for the p-in/p-out combination and more than one order of magnitude lower for the s-in/s-out combination.

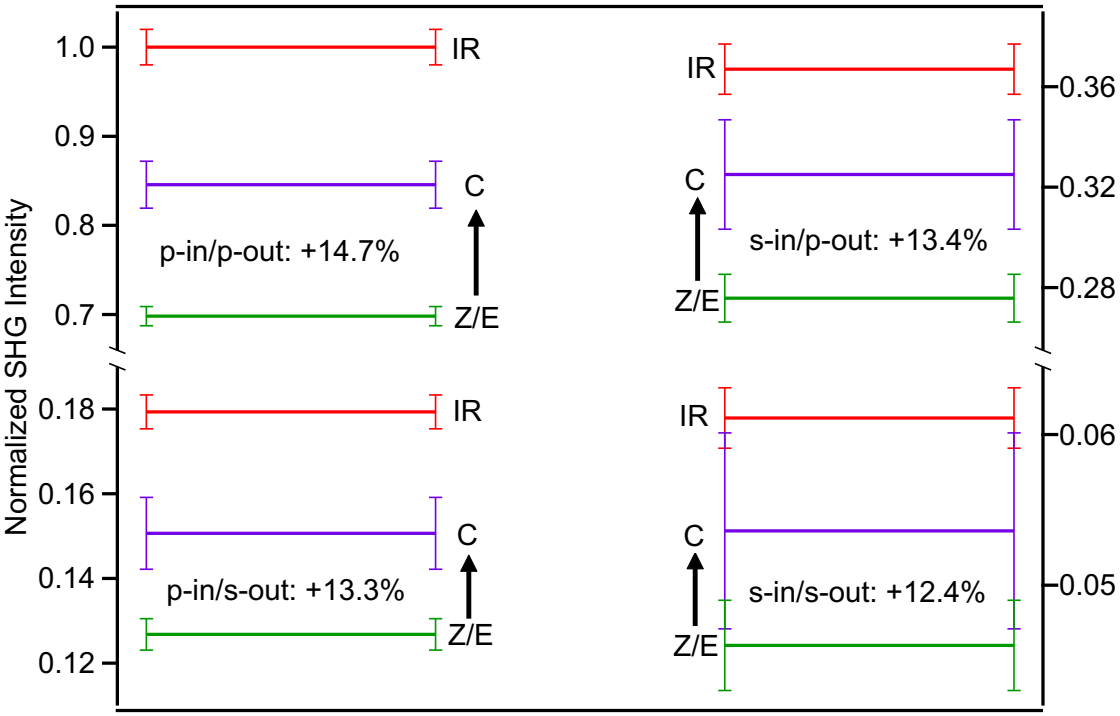

Figure 3.16: SHG signal level of the three states for different polarization combinations. All signal levels are referenced to the IR-level for p-in/p-out polarization.

Based on the observation that the highest signal level was measured for p-in/p-out and the assumption that the main contribution of the SHG signal is generated by the delocalized π-electron systems, the conclusion can be drawn that the molecules are oriented mainly perpendicular to the surface. The assumption of mainly standing molecules is further supported by the very low signal level for the s-in/s-out combination. Despite the large variance in the signal level for the different polarization combinations the NLO contrast between the open- and closed-form is very similar for all combinations. In contrast to the differences in the switching behavior between the IR-state and the open-

and closed-form, the IR-state still has the same polarization dependence as the open- and closed-form, which supports the interpretation that the IR-state is located at the fulgimide molecule.
In summary, for the 3-indolylfulgimide with alkyne linker three states (IR, open, closed) were measured. As for the 2-indolylfulgimide only the open-form is thermally stable and the two other forms decay thermally into the open-form. Thus the IR-state is not specific to the 2-indolylfulgimide, but rather due to an interaction of the fulgimide with the new phenyl linker. Compared to the same 3-indolylfulgimide immobilized by an amide linker the cross-sections of the switching between the open- and closed-form are reduced by up to one order of magnitude. Similar cross-sections have been measured for the 2-indolylfulgimide with the alkyne linker. The orientation of the 3-indolylfulgimide seems to be more upright than the 2-indolylfulgimide and similar to the 3-indolylfulgimide with amide linker.

3.4 Comparison with simulations

To get a deeper understanding and to quantify the observations of the experimental work DFT calculations of all systems discussed in this thesis were performed by Clemens Rietze in the group of Prof. Peter Saalfrank at the Institut für Chemie at the Universität Potsdam.
As a first step a structure optimization of the full system of the fulgimide including the alkyne linker was done with hybrid-DFT based on the B3LYP/6-31G* level. The alkyne linker was reduced to a C_2H_5 to reduce calculating time. It was shown before that the influence of a longer alkin chain has only vanishing influence to aromatic systems [109]. To calculate the thermal transfer rates potential surfaces were scanned with locked degrees of freedom of the alkyne linker. For the E-/Z-isomerization the diederangle and for the ring opening reaction (C-form to E-form) the C-C distance was scanned. The resulting guess were used for the QST3-calculation. For the hyperpolarization of the optimized gas phase structures the 6-311++G** basis set was used as a foundation. The basis set includes the polarization functions for all atoms and diffuse functions. The hyperpolarization was calculated both with Hartree-Fock level (coupled perturbed HF) and Møller-Plesset perturbation theory (MP2 level) with the GAUSSIAN09 program package [110]. Due to high computational costs the dynamic (frequency dependent) hyperpolarizations $\beta_{ijk}(-2\omega;\omega;\omega)$ were calculated based on the static ones by the method of Champagne [111, 112]. The frequency-dependent calculations were done with a frequency of $\omega = \frac{c}{2\pi\lambda}$ with $\lambda = 800\,\mathrm{nm}$ corresponding to the laser wavelength used in the SHG experiments.

3.4.1 Thermal stability

For all three systems a thermodynamic analysis was done. Comparing the free enthalpy of the different photochromic states of the molecules shows that the E-form is the stablest form independent of the fulgimide or spacer (see table 3.1). Furthermore, only a small difference between the energetic level of the two open-forms was observed. In

Table 3.1: Energetic differences between the different photochromic forms of the fulgimide samples (calculations were performed by Clemens Rietze, in the group of Peter Saalfrank, Universität Potsdam).

Sample	ΔG(C-Z) [eV]	ΔG(C-E) [eV]	ΔG(Z-E) [eV]
2-indolylfulgimide	0.21	0.25	0.05
3-indolylfulgimide	0.16	0.21	0.05
2-indolylfulgimide + Spacer	0.24	0.27	0.02

addition to the free enthalpy the excitation energies of the different forms were calculated. The energetic barrier of the C-form is for all molecules around 1.6 eV. For the 2-indolylfulgimide a value of 1.57 eV, for the 3-indolylfulgimide a value of 1.64 eV, and for the 2-indolylfulgimide with spacer a value of 1.60 eV has been calculated. Thus the observed thermal instability of the C-form can not be explained by the simulations. Furthermore, the stabilization of the C-form due to the spacer and the therefore large influence of the spacer can not be verified by the simulations. Only the E-form as the energetically stablest form is confirmed.

3.4.2 Molecular orientation and hyperpolarizations

To increase the understanding of the polarization-resolved measurements the first order hyperpolarizability β, which corresponds to the second order susceptibility $\chi^{(2)}$ on a molecular level, was calculated. Based on the tensor elements β_{ijk} the hyperpolarizability vector $\tilde{\beta} = (\tilde{\beta}_x, \tilde{\beta}_y, \tilde{\beta}_z)$ was calculated by:

$$\tilde{\beta}_i = \beta_{iii} + \frac{1}{3}\sum_{j\neq i}(\beta_{ijj} + \beta_{jij} + \beta jji) \tag{3.4}$$

From the hyperpolarizability vector the mean hyperpolarizability of the molecules was calculated by:

$$\tilde{\beta}_0 = \sqrt{(\tilde{\beta}_x^2 + \tilde{\beta}_y^2 + \tilde{\beta}_z^2)} \tag{3.5}$$

Finally an asymmetry value a to compare the perpendicular component and the parallel component of the hyperpolarizability vector in regard to the surface was calculated:

$$a = \left|\frac{\tilde{\beta}_z}{\tilde{\beta}_{xy}}\right| \text{ with } \tilde{\beta}_{xy} = \frac{1}{\sqrt{2}}\sqrt{\tilde{\beta}_x^2 + \tilde{\beta}_y^2} \tag{3.6}$$

The results of the simulations are summarized in table 3.2. Based on the calculations an attribution of the polarization-resolved measurements could be done. Comparing the calculated results with the measured SHG intensities a few conclusions can be drawn.

Table 3.2: Dynamical hyperpolarization parameter for $\lambda = 800\,\mathrm{nm}$ calculated on MP2-level. All value are given in atomic units (calculations have been performed by Clemens Rietze, in the group of Peter Saalfrank, Universität Potsdam).

Parameter	C-form	E-form	Z-form
	2-indolylfulgimide		
$\tilde{\beta}_x$	-5281.28	1147.46	-16005.91
$\tilde{\beta}_y$	-4552.29	908.04	-14479.16
$\tilde{\beta}_z$	-23105.54	-3281.10	-17856.71
β_0	24134.65	3592.61	28012.45
a	4.69	3.17	1.17
	3-indolylfulgimide		
$\tilde{\beta}_x$	-13115.57	7707.18	1446.58
$\tilde{\beta}_y$	-25746.71	-2125.57	-598.70
$\tilde{\beta}_z$	-63228.99	-1060.30	1147.02
β_0	69518.46	8064.92	1940.79
a	3.09	0.19	1.04
	2-indolylfulgimide + Spacer		
$\tilde{\beta}_x$	4571.26	-615.42	-17320.99
$\tilde{\beta}_y$	-4086.70	-4449.59	-4943.58
$\tilde{\beta}_z$	1488.73	-6195.56	461.16
β_0	6309.82	7652.62	18018.56
a	0.34	1.95	0.03

First of all the attribution of the higher SHG signal level induced by UV illumination to the closed-form is confirmed by the simulations, which show significant higher hyperpolarizabilities for the C-form in comparison to the E-form. The higher hyperpolarizability of the C-form in comparison to the E-form can be explained by the conjugated π-system and therefore high delocalization of electrons, which is created by the ring-closure reaction [38, 39]. For the 2-indolylfulgimide with spacer the hyperpolarizabilites for the C- and E-form are similar. This can be explained by a large rotation of the molecule due to the CH_2 spacer leading to a orientation of the π-system mostly parallel to the surface and thereby suppressing the high change in hyperpolarizability in z-direction. Comparing the x- and y-components of the C-form with the E-form still results in a higher hyperolarizability of the C-form compared to the E-form.

Secondly a comparison of the relative amplitude of the z-component compared to the x- and y-components with the polarization-resolved measurements reveals a large consistency. It can be assumed that with the p-in/p-out measurement mostly the z-component

and with the s-in/s-out measurement mostly the x- and y-components are probed. While the mixed polarization combinations probe mixtures of these components. Thus by comparing the simulated hyperpolarizabilities and the SHG signal levels a rough estimate of the molecular orientation can be done. For the 3-indolylfulgimide the highest signal levels were measured for p-in/p-out polarization with nearly 3 times more count rate than for any other combination. Furthermore, the signal of the s-in/s-out combination is largely suppressed (under 10 % of the signal level of p-in/p-out). This result is mirrored by the hyperpolarizations calculated for the C-form. Thus a orientation of the delocalized π-electron system in the closed-form perpendicular to the surface as calculated by the simulations can be confirmed. This result is similar to the results of Schulze for the 3-indolylfulgimide with amid linker [74]. Thus the change of the linker molecule did not change the orientation of the molecules significantly. Going to the 2-indolylfulgimide the orientation of the π-system changes. While the simulated hyperpolarizations for the C-form show a similar behavior to the polarizations of the 3-indolylfulgimide in the polarization-resolved SHG measurements slight differences can be observed. The signal of the p-in/p-out combination is only a factor of two larger than the s-in/s-out combination and instead of the p-in/p-out combination the p-in/s-out combination is the largest by roughly 20 % of the p-in/p-out signal. It is therefore assumed that the delocalized π-electron system and with it the fulgimide is tilted out of a fully perpendicular orientation, but still the major contribution is perpendicular to the surface. Finally in the simulations the spacer unit introduces a large tilt of the molecules to a nearly parallel orientation. This can be confirmed by the SHG measurements, because here the s-in/s-out combination showed more than two times the signal of the p-in/p-out combination, while the dominant contribution has been measured for p-in/s-out. Thus the relation between the perpendicular and the parallel component are is inversed compared to the system without spacer.

3.5 Discussion

Three different systems based on fulgimide derivatives were investigated. In all three systems the fulgimides were immobilized by an alkyne linker on a H-terminated silicon surface. Two 2-indolylfulgimide samples were created by attaching the fulgimide to the alkyne with a phenyl ring. In one of the samples a CH_2 spacer was introduced to decouple the two parts from each other. The third sample was made of a 3-indolylfulgimide attached by a phenyl ring to the alkyne linker. For comparison the results measured by Michael Schulze on the similarly prepared 3-indolylfulgimide immobilized by an amide linker are used [73, 74]. The main results including thermal stabilities and cross-sections are summarized in table 3.3.

All systems incorporating the phenyl ring and alkyne linker show three different signal levels while two of the levels can be assigned to the open- and closed-form of the fulgimide molecules, the third level, introduced by high intensity IR-light, is unexpected. Using the amide linker does not lead to such a third level as shown on the 3-indolylfulgimide [74]. Investigations on the surface with only the alkyne linker and with the phenyl ring

Table 3.3: Summary of the main results of all fulgimide samples of this work and the sample investigated by Schulze *et al.* [74].

	2-indolylfulgimide (alkyne linker)	2-indolylfulgimide (alkyne linker + CH_2 spacer)	3-indolylfulgimide (alkyne linker)	3-indolylfulgimide (amide linker)
General behaviour	3 SHG intensities (open/closed/IR-state)	3 SHG intensities (open/closed/IR-state)	3 SHG intensities (open/closed/IR-state)	2 SHG intensities (open/closed)
NLO contrast (open $\leftrightarrow$ closed)	$20 \pm 1\,\%$	$22 \pm 3\,\%$	$25 \pm 1\,\%$	$17 \pm 6\,\%$
Thermally stable	open-form	open- and closed-form	open-form	open- and closed-form
Thermal decay	$\tau_{IR\to o} = 424 \pm 30\,\mathrm{s}$ $\tau_{c\to o} = 302 \pm 30\,\mathrm{s}$	$\tau_{IR\to o} = 199 \pm 67\,\mathrm{s}$	$\tau_{IR\to o} = 96 \pm 18\,\mathrm{s}$ $\tau_{c\to o} = 238 \pm 74\,\mathrm{s}$	
Cross-sections:				
$\sigma_{o\to c}$	$3.4 \pm 0.6 \cdot 10^{-19}\,\mathrm{cm}^2$	$2.0 \pm 0.7 \cdot 10^{-18}\,\mathrm{cm}^2$	$7.1 \pm 1.3 \cdot 10^{-19}\,\mathrm{cm}^2$	$2.3 \pm 0.3 \cdot 10^{-18}\,\mathrm{cm}^2$
$\sigma_{c\to o}$	$4.2 \pm 0.5 \cdot 10^{-20}\,\mathrm{cm}^2$	$1.2 \pm 0.5 \cdot 10^{-19}\,\mathrm{cm}^2$	$1.3 \pm 1.3 \cdot 10^{-19}\,\mathrm{cm}^2$	$1.2 \pm 0.3 \cdot 10^{-18}\,\mathrm{cm}^2$
$\sigma_{o\to IR}$	$3.0 \pm 0.3 \cdot 10^{-23}\,\mathrm{cm}^2$	$1.0 \pm 0.3 \cdot 10^{-24}\,\mathrm{cm}^2$	$5.9 \pm 0.2 \cdot 10^{-23}\,\mathrm{cm}^2$	
$\sigma_{c\to IR}$	$5.6 \pm 0.8 \cdot 10^{-23}\,\mathrm{cm}^2$	$8.9 \pm 3.2 \cdot 10^{-25}\,\mathrm{cm}^2$	$7.7 \pm 0.2 \cdot 10^{-23}\,\mathrm{cm}^2$	
$\sigma_{IR\to o}$	$1.5 \pm 0.3 \cdot 10^{-19}\,\mathrm{cm}^2$	$4.0 \pm 0.5 \cdot 10^{-19}\,\mathrm{cm}^2$	no influence of illum.	
$\sigma_{IR\to c}$	$1.9 \pm 0.3 \cdot 10^{-19}\,\mathrm{cm}^2$	$1.4 \pm 0.2 \cdot 10^{-18}\,\mathrm{cm}^2$	down: $6.2 \pm 0.8 \cdot 10^{-19}\,\mathrm{cm}^2$ up: $3.7 \pm 1.4 \cdot 10^{-19}\,\mathrm{cm}^2$	

attached to the alkyne linker did not show any IR-light dependence. Therefore it is assumed that the origin of the IR-state lies in the interaction between the fulgimide and the phenyl ring. From the polarization-resolved measurements a strong correlation of the signal of the IR-state with the signals of the other two states was observed. Despite the significantly different polarization behavior of the three systems the IR-state always shows the same polarization-resolved behavior as the open- and closed-form, even for the tilted 2-indolylfulgimide with CH_2 spacer. It can therefore be assumed that the effect is localized on the fulgimide and not on the phenyl ring, which should be orientated similar for all investigated systems.
In the case of the direct attachment to the phenyl ring, independent of the fulgimide derivative, only the open-form of the molecules were stable. This is highly unexpected for fulgimide derivatives, because usually both the open- and the closed-form are highly stable to thermal influences [38, 94, 105, 106]. Decoupling of the fulgimide from the phenyl ring, as it was done with the CH_2 spacer, brought the thermal stability of the closed-form back. Comparing the fulgimide attached with the amide linker, where both open- and closed-form are thermally stable, leads to the conclusion that the phenyl ring with its π-electron system destabilizes the closed-form of the fulgimides. A general destabilization of the switching states should result in molecules switching to the open-form, which is globally the energetically lower lying level [24, 77]. This is supported by the simulations, which also assign the global minimum to the open-form, but the lowered barrier is not mirrored in the calculations.
Comparing the cross-sections for the different systems and processes three observations are important for the further interpretation: (1) The cross-section to switch into the IR-state are at the order of $10^{-23}\,\mathrm{cm}^2$, while the cross-sections of the ring opening and closure reaction are in the order of magnitude of $10^{-19}\,\mathrm{cm}^2$, independent of the fulgimide derivative. (2) The cross-sections of the switching process between the open- and the closed-form are increased by an order of magnitude for the 2-indolylfulgimide by introducing the spacer and for the 3-indolylfulgimide by changing the linker. So in both cases reducing/removing the influence of the phenyl ring increased the switching cross-section. Furthermore, in the case of the 2-indolylfulgimide the spacer reduced the cross-sections for switching into the IR-state by over one order of magnitude. (3) The thermal stability of the IR-state depends largely on the incorporated fulgimide and the decay time has been reduced by a factor of two by introducing the spacer unit for the same fulgimide. For comparison, the measured decay times of the IR-state are: $\tau_{IR} = 424 \pm 30\,\mathrm{s}$ for the 2-indolylfulgimide, $\tau_{IR} = 199 \pm 67\,\mathrm{s}$ for the 2-indolylfulgimide with spacer, and $\tau_{IR} = 96 \pm 18\,\mathrm{s}$ for the 3-indolylfulgimide. While the thermal decay time for the closed-form of the fulgimides is more similar: $\tau_c = 302 \pm 31\,\mathrm{s}$ for the 2-indolylfulgimide versus $\tau_c = 238 \pm 74\,\mathrm{s}$ for the 3-indolylfulgimide.
Combining the above results a strong influence of the phenyl ring on the functionality of the fulgimide has been observed. It seems to destabilizes the otherwise thermally stable closed-form of the fulgimides and is most likely involved in the creation of the new IR-state. A reduction of the influence of the phenyl ring to the fulgimide led to a system were the IR-state is still created in a more destabilized form, while the thermal stability of the closed-form is not destroyed.

The nature of the IR-state is still unclear. From the measurements it is clear that it overwrites the information of the open- and closed-form, because after switching into the IR-state the systems decays back into the signal level of the open-form independent of the before used illumination. Especially for the 2-indolylfulgimide with spacer unit, where the closed-form is thermally stable, the influence of the molecular state before switching into the IR-state to the decay of the IR-state was explicitly tested. For the 3-indolylfulgimide the switching from the IR-state directly to the closed-form seems to be not possible, because the signal curve goes below the signal level of the closed-form and then up again. This behavior could also be expected for the independent process of thermal decay into the open-form and a much slower switching into the closed-form. Even more for the 3-indolylfulgimide no influence of the illumination with UV or visible light to the decay could be measured, while for both 2-indolylfulgimide setups the decay of the IR-state has been significantly altered by the illumination. Therefore the IR-state seems to depend on the molecular species (2- or 3-indolylfulgimide) and to interact with the open- and closed-form. It seems not to be a superposition of the SHG signal to the signal of the open- or closed-form. There are some noteworthy possibilities of processes, which could be the reason for the IR-state.
One possible explanation could be the up to now neglected Z-form of the fulgimides. Usually only a low amount of molecules are in the Z-form, because the illumination wavelength for the switching processes between the two forms are similar and only the E-form can be transfered to the C-form and back. Therefore under UV illumination an equilibrium between the E- and Z-form is created, which is depopulated via the E-form to the C-form, where the back process to the E-form is not driven by UV light. Illumination with visible light switches the C-form only to the E-form leading to high populations of E-form molecules. In the end in neither case the Z-form is populated with a significant amount of molecules. Using polar solvents can shift the absorption peaks of all forms, especially a shift of the peak maxima of the Z-form compared to the E-form can be created. Assuming a different peak maximum for the Z-form compared to the E-form induced by the electron donating phenyl group and a two photon process of the IR-photons leading to an energy transfer corresponding to 400 nm, while the illumination with the diode has been at 365 nm, could explain the switching into the Z-form by the IR-light. This interpretation is supported by the low cross-sections for the switching processes with IR-light, which are up to six orders of magnitude lower than their counterparts with UV or visible light. Furthermore, the assignment of the IR-state to the Z-form would explain why in all three samples the thermal decay of the IR-state goes directly to the E-form, even coming from the C-form before. Strictly against the interpretation of the IR-state as Z-form of the fulgimides are standing the observed switching procedures and differences in the cross-sections for switching with IR-light. With the interpretation of the IR-state as Z-form the illumination with visible light should not have any influence to the fulgimides. This could only be verified for the 3-indolylfulgimide for both 2-indolylfulgimide systems a significant increase in the transfer time from the IR-state to the E-form has been measured. Furthermore, a seemingly direct switching with UV light to the C-form has been observed for the 2-indolylfulgimides. Comparing the cross-sections for the processes E-form to IR-state

and C-form to IR-state for both the 2- and the 3-indolylfulgimide the cross-section for the switching into the IR-state coming from the C-form is higher than for coming from the E-form. This speaks against the interpretation of the IR-state as Z-form, because for the switching process from the C-form to the Z-form the molecules must first brought to the E-form and then to the Z-form, which is in direct contrast to the measured cross-sections. Furthermore, the process C-form to E-form should not be driven by UV light at all. Even considering the thermal decay of the C-form into the E-form and then a switching of the E- to the Z-form can not be supported by the measured values. All in all the assignment of the IR-state to the Z-form seems to be reasonable at the first glance, but based on the measured processes and their cross-sections it can be definitely excluded.
For the very similar species of fulgides the dependence of the switching process between the E- and C-form in different solvents led to the assumption of a polar excited state of the fulgides [25]. In the polar-form a positive charge accumulation takes places at the nitrogen atom and a corresponding negative charge accumulation on the opposite oxygen atom. Polar solvents stabilize this excited polar-form in fulgides and fulgimides, which leads to a reduced quantum yield of the reactions [24, 25, 87]. Considering the electron donating nature of the phenyl [113] ring located in close vicinity of the oxygen, which is negatively charged in the polar-form, a stabilization of the negative charge can be assumed. Based on these considerations an excited state with a high dipole moment stabilized by the phenyl ring could be assumed and the IR-state could be attributed to the polar-form. In this case most of the measured results could be explained. First of all it would be possible to switch between all three forms (E-form, C-form, polar-form) directly. Secondly the polar-form would overwrite the information of the previous state. For both fulgimides the thermal decay channel is into the open-form. Thirdly the higher stability of the polar-form of the 2-indolylfulgimide compared to the 3-indolylfulgimide could be explained by the different molecular orientation, which favors the polar-form for the 2-indolylfulgimide. Fourthly the lowered stability of the IR-form introduced by the spacer could be explained by the lowered influence of the phenyl ring, which stabilizes the polar-form. Finally the high NLO contrast for the IR-state would fit very well, because the induced dipole would lead to a significant increase of the SHG signal. Based on the low cross-sections for switching into the polar-form, it can be explained either by the very low absorbance of the fulgimides at 800 nm or the switching process is driven by a two photon process corresponding to an excitation of 400 nm. Against this interpretation stands the usually ultrashort decay time (a few picoseconds) of the intermediate states in the switching process of fulgimides [24, 87]. Increasing the decay time by 12 orders of magnitude by introducing the phenyl ring has to be considered as physically unrealistic. In comparison switching fulgides in polar solvents compared to non-polar solvents has led to an increase by a factor of 2 [25].
Based on the considerations above a clear assignment of the IR-state is difficult. From the comparison of the 3-indolylfulgimide with amide and alkyne linker the IR-state has to be based on the interaction with the phenyl ring and fundamentally influences the fulgimide. From a fundamental point of view an explanation of this effect and the creation of a new state in the fulgimide system could lead to a greater understanding

of the photo-physics, which could lead to new applications of such a system. For the further application of fulgimides as photo-switchable surface layer the influence of the anchor group has to be considered.
Independently of the IR-state and the influence of the phenyl ring SHG has been proven to be a powerful tool to investigate sub-monolayer coverages of functional molecules. Due to the high surface/interface sensitivity of the SHG method the fulgimide molecules are the main signal origin and over 30 % of the signal change of the total signal amplitude could be achieved by switching between the open- and closed-form. Furthermore, compared to other systems very high cross-sections in the range of 10^{-19} - $10^{-18}\,\mathrm{cm}^2$ could be achieved. Compared to most of the experiments on fulgimides in our case they have been immobilized on a silicon surface. In regard of a possible application for data storage, spatially resolved sensory or for photo-reactive materials the immobilization of full functional molecules is an important step towards the application. Combining two laser beams even high 3-dimensional resolution based on SHG could be imagined.

4 Ultrafast Excited State Dynamics in Organic Thin Films

Understanding the ultrafast electronically excited state dynamics in organic semiconductors after optical excitation is crucial for the optimization of organic optoelectronic devices [7, 41]. For instance, in organic solar cells formation of charge transfer states and the separation of charges is a key component for efficiency [7]. Competing relaxation pathways can highly suppress the efficient charge separation. Ultrafast energy transfer to self-trapping sates for example has been reported to occur on similar time scales as charge transport [51, 52]. Therefore, investigations of the ultrafast dynamics in organic thin films are important for the understanding of decay mechanisms and optimization of the films.

This chapter presents, and then discusses the results of the ultrafast pump/probe experiments on the two different organic semiconductors diindenoperylene (DIP) (structure see figure 4.2) and n,n'-bis-(2-ethylhexyl)-1,7-dicyanoperylene-3,4:9,10-bis(dicarboximide) (PDIR-CN_2) (structure see figure 4.11). Possible electronically excited states at the interface in a bilayer configuration are also examined.
After an overview over the dynamics of optically excited states, their decay mechanisms, and their role in organic solar cells given in section 4.1, the preparation of the samples is presented in section 4.2.
Section 4.3 poses a presentation and discussion of the results of the measurements on thin DIP layers on sapphire and silicon. On sapphire, two different kinds of DIP films were created by changing the substrate temperature during film preparation (see section 4.2). The DIP film evaporated on a cold sapphire substrate is marked in this thesis as DIP (LT). The intrinsic excited state dynamics in DIP were investigated on sapphire and the influence of trap states at the interface on the dynamics were investigated on silicon oxide in direct comparison to the results on sapphire.
In section 4.4 the results of the ultrafast TR-SHG investigations on thin PDIR-CN_2 films on sapphire are discussed. On all samples, especially on the pure PDIR-CN_2 sample, it was possible to resolve signal oscillations in the TR-SHG measurements. The discussion of the origin of these oscillations can be found in section 4.6.
With the full understanding of the excited state dynamics of the single materials, bilayers of DIP and PDIR-CN_2 were studied to investigate the interaction of excited states at the donor/acceptor interface with focus on the formation of CT-excitons. In the course of this thesis, three differently prepared bilayer samples were investigated. The three bilayers were PDIR-CN_2 on DIP (PDIR-CN_2/DIP), PDIR-CN_2 on DIP (LT) (PDIR-CN_2/DIP (LT)), and DIP on PDIR-CN_2 (DIP/PDIR-CN_2). All bilayers were made on

sapphire substrates under the same conditions as the single layers of DIP and PDIR-CN_2. The results are presented in section 4.5.1 for PDIR-CN_2/DIP, in section 4.5.2 for DIP/PDIR-CN_2, and in section 4.5.3 for PDIR-CN_2/DIP (LT).
The chapter is completed by a conclusion summarizing the results (section 4.7).

4.1 Excited states and their dynamics in organic semiconducting molecules

The interaction of visible light and low energy UV light in the wavelength regime of 200-1000 nm with organic molecules usually leads to absorption of photons by the organic molecules, because the optical gaps of the organic molecules lie in this regime. This section discusses the usual case of one photon absorbed by one molecule and the electronically excited state processes most relevant for the present thesis. For a more extensive description of the dynamics of excited states in organic molecules see Ref. [50, 114, 115].
The absorption of the photon leads to an excited molecule. This is only possible when the energy of the photon corresponds to the energetic difference between the initial and the final state. In general two different excited forms depending on the overall spin configuration are discussed: singlet and triplet state. In case of the singlet state, the net angular momentum of the system is zero and in the triplet case, the total spin is one. In the ground state the molecules are singlets and all electrons are coupled. Energy transfer in the molecule depends on the transfer moment, which is composed of the electronic transition moment, the spin overlap integral, and the overlap integral of the initial and the final wave function of the nuclear vibrations. In case that any one of the three parts is zero the transfer moment becomes zero and the transition is called forbidden. Transitions with a transfer moment unequal to zero are called allowed. Based on the transfer moment, three selection rules can be created: (1) The electronic transition moment depends on the symmetry of the wave functions of the involved states. In practice, symmetry forbidden transfers can also be observed due to vibronic coupling between the electronic and the nuclear wave functions. (2) The spin overlap depends on the spin multiplicity of the initial and the final state. Transitions without a change of spin multiplicity are allowed and transitions with a change are forbidden. Therefore transitions from singlet to singlet and triplet to triplet states are allowed and the direct transitions between singlet and triplet states are forbidden. The spin selection rule can be weakened by spin-orbit coupling, which scales with the fourth power of the atomic number. It is therefore rarely observed in purely organic molecules. (3) The electronic excitations appear on timescales which are fast in comparison to the nuclear motion (Born-Oppenheimer approximation). Therefore only vertical transitions are allowed. This approximation is called Franck-Condon principle. Based on the spin selection rule, the absorption of light by a non-excited molecule leads to an excited singlet state, because the ground state has a singlet character and the photon can not change the spin of the electron. Furthermore, the excited state is usually not the vibronic ground state of the excited electronic state, because the transition to the vibronic ground state is often not

possible based on the Franck-Condon principle. This means a so-called "hot" excited state is created. An excited molecule can also absorb an additional photon and higher electronic states can be populated. These spin-allowed processes are *singlet* → *singlet* and *triplet* → *triplet absorption*.

Jablonski diagrams are used to visualize the possible interactions of light with molecules and the resulting excited state dynamics. In a Jablonski diagram the electronic states (singlet and triplet multiplicities) are drawn as thick horizontal lines and the vibronic sub-level of the electronic states are drawn by thin horizontal lines. Light involved transitions are visualized as vertical (Franck-Condon principle) arrows and non-radiative arrows are marked as wavy arrows. In figure 4.1 the processes in a single molecule discussed here are visualized and a list of additional processes based on the interaction between neighboring molecules is given. All processes mentioned in figure 4.1 are discussed briefly below.

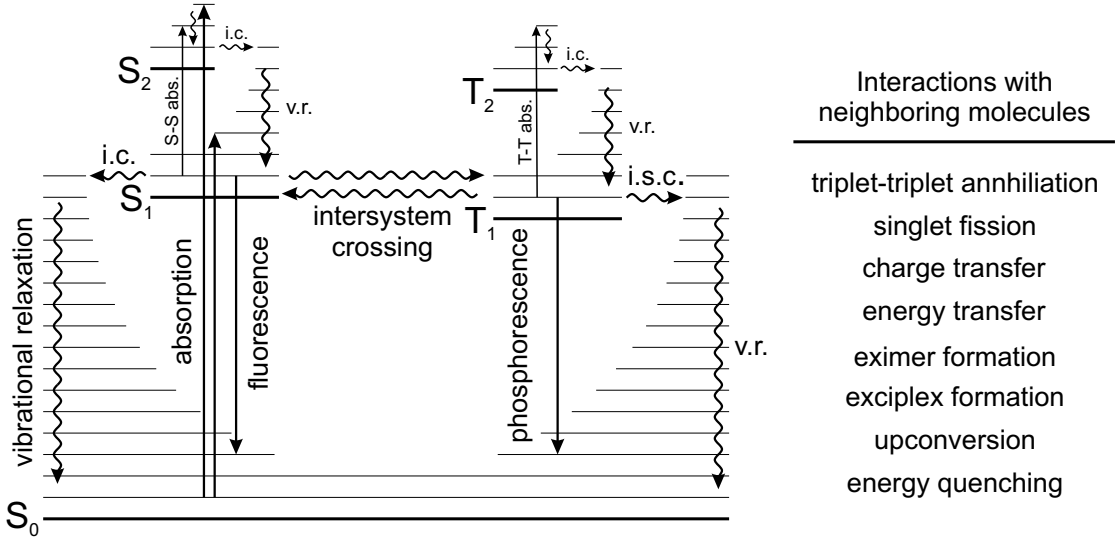

Figure 4.1: Jablonski diagram of the excited state processes of a generic organic molecule after light absorption. Further processes based on the interaction with a second molecule are summarized on the right.

A few deexcitation and energy transfer processes can take place after absorption of a photon. As mentioned before, the initial excitation by a photon usually leads to a hot excitation. The first deexitation is thus the thermalization of the energy to the surrounding molecules called *vibrational relaxation* (v.r.). It takes place on a femto- to picosecond timescale and is usually faster than any of the other transfer processes [50]. The other processes usually start from the vibronic ground state. The influence of this vibronic excess energy to other energy and charge transfer processes is still lively discussed. Beginning with the vibronic ground state three cases are considered:

Radiationless Deactivation
Radiationless deactivation takes place between two isoenergetic vibrational levels of different electronic states driven by an increase in entropy and followed by the ultrafast vibrational relaxation. The radiationless deactivation is the dominant process inside the singlet and triplet manifolds ($S_n \rightarrow S_1$ and $T_n \rightarrow T_1$) and usually takes place on a picosecond timescale. For the final deexcitation of $S_1 \rightarrow S_0$, the transition is hindered by the symmetry selection rule and takes place on a nano- to microsecond timescale. Inside one spin multiplicity, the radiationless deactivation is called *internal conversion* (i.c.). Additionally, the spin forbidden radiationless deactivation between the singlet and triplet multiplicities can take place. It is then called *intersystem crossing* (i.s.c.). The intersystem deexcitation process $T_1 \rightarrow S_0$ usually happens on a millisecond to second timescale. Usually, the intersystem crossing is a forbidden process, but it is strongly influenced by heavy atoms and the coupling between the involved states.

Radiative Deactivation
The deexcitation of the molecules can also take place under spontaneous emission of a photon. Usually the radiative deactivation only takes place at the lowest excited state of the corresponding multiplicity. The process is called *fluorescence* for spin-allowed and *phosphorescence* for spin forbidden transitions. Fluorescence takes place on a nanosecond timescale and phosphorescence can even occur on a timescale of seconds. Another important process composed of intersystem crossing and fluorescence is called *delayed fluorescence*. If the lowest excited singlet and triplet states are similar in energy, an intersystem crossing to the triplet followed by a thermally-induced intersystem crossing back to the singlet state can occur. The fluoresence of the singlet state is then delayed and depends on the triplet population. This kind of delayed fluorescence is called E-type delayed fluorescence.

Intermolecular Interactions
In the case of a solution or solid material composed of one molecular species or even different species further deexcitation channels are created. First of all a second type of *delayed fluorescence* (P-type) can occur. In this case, two excited molecules in the triplet state with a total singlet character interact and form one molecule in the ground state and one in an excited singlet state, followed by fluorescence of the excited molecule. The process is also known as *triplet-triplet annhiliation*. Also, the reverse process called *singlet-fission* can be observed in some systems. Here, one molecule in the excited singlet state and one molecule in the ground state interact and form two triplet states with total singlet character. Both processes can be ultrafast (femto- to picosecond timescale), because despite the change of singlets and triplets both processes are spin-allowed. Furthermore, the electron donating/accepting properties of excited molecules are increased and they can act as electron donor or acceptor and a *charge transfer* takes places. In addition to a charge transfer, *excimers* (excited dimer) for one molecular species and *exciplexes* (excited complex) for different molecular species can be formed by energy transfer between two neighboring molecules. Excimers and exciplexes are bimolecular species and only exist in the excited form. In the non-excited state the molecules are not

coupled. By energy transfer to an already excited molecule *upconversion* can take place, leading to a higher excited state of one molecule. Finally, by *energy transfer* (singlet to singlet, or triplet to triplet) to a different molecular species without further interaction, excited states can be quenched. This process often takes place at metallic interfaces.

In addition to the excited dynamics in organic molecules already discussed, a few quasiparticles play an important role in the discussion of excited organic thin films. The discussion of excited states in semiconducting materials presented here is based on the book of Schowerer and Wolf [116]. Excitons are the species mainly discussed. They are formed in a semiconducting film after optical excitation. An exciton is a neutral quasiparticle made of an electron and the corresponding hole, which are bound by the electrostatic coulomb force. An exciton can transport energy without transporting a net electric charge. Excitons are of key importance in organic solar cells, because they are the usual results of an excitation of the active material by light, and charge separation into two independent charge carriers can produce an electric current. In general, the two limiting cases of *Wannier-Mott* and *Frenkel excitons* are considered. Additionally, textitcharge-transfer excitons play an important role in organic thin films and devices.

Wannier-Mott Exciton
The Wannier-Mott exciton describes the limiting case for large distances between electron and hole of an order of magnitude higher than the unit cell of the crystal. The electron is treated as a delocalized electron cloud, which is around the hole. The coulomb interaction is screened by the material between electron and hole, which leads to usually very low binding energies in the order of 0.01 eV. This is the normal case in inorganic semiconductors such as Si or GaAs.

Frenkel Exciton
Frenkel excitons describe the other limiting case of excitons in materials with small dielectric constants. Here, the coulomb interaction between electron and hole is high and the distance between electron and hole is in the order of the unit cell. In organic molecular crystals both charges can be located on the same molecule. In this case they are also called molecular excitons. Frenkel excitons have a much higher binding energy than Wannier-Mott excitons, usually 0.1 eV to 1 eV.

Charge-Transfer Exciton:
The term charge-transfer exciton (CT-exciton) is used in organic molecular semiconductors for neutral but polar excitations, which span over at least two molecules, but in general are larger than the structural units. Their properties lie in between the Wannier-Mott and the Frenkel exciton. They can be found in single material semiconductors as well as in compounds made of different molecular species. In such multi-material compounds they are usually the dominant lowest excitation and are of great importance for organic devices [9, 117].

In inorganic semiconductors, weakly bound Wannier-Mott excitons are formed, which can be easily separated by a built-in electric field due to differently doped regions of the semiconductor. In their organic counterparts, the excitons are strongly bound. Separating the excitons usually needs two component solar cells with a donor and acceptor compound. At the donor/acceptor-interface, the Frenkel excitons can relax into CT-excitons, which can be separated into free charge carriers at the interface. A more extensive description of the different excitations in organic materials and their application in organic devices is given by Schowerer and Wolf [116]. For an efficient charge separation, the CT-state formation and dissociation has to be fast compared to other relaxation effects [7, 41]. Therefore, the ultrafast excited state dynamics in the single organic layers are of major importance for an efficient charge separation in bilayer systems [51, 52].

4.2 Sample preparation

All samples investigated in this chapter were prepared by Valentina Belova in the group of Prof. Dr. Frank Schreiber at the Institut für Angewandte Physik, Eberhard-Karls Universität Tübingen, Germany. The samples were prepared by organic molecular beam deposition [118, 119] in an ultrahigh vacuum (UHV) chamber on sapphire (CrysTec, single crystal, (001) surface, both sides polished) and silicon (Si-Mat, doped with boron, resistance: 17-23 Ωcm, cut along (100) crystal plane) substrates. The silicon substrates were covered with a native oxide layer of approximately 2 nm. All substrates were cleaned in an ultra -sonic bath using acetone and isopropanol. They were heated to 650 K in the UHV chamber before deposition of the molecules and were kept at 297 K during evaporation of the organic molecules. Samples marked as "(LT)" for low temperature were evaporated on substrates held at 220±10 K. The pressure during deposition was 1 x 10^{-9} mbar. Deposition rates of 0.5 nm/min for DIP on silicon, 0.3 nm/min for DIP on sapphire, and 0.3 nm/min for PDIR-CN_2 on sapphire and during bilayer deposition were used and controlled by a water-cooled quartz crystal microbalance calibrated by X-ray reflectivity. The nominal thickness for each single layer was 20 nm, which led to 40 nm (each layer 20 nm) for the bilayer films.

For the deposition method used here both DIP and PDIR-CN_2 form well-defined polycrystalline films [120, 121]. For DIP, an upstanding structure with a herringbone-like substructure parallel to the substrate is formed on both sapphire and SiO_2 (see figure 4.2b) [120]. The homogeneity of the film structure was investigated by X-ray reflectivity (XRR) measurements on the DIP and PDIR-CN_2 films by Valentina Belova. No significant difference between the structures was found. Therefore any change in the dynamics going from sapphire to silicon oxide is related to a change in the excited state properties due to the silicon oxide and not to a different film structure. Additionally, optical absorption data was provided by Valentina Belova. The results for the DIP layers investigated in this thesis are shown in figure 4.2c, and for PDIR-CN_2 in figure 4.11b.

4.3 Diindenoperylene (DIP)

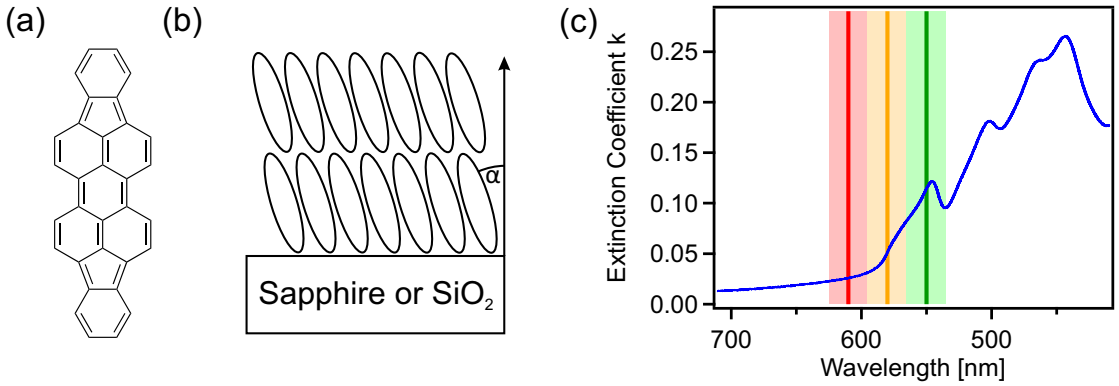

Figure 4.2: (a) Molecular structure of diindenoperylene (DIP). (b) Crystal structure of DIP on weakly interacting substrates. (c) Extinction curve of DIP (measured by Valentina Belova, Universität Tübingen).

DIP is a well-studied organic semiconductor with many promising properties [122–125]: (1) DIP forms highly ordered films on different substrates [120, 126–128], which enables a polarization-resolved separation of different excited states due to their orientation. The molecular structure and the thin film configuration on weakly interacting substrates is shown in figure 4.2a and b. (2) DIP has a high resistivity to environmental influences [45, 46] and can easily be handled outside of an ultrahigh vacuum environment, which is important for applications in solar cells. (3) It has a high exciton diffusion length [129], which is important for the transfer of the excited states to the donor/acceptor interface. It was used in a variety of devices, like bilayer organic photovoltaic devices (OPVs) [122, 130, 131] and organic field effect transistors [132, 133]. Recently, DIP has been investigated with time-resolved photoluminescence and transient absorption to gain insights into the fundamental decay dynamics in solution and thin films on a picosecond to nanosecond timescale [125]. In DIP films, no indication for long-lived singlet exciton states of singlet fission has been found, contrary to crystals with similar packing motifs such as crystalline anthracene [134, 135], perylene [136, 137], tetracene [138], and pentacene [139–141]. However, so far the dynamics on the ultrafast femtosecond timescale are unresolved and the basic photophysics of DIP are not fully understood.

In the following, the excited state dynamics in DIP films adsorbed on the two different substrates sapphire and SiO_2 are investigated. The different substrates were chosen for the following reasons: Sapphire generates nearly no SHG signal, no excitation and therefore no signal change is introduced by the pump pulse and it does not interact electronically with the DIP molecules. For SiO_2 a large contribution to the SHG signal from the symmetry breaks in and at the interfaces of the native silicon oxide layer is expected. Additionally, interactions of excited states in DIP with the silicon oxide can occur. Especially charge trapping in oxide traps at the silicon oxide surface is energetically favorably [133, 142].

4.3.1 DIP on sapphire

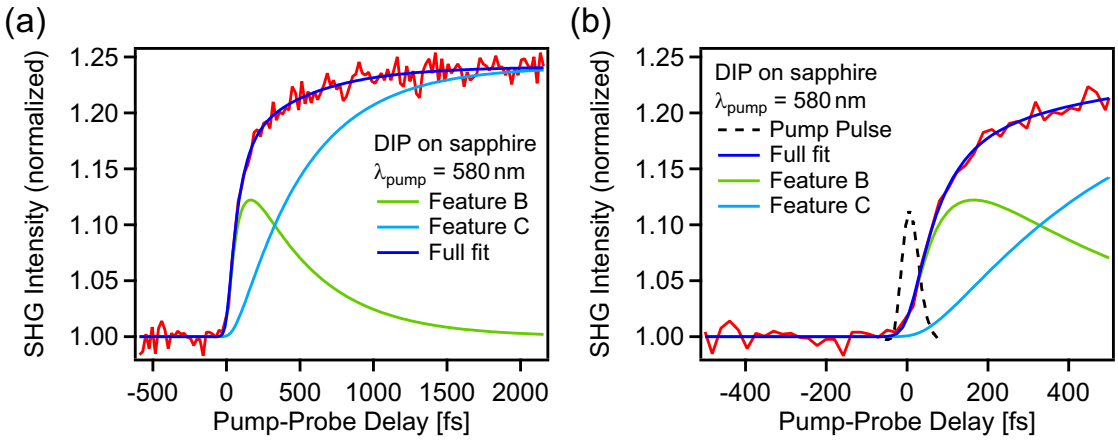

Figure 4.3: TR-SHG measurement of DIP on sapphire. (a) TR-SHG results for a pump-probe delay of up to 2 ps overlaid with the results of a three-step first-order kinetic model (see text). (b) Enlarged view of the data below 500 fs, including the temporal width of the pump pulse to visualize the delayed SHG signal increase.

The TR-SHG results of DIP on sapphire are presented in figure 4.3a and a detailed view of the first 500 fs after optical excitation is given in figure 4.3b. Shortly delayed after the pump pulse, a strong SHG signal increase of nearly 25 % is observed. The signal increase is composed of two components, a faster and a slower one (feature B and C). In addition to the short delay, the rise of the pump pulse is much steeper than the signal increase and the signal still increases after the pump pulse has passed (see figure 4.3b). This observation clearly indicates that the rise of the signal does not come from the initial excitation by the pump pulse. Thus the initial excitation does not lead to a signal change. Moreover, the decay of the initially excited species (labeled as A) leads to the generation of a second excited species (feature B), which is seen in the TR-SHG trace. In the next step, the decay of B leads to the rise of a third species (feature C), which can be traced by the slow component of the signal rise. A three-step process subsequently describes the data very well. To model the data a three-step first-order kinetic model (state A, B, C), which was convoluted with a Gaussian function to model the intensity distribution of the excitation laser pulse, was used:

$$\begin{aligned} f(t) = A \cdot e^{-k_{\mathrm{AB}} x} + B \frac{k_{\mathrm{AB}}}{k_{\mathrm{BC}} - k_{\mathrm{AB}}} (e^{-k_{\mathrm{AB}} t} - e^{-k_{\mathrm{BC}} t}) \\ + C(1 - \frac{k_{\mathrm{BC}}}{k_{\mathrm{BC}} - k_{\mathrm{AB}}} e^{-k_{\mathrm{AB}} t} + \frac{k_{\mathrm{AB}}}{k_{\mathrm{BC}} - k_{\mathrm{AB}}} e^{k_{\mathrm{BC}} t}) \end{aligned} \tag{4.1}$$

A, B, and C are the TR-SHG signal changes due to the three involved species and k_{AB}, k_{BC} are the transfer constants between the states. All later shown transfer times are the inverse of the transfer constants. A decay of state C was not included in the model,

due to the completely different timescale of the decay compared to the time window of the measurements (compare figure 4.4a). During the fits all amplitudes were kept independent and the amplitude of the initial excitation (state A) was held at zero. The width of the Gaussian function was calculated from SFG cross-correlation measurements on the sample (compare figure 2.2b). As can be seen in figure 4.3, the measured TR-SHG trace is convincingly described by the model. From the fit, the times of 71±19 fs for the transfer from A to B and 471±100 fs for the transfer B to C can be extracted.
To investigate the dynamics for longer time scales, a measurement of up to 40 ps was performed. The result is shown in figure 4.4a. The data was modeled by an direct excitation and a single exponential decay. It is to be noted that the ultrafast processes could not be resolved in this measurement and are therefore ignored. From the single exponential fit, a decay constant of 680±110 ps is obtained. Picosecond time-resolved measurements on similar DIP films have identified a biexponential decay with the time constants of 166 ps and 1.1 ns [125]. The value found here could be interpreted as a superposition of these two time constants. Due to the comparably short time window, a differentiation of these time constants is not possible from the TR-SHG measurements and lies beyond the scope of these thesis.
To gain deeper insights into the ultrafast excited state dynamics of DIP films and the underlying decay processes, pump pulse intensity- and energy-resolved as well as probe pulse polarization-resolved measurements were conducted. The results are shown in figure 4.4b-d. All this data can be accurately described by the three-step kinetic model, introduced above.
The results of the pump pulse intensity-resolved measurements presented in figure 4.4b show an increase of both amplitudes for low intensities up to approximately 50 μJ/cm^2. For higher pump intensities, a saturation takes place. The amplitude of feature B saturates at a higher level compared the amplitude of feature C. The variation in the amplitudes after saturation can be explained by small inhomogeneities of the sample, which causes laser spot dependent intensity changes. It is to be noted that the dynamics determined above are not influenced by these variations i.e. transfer times do not change. Despite the variations the difference in the NLO contrast between the amplitude of feature B and C does not change in the saturation regime. This can be taken as further proof of a coupling between state B and C as proposed in the kinetic model. The initial rise of the amplitudes is explained by an increased number of excited species, which scales linearly with the pump intensity. The reason for the saturation after 50 μJ/cm^2 is most likely due to exciton-exciton annihilation. An explanation for the higher saturation level of feature B compared to C may be an incomplete transfer of state B to C.
As the next step, pump pulse energy-dependent measurements as shown in figure 4.4c were performed. For these experiments the pump pulse wavelength was tuned to 610 nm, 580 nm, and 550 nm respectively, covering the first rise of the extinction spectrum with the lowest one (550 nm) being resonant with the first excitation as shown in figure 4.2c [123, 125]. All three measurements were done with a pump intensity of 135 μJ/cm^2 lying in the saturation regime (see figure 4.4b). The measurements basically show the same behavior, a two component rise, as discussed before, but with an increase in amplitude for short delay times. Modeling the data with the three-step kinetic function

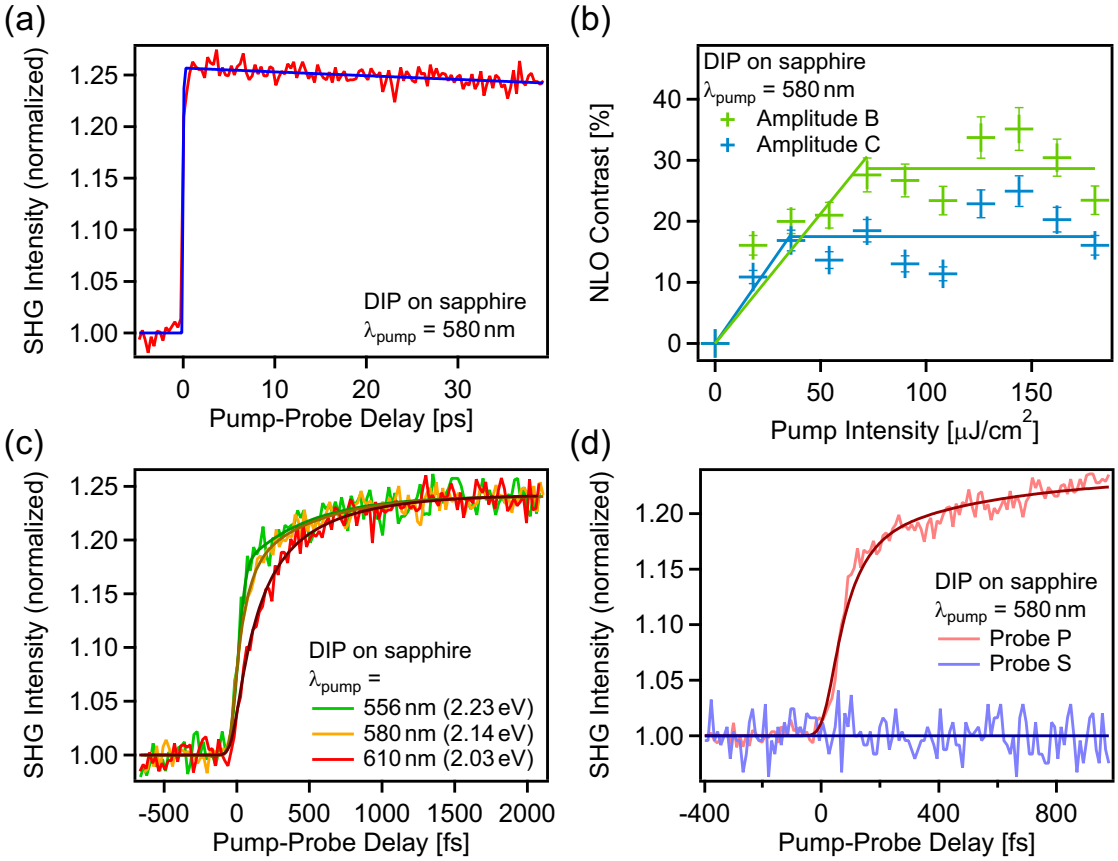

Figure 4.4: (a) Single exponential decay for high pump-probe delays. (b) Amplitudes of features B and C fitted from the kinetic model (see figure 4.3). (c) Dependence of the TR-SHG signal on the excitation (pump) photon wavelength. (d) TR-SHG signal as a function of probe beam polarization (s- or p-polarized beam, see figure 2.4).

makes it clear that the first transfer time becomes shorter for lower excitation wavelengths, while the transfer time from B to C does not change. The transfer times for A to B extracted by the model are 140±60 fs at 610 nm, 71±19 fs at 580 nm, and 19±30 fs at 550 nm. This means for resonant excitation with 550 nm the relaxation is the fastest and it gets slower for the off-resonant excitations. For similar aromatic molecules, namely 3,4,9,10-perylenetetracarboxylic dianhydride (PTCDA) and N,N′-dimethylperylene-3,4,9,10-dicarboximide (MePTCDI), similar decay times of 65 fs for MePTCDI and 100 fs for PTCDA have been observed. They have been attributed to excitonic intraband relaxation [143].

Changing the polarization of the probe beam from p- to s-polarization has a pronounced impact on the SHG signal as can be seen in figure 4.4d. None of the dynamics, which are resolved with p-polarized light, can be detected with s-polarized light. As described in section 2.2.2, the s-polarized light only probes excitations parallel to the surface, while with p-polarized light both parallel and perpendicular components are probed. Hence,

the main component of the excitations behind feature B and C is oriented perpendicular to the surface and can therefore only be probed by the p-polarized light. Detailed X-ray diffraction measurements have revealed that DIP molecules adopt an adsorption geometry in which the long axis of the molecules is aligned perpendicular to the surface [120]. Based on these examinations, it can be concluded that the transition dipole moment of both excitations B and C are oriented parallel to the long molecular axis.

Merging together all results discussed above, an assignment of the three excited states and their dynamics can be done (see figure 4.5): The state labeled as A is most likely attributed to delocalized (hot) excitons, which localize via intraband relaxation forming molecular (Frenkel) excitons (state labeled as B). In case of the resonant excitation (550 nm), the relaxation becomes much faster compared to the off-resonant excitations. For the molecular exciton in DIP the transition dipole is oriented mostly parallel to the long molecular axis [144], which clearly explains the disappearance of the SHG signal change by the exciton for s-polarized light. Time-resolved measurements of similar DIP films studying the excited state dynamics in the picosecond time regime proposed that after 1 ps the main excitation is an excimer-like state [125, 145]. Following this proposal, the state labeled with C is assigned to an excimer. Excimer formation is a common property of perylene. Thus, the molecular exciton decays on a timescale of 471±100 fs via a charge transfer between an excited molecule and a non-excited neighboring molecule forming an excimer. Simulations have shown that a dimer formation of DIP is reasonable on a timescale of 400-500 fs and that grain boundary or defects are needed to give the DIP molecules enough freedom for reorganization [51]. The transition dipole moment of this excimer state is mainly orientated perpendicular to the surface and is therefore not detectable with s-polarized light [144]. Finally, it decays on a timescale of 680 ps back to the ground state. As discussed above, this value could be the superposition of the time constants of 166 ps and 1.1 ns as was observed with time-resolved photoluminescence [125]. A schematic visualization of the results discussed above is given in figure 4.5. In the scheme a second alternative assignment discussed below is shown for comparison.

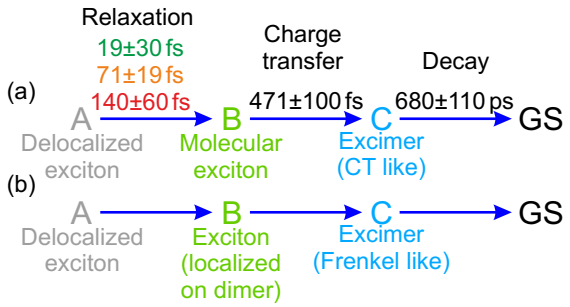

Figure 4.5: Electronically excited state dynamics in DIP films on sapphire after optical excitation. The different relaxation times for the delocalized exciton correspond to varying excitation energies (see figure 4.4(c) and text). (a) and (b) slightly different assignments based on two different simulation approaches discussed in the text.

Based on recent simulations in the groups of Engels and Engel, a slightly different assignment of the excited state dynamics has to be considered. In their simulations on DIP dimers in the gas phase, the lowest energetic state does not have CT-character, but is Frenkel-like [146]. Additional simulations on the similar PTCDI [147] and PTCDA [148] showed that the surrounding molecules stabilize the Frenkel state even more than the CT-states. The difference in the results compared to earlier simulations by Gisslén *et al.* [144], which resulted in the CT-state as the state with the lowest energy, is caused by the simulation approach used. In the approach of Gisslén *et al.* [144], the charges of the CT-states of the dimer were calculated as localized on the single molecules, which leads to strong dipole moments, that are stabilized by a polarizable environment. The CT-state is further stabilized by the electrostatic attraction between the two monomers. The dimer approach of Engels *et al* [149] results in a suppression of this localization by the high symmetry of the system. In this, the dipole moment of the CT-state nearly diminishes due to the delocalization of the CT-state over the full dimer, which results in a lower stabilization and thus the Frenkel-like excitation of the dimer becomes the lowest excited state. Additionally, the simulations showed that the first step after optical excitation is a relaxation to the CT-state of the dimer on an ultrafast timescale. Applying these new calculations to the measured TR-SHG data, state A can still be assigned to the delocalized exciton, which then relaxes onto a exciton localized on a DIP dimer (B) and finally relaxes via a conical intersection into a Frenkel-like excited dimer state (C). The timescales according to the simulations are 200 fs for the first step and 400-500 fs for the second step. In the experiment, the first step is significantly faster (19-140 fs), but the second transfer time of 471±100 fs concurs perfectly with the predicted relaxation time. A direct relaxation of the initial excitation to the lowest Frenkel-like excited dimer state is forbidden according to the simulations, because a deformation of the DIP molecules is needed, which is supported by the three-step model needed to describe the experimental data.
The difference between the two interpretations lies in the character (Frenkel vs. CT) of the lowest excited state in DIP crystals, which depends on the involved model used for the simulations. In both cases, an excited dimer formation is the key process leading to a relaxation of the initially excited state into a lower-lying state, which has excimer character. Independent of the assignment, the ultrafast relaxation of the optical excitation of DIP is supported by the TR-SHG measurements.

4.3.2 DIP on silicon

Based on the understanding of the intrinsic excited state dynamics in DIP on sapphire, the influence of the silicon substrate with a native oxide layer (SiO_2) on the dynamics is investigated. Compared to sapphire, the silicon substrates have an additional source of SHG intensity coming from the symmetry breaks in a silicon oxide and at the interface to the bulk silicon. This leads to an increase of background signal, which reduces the relative signal changes by the DIP layer and thereby the signal to noise ratio. Furthermore, interactions between optically excited DIP molecules and trap states at the silicon oxide surface were determined in organic field effect transistors [133]. However so far, no

investigations on the ultrafast timescales of the charge trapping at the DIP SiO_2 interface have been done.
Compared to the TR-SHG measurements on DIP/sapphire (see figure 4.3), the results on DIP/SiO_2 (see figure 4.6a) show a different behavior. First, the relative signal change is largely reduced to only 5 % compared to the 25 % for DIP/sapphire, which leads to a highly reduced signal to noise ratio. This reduction is attributed to the higher background signal from the SiO_2 substrate, as mentioned before. Second, an additional very short-lived component (labeled as D) arises, which is directly populated by the pump pulse. The decay of feature D is obviously faster than the rise of the next feature (B). A direct population of B from D can therefore be excluded. This is confirmed by the pump pulse intensity-dependent measurements shown in figure 4.6b. In the saturation regime above 50 $\mu J/cm^2$, the difference between the NLO contrast of D and B or C changes significantly for different pump intensities, while B and C possess the same behavior. Additionally, the amplitude of D rises much more steeply compared to the amplitudes of B and C.

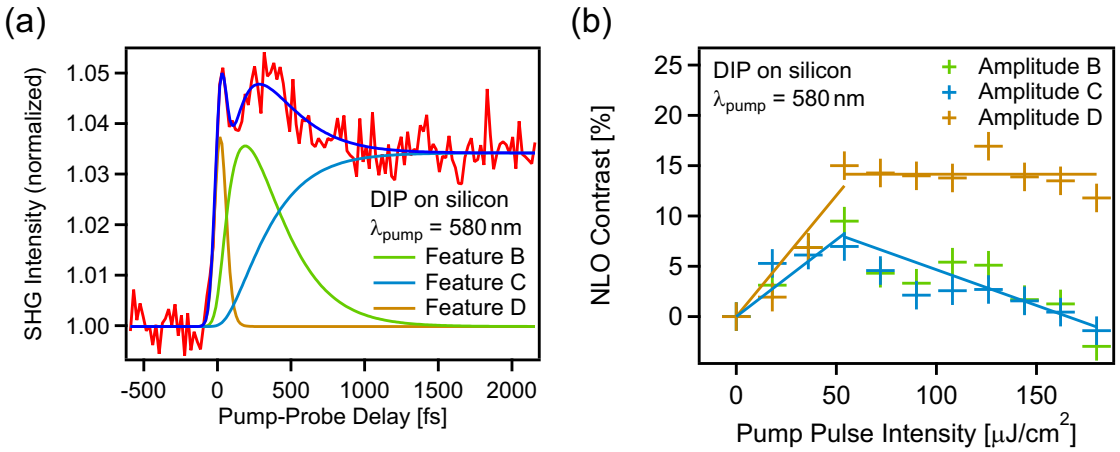

Figure 4.6: TR-SHG of DIP on SiO_2. (a) TR-SHG signal for time delays of up to 2 ps. The result of a three-step fit with an additional independent component (labeled as D) is included (see text). (b) Pump laser intensity-dependence of the amplitudes of the features B, C, and D of the fit of (a).

In order to describe the TR-SHG data (figure 4.6a), the fit model from DIP/sapphire was modified by an additional directly populated excited state (feature D), which decays independently of the three-step dynamics of A, B, and C. No influence of D to the dynamics of the other three states was implemented. The model gives a decay constant of 22±14 fs for the new feature D and transfer times of 157±80 fs for A to B and 207±95 fs for B to C.
To gain further information on the involved excited states leading to the TR-SHG signal changes, polarization-resolved measurements were performed. The results of these measurements are shown in direct comparison to the results on DIP/sapphire, scaled to the same relative signal changes to highlight the different dynamics (figure 4.7). For DIP on SiO_2, the relative amplitude of feature C compared to the amplitude of B

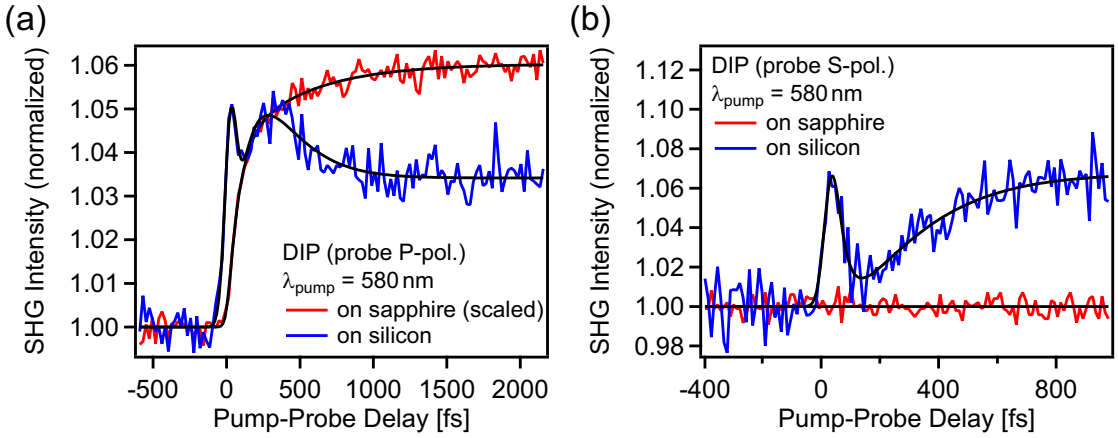

Figure 4.7: Polarization-resolved TR-SHG traces of DIP on SiO_2. (a) Comparison of the traces of DIP on the two substrates for the p-polarized probe pulse and (b) for the s-polarized probe pulse.

is reduced compared to the amplitudes on DIP/sapphire in the p-polarized measurement. In the case of s-polarized light, for which no pump pulse induced SHG changes were found on DIP/sapphire, a clear signal coming from feature C could be resolved here. Thus the behavior of feature C changes drastically for DIP on SiO_2 compared to DIP/sapphire. Assuming a similar orientation and ordering of the DIP films on both substrates [120, 127, 128], the corresponding transition dipole moment of the electronically excited state is obviously not oriented parallel to the long molecular axis anymore as found for DIP/sapphire. In contrast, the orientation of feature B did not change.

Comparing the results on the excited state dynamics on DIP/SiO_2 with DIP/sapphire a clear influence of the substrate is found. Apart from a new short-lived feature (D) with a lifetime of 22±14 fs, particularly the properties of feature C are different on SiO_2. Generally, the following processes influencing the excited states dynamics may be considered: (1) Independent of the DIP, electrons could be excited in SiO_2 by multi-photon processes due to the high pump pulse intensities, which then undergo self-trapping [150, 151]. (2) SiO_2 has a high density of trap states at the surface, which are energetically favorable for excited electrons in DIP [133, 142]. (3) An optically induced electron transfer from native oxide to the DIP molecules could be relevant. (4) Momentum relaxation due to scattering processes can take place on ultrashort timescales in silicon (32 fs) [152]. Most likely the latter can be associated with feature D, which has no influence in the excited states dynamics in the DIP film. It is assumed that the initial excitation still leads to delocalized excitons (feature A) in the DIP film, followed by a localization of a time scale of 157±80 fs (intraband relaxation), which leads to the generation of localized excitons (feature B) as suggested for DIP/sapphire. Contrary to the DIP/sapphire system, the polarization-resolved measurement clearly indicates that the following excimer formation is suppressed by a faster process leading to a different excited species. As mentioned above, SiO_2 possesses a high density of energetically favorable trap states at the interface. Therefore, feature C may be attributed to the trap states on SiO_2 and

the transfer time of 207±95 fs from feature B to feature C describes the charge trapping at the DIP/SiO_2 interface, which is more than two times faster than the formation of excimer states in DIP on sapphire (471±100 fs). Figure 4.8 summarizes the assignments described here.

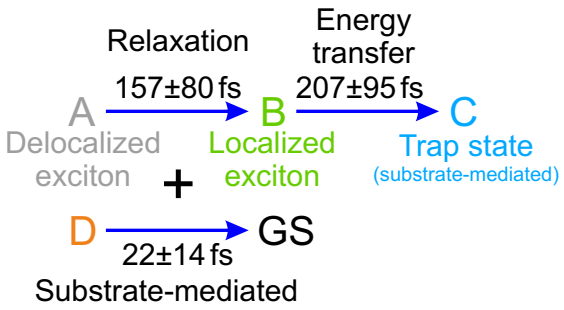

Figure 4.8: Proposed processes in DIP on SiO_2 after optical excitation at 580 nm (see text).

4.3.3 DIP (LT) on sapphire

Another DIP layer was prepared by the evaporation of DIP on a cold sapphire substrate at 220±10 K (see section 4.2). The aim of this procedure was to create a more lying structure of the DIP molecules [120], to increase the orbital overlap between DIP and PDIR-CN_2 in the bilayer configuration (see below). It is to be noted that a substrate temperature of around 220 K is not low enough to create a fully lying structure and therefore large areas of standing DIP are still expected [120]. Figure 4.9 shows the TR-SHG results.
The TR-SHG trace of DIP (LT) (figure 4.9a) looks very similar to the trace of DIP. The only apparent difference are oscillations, which are modeled by a damped sine oscillator and are discussed separately in section 4.6. To describe the dynamics, the same three-step first-order kinetic model in equation (4.1) with an additional damped oscillator was used to model the data. The model describes the measurement accurately and the following times were calculated: 26±8 fs for the transfer from A to B and 350±105 fs for the transfer from B to C. In figure 4.9b, the decay of the signal for the picosecond timescale is shown. Here, the behavior of the thin DIP (LT) film is again very similar to the DIP film and a single exponential decay was used to describe the decay. From the single exponential decay a decay time of 600±112 ps was extracted. In figure 4.9c, the dependence of the TR-SHG trace on the wavelength of the pump beam is presented. As before on the DIP film, the curves get steeper with increasing pump energy. Comparing DIP and DIP (LT), the only obvious difference can be seen in the s-polarized probe beam measurements (figure 4.9d). Here, no signal change could be detected for DIP, but on DIP (LT) a clear decrease of the signal can be seen. Because of the assumption that the structure of the DIP (LT) film is similar to the DIP film, but has some lying areas, the model developed for the p-polarized measurements was used for the s-polarized measurements. Due to the low signal to noise ratio of the s-polarized measurements, the transfer times of the p-polarized fits were used as fixed parameters during the fitting

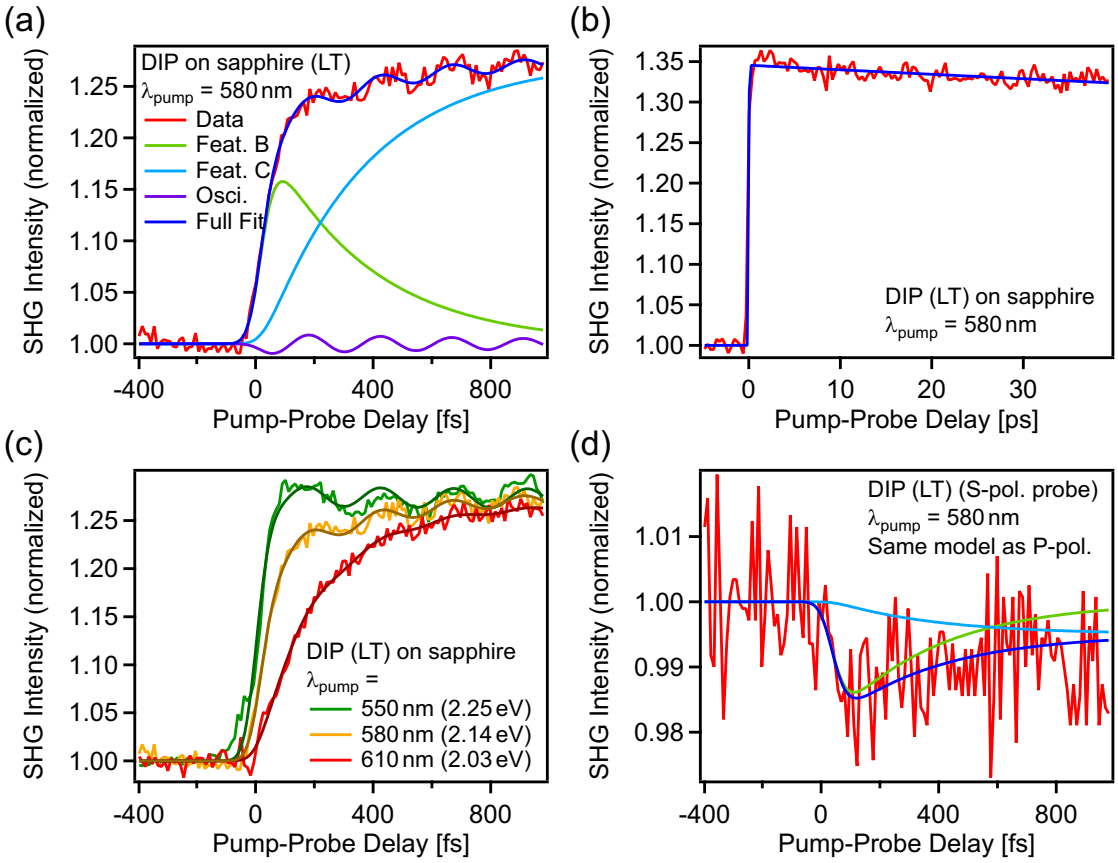

Figure 4.9: TR-SHG measurement of DIP evaporated on cold sapphire. (a) TR-SHG results for a pump-probe delay of up to 2 ps overlaid with the results of a three-step first-order kinetic model with an additional oscillating term. (b) Result for a pump-probe delay of up to 40 ps overlaid with a single exponential decay. (c) Pump wavelength dependence of the TR-SHG trace. (d) Measurement with s-polarized probe beam. The measurement was modeled with the three-step first-order kinetic model used for p-polarized probe beam (see (a)).

routine and only the amplitudes of the different features were kept free. As can be seen in figure 4.9, the model describes the data very well and the fit converged perfectly.

Based on the high similarities between the results on DIP and DIP (LT) and the assumption that the structure of the thin films is similar, the interpretation of the results is the same as for DIP (see section 4.3.1), with the exception that there are crystal areas where the molecules are lying flat instead of standing up [120]. Therefore the assignment of the different features is that in the DIP (LT) film, the initial excitation of delocalized excitons (A, not visible) relaxes on an ultrafast time-scale dependent on the excitation wavelength into the molecular exciton. For a resonant excitation, this process is the fastest. Afterwards, the molecular excitons form excimer states between two adjacent molecules independent of the excitation wavelength and finally the excimers decay in a few hundred picoseconds back to the ground state. The difference here is that, because

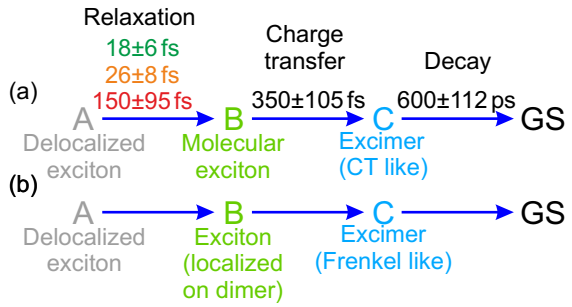

Figure 4.10: Proposed model for the excited state dynamics of DIP (LT) on sapphire after optical excitation. (a) and (b) slightly different assignments based on two different simulation approaches discussed in section 4.3.1.

of some lying DIP molecules, the signal of the molecular exciton and of the excimer have a component parallel to the surface. As will be discussed later, these lying areas are an important finding and have a large influence on the interaction between DIP and PDIR-CN_2 at their interface. With the slightly different structure, the excimer formation is faster. It can be explained by the higher disorder in the DIP (LT) film, which leads to an increased number of grain boundaries and defects in the DIP film and therefore lowers the barriers hindering the dimer formation [51]. As it was for DIP the alternative simulation approach of Engel and Engels has to be considered. Based on the alternative approach the assignment is: (A) to (B) localization of the initially delocalized exciton on a dimer unit followed by the relaxation into a lower-lying Frenkel-like excitation of the dimer (C). Similar to the approach discussed above, the faster transfer from (B) to (C) in DIP (LT) compared to DIP can be explained by the higher amount of disorder in the DIP (LT). The resulting assignments of both approaches are presented in figure 4.10. For a detailed discussion of the two approaches and the corresponding assignments see section 4.3.1.

4.4 The perylene diimide derivative PDIR-CN_2 on sapphire

PDIR-CN_2 (n,n'-bis-(2-ethylhexyl)-1,7-dicyanoperylene-3,4:9,10-bis(dicarboximide)) belongs to the class of perylene diimides (PDIs), which are well-known organic molecules. The structure of the PDIR-CN_2 molecules is shown in figure 4.11. PDIs are commonly known for their use as high performance pigments and dyes [153]. In the recent years, they have gained additional attention as acceptor materials [44, 154], because, like DIP, they have very promising properties for the application in solar cells. They have high chemical, thermal, and photochemical stabilities [47], which is what already made them common as pigments and dyes [153]. Furthermore, they exhibit a high absorption in the visible regime, which gives them an advantage over the usually used fullerenes [44, 154]. In addition, their optical properties can be easily modified to match the desired absorption regime, by adding functional side groups at the bay positions of the perylene core [47, 121, 155, 156]. By introducing side chains at the imide positions, the molecules can

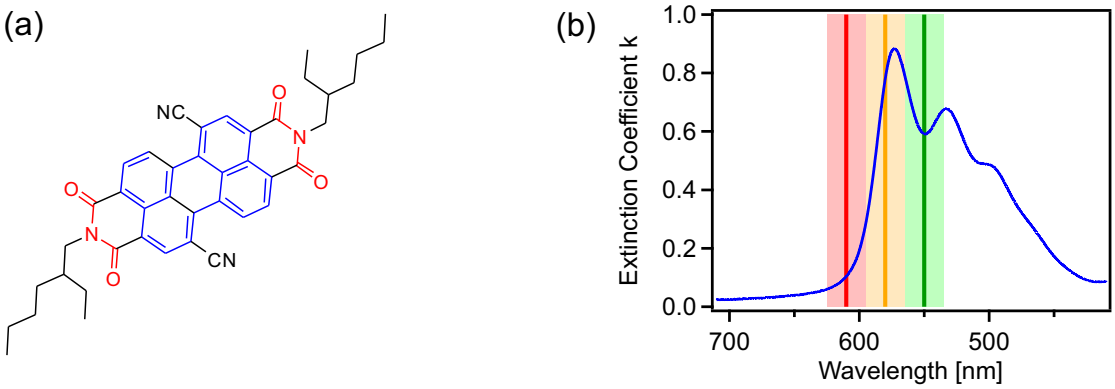

Figure 4.11: (a) Molecular structure of PDIR-CN_2. (b) Extinction curve of a thin PDIR-CN_2 film (measured by Valentina Belova, Universität Tübingen).

be made solvable and the crystalline structure in thin films can be tailored [157]. In recent years organic solar cells with reasonable efficiencies [156, 158, 159] and ambient stable field effect transistors have been realized with PDIR-CN_2 [160]. Despite the successful use in organic devices, the fundamental electronically excited state dynamics of PDIR-CN_2 have not been investigated so far.
The TR-SHG results for PDIR-CN_2 on sapphire are shown in figure 4.12a. With the arrival of the pump pulse, a steep increase of the signal which perfectly fits to the broadness of the excitation pump pulse can be seen. This means, in contrast to DIP on sapphire as discussed above, the initial excitation by the pump pulse is visible in the TR-SHG trace. In addition to the initial rise, a second slower increase of the signal for around 800 fs was detected. After 800 fs no further signal change was detected on the ultrafast timescale. The TR-SHG signal is overlaid by an oscillation which starts with the excitation. For pump probe delays in the picosecond regime (figure 4.12b), a decay of the signal back to the non excited level can be seen.
To model the ultrafast data a two-step first-order kinetic model (feature A and B) was chosen:

$$f(t) = A \cdot e^{-k_{\mathrm{AB}}x} + B(1 - e^{-k_{\mathrm{AB}}x}) \tag{4.2}$$

A and B are the amplitudes of the two features and k_{AB} is the transfer time between the two states. As before, the model was convoluted with a Gaussian function to describe the intensity distribution of the pump pulse. The width of the excitation pulse was determined by SFG cross-correlation measurements between pump and probe pulse on the sample. The TR-SHG trace is overlaid by an oscillation, which is excited by the excitation pulse. The oscillations were modeled by an sine oscillator with exponential damping, which is independent of the two step model. An additional short-lived component (C) is needed to describe the short-lived feature directly decaying after the excitation, otherwise the initial peak is not described by the model. This additional feature is not part of the oscillations and can not be described with the two step model, because it

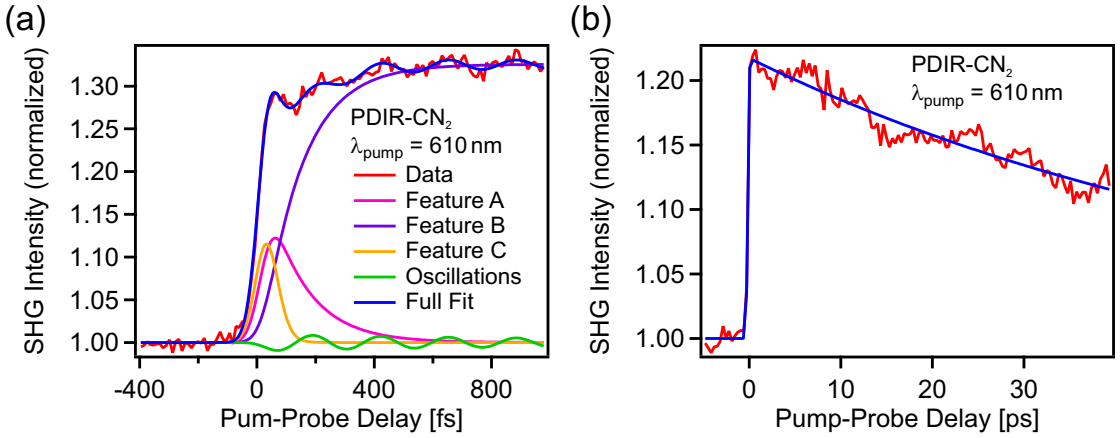

Figure 4.12: TR-SHG results of PDIR-CN_2 on sapphire. (a) TR-SHG results for a pump-probe delay up to 1 ps overlaid with the results of a two-step first-order kinetic model expanded by an additional independent decay (see text). (b) Decay of the excitations on a 40 ps timescale overlaid with a single exponential decay.

decays faster than the rise of the other components. The separation is supported by the measurements shown below. Including all features the model becomes:

$$f(t) = A \cdot e^{-k_{\mathrm{AB}}x} + B(1 - e^{-k_{\mathrm{AB}}x}) + C \cdot e^{-k_{\mathrm{C}}x} + O \cdot e^{-k_{\mathrm{O}}x} \cdot \sin(\omega x) \qquad (4.3)$$

where A and B denote the two step model, C and k_C describe the additional feature, and O, k_O and ω describe the oscillations including an exponential damping. With the model, the following dynamics were determined: Feature A is directly excited by the pump pulse and the transfer time to B is 131±25 fs. Feature C is directly excited by the pump pulse and decays in 20±10 fs. The oscillations have a period of 271±2 fs, which corresponds to a frequency of 123±1 cm^{-1} and are damped with a decay time of 1500±500 fs. For this, the damping was calculated from fits to TR-SHG data measured for up to 2 ps. A detailed discussion of the origin of the oscillations can be found in section 4.6.

The decay of feature B can be described by a single exponential decay, excluding the ultrafast processes, which are not resolved in the long time window measurement. From the single exponential fit of the TR-SHG measurement of the picosecond time window the decay time of 62.4±1.8 ps was extracted (see figure 4.13b).

To get a deeper understanding of the excitation behavior of the PDIR-CN_2 film and the processes behind the model, pump energy-, pump intensity-, and probe polarization-resolved measurements, which are discussed below, were performed.

The results of the pump energy-resolved measurements are shown in figure 4.13a. A clear increase of the initial signal change going from the excitation wavelength of 610 nm to 556 nm can be seen. In the inset of figure 4.13a the difference between the measurements at 556 nm and 610 nm is shown. The difference can be perfectly described by a directly excited state, which decays with a single exponential decay, with a decay time

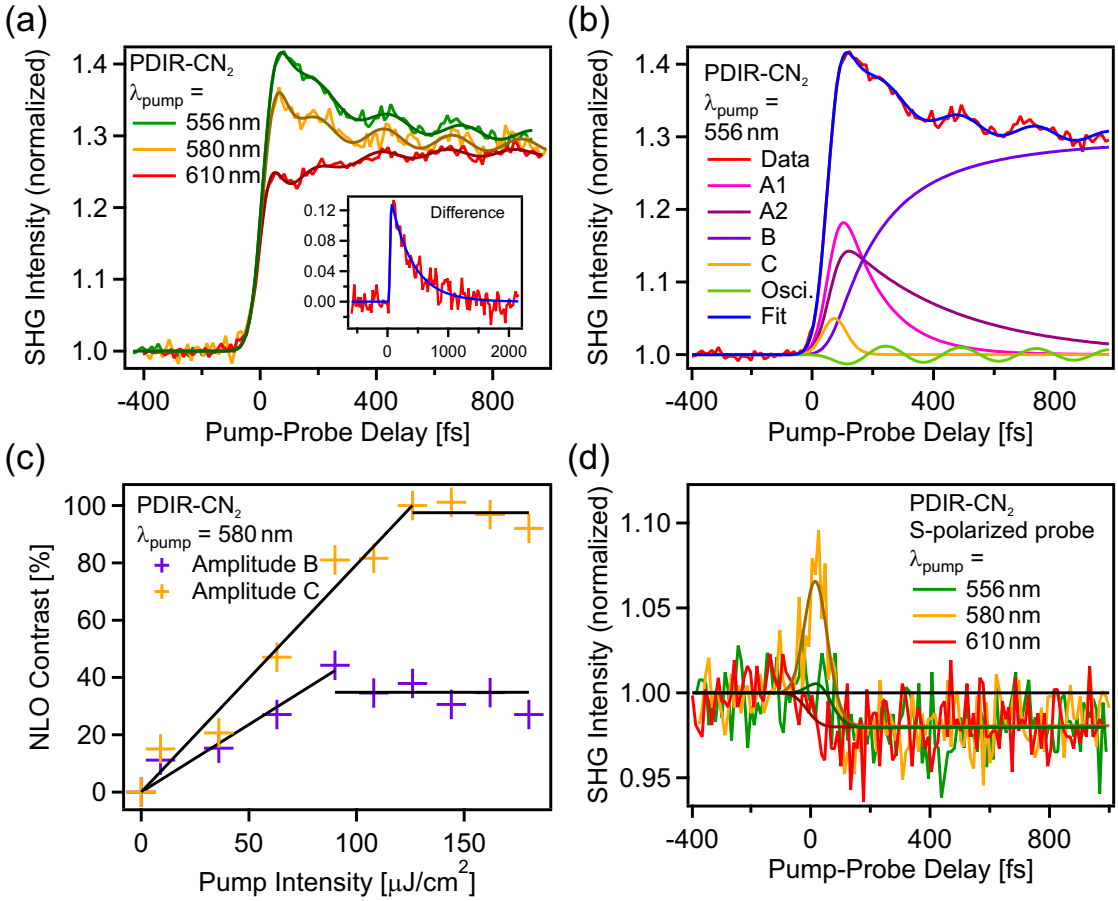

Figure 4.13: (a) Dependence of the TR-SHG trace on the pump wavelength. Insert: Difference between the TR-SHG response for a pump wavelength of 556 nm and 610 nm. (b) TR-SHG trace for 556 nm overlaid with an expanded fit model (see text). (c) Pump intensity dependence of the amplitudes of feature B and C. (d) Dependence of the TR-SHG trace on the pump wavelength for s-polarized probe light.

of 369±25 fs. This new decay channel has a different decay time compared to all of the species considered in the model used for the excitation with 610 nm. Therefore a new component was added to the model. From the extinction measurement (see figure 4.11b), it can be concluded that the additional feature most likely results from excitation of a vibronic transition. Thus the model is expanded by an excited state, which is directly pumped by the pump pulse and relaxes into state B. The expanded model is described by:

$$f(t) = A1 \cdot e^{-k_{\mathrm{A1B}}x} + A2 \cdot e^{-k_{\mathrm{A2B}}x} + B\left(1 - \frac{A1}{A1+A2}e^{-k_{\mathrm{A1B}}x} - \frac{A2}{A1+A2}e^{-k_{\mathrm{A2B}}x}\right) + C \cdot e^{-k_{\mathrm{C}}x} + O \cdot e^{-k_{\mathrm{O}}x} \cdot \sin(\omega x) \tag{4.4}$$

With A1 denoting the old feature A and A2 describing the additional excited feature for

higher excitation energies. The new expanded model was used to fit the TR-SHG traces for an excitation wavelength of 556 nm. The result is shown in figure 4.13b. As can be clearly seen, the data is described very well by the expanded model.
As the next step, the influence of the pump intensity on different features was investigated. Figure 4.13c presents the amplitudes of features B and C as a function of the pump intensity. For better clarity, the amplitudes of A1 and A2 are not shown, because they exhibited the same behavior as feature B. Feature B shows a linear increase with increasing pump intensity up to 80 μJ/cm^2 and saturates afterwards at a NLO signal change of roughly 30 %. The amplitude of feature C increases linearly as well, but the increase is steeper and the saturation takes place at a higher level (near 100 % NLO contrast) for a higher pump intensity (120 μJ/cm^2). Despite the large changes in the excitation amplitudes, no change of the involved time dynamics was detected. This leads to the assumption that feature C belongs to a process, which is independent of the process involving features A and B.
Finally, s-polarized probe beam measurements were conducted for all three excitation wavelengths (figure 4.13d). The excitation by light with a wavelength of 610 nm led to a small decrease of the signal. The data was fitted by a single exponential decay convoluted with the Gaussian excitation. Because of the small signal change and the corresponding low signal to noise ratio, it makes no sense to fit a more complex function to the data. In the exponential decay function, the decay time was fixed at 62 ps corresponding to the decay time measured with p-polarized light. For the 580 nm excitation, an additional feature with a positive amplitude and a decay time of 20 fs can be seen. It has the same decay time as feature C, which was needed to describe the p-polarized data fully. For the excitation with 556 nm, the amplitude of this feature is strongly reduced compared to the excitation with 580 nm.
Based on the results described above, an assignment of the features is discussed. Feature A1 is assigned to the initial excitation by the pump pulse, which relaxes to the vibrational ground state of the first excited state (S1). The additional feature A2 is introduced by the excitation of a higher vibrational level than A1 within the first excited state (S1). This can also be seen in the extinction spectra (figure 4.11b). The lowest excitation energy only has an overlap with the first feature in the extinction spectra, whereas the higher excitation energies show an overlap with the next vibronic feature. This interpretation is supported by the relative increase of the amplitude of A2 with increasing pump energy (figure 4.13a). The decay time of 369$\pm$25 fs of the higher excitation of S1 is approximately three times higher than the relaxation time of the lower one (131$\pm$25 fs). This can be explained on the one side by a lower overlap of the wave functions of the two involved states and on the other side by the higher amount of energy, which has to be released to the surrounding material. The measurements with s-polarized light only showed very small signal changes. For PDI molecules, it has been shown that the singlet excitons are oriented along the molecular axis [154]. Similar PDIs to PDIR-CN_2 form ordered films with a layer by layer structure perpendicular to the surface on weak interacting substrates like sapphire and silicon oxide [121]. In these structures, the PDI cores are slightly turned out of the plane perpendicular to the surface. This can explain the low decrease of the TR-SHG signal. The additional ultrafast process (C) could be separated

from the other excitation dynamics by pump intensity and probe polarization-resolved measurements. Its SHG response still increases after saturation of the excitonic species (A+B) is reached. Additionally, for s-polarized light it shows a large increase for a resonant excitation of the lower vibronic level (see figure 4.11b and figure 4.13d). Even though it can be seen for all excitation energies in the p-polarized measurements, the highest amplitude of feature C was measured for the excitation with 580 nm. Therefore it seems to be coupled to this excitation. It might be a polarization change of the molecules due to the resonant excitation into the vibronic state, which decays ultrafast on a timescale of 20 fs after excitation. The decay of the TR-SHG signal of 62.4±1.8 ps is attributed to the electronical decay from the excitonic state to the ground state of the molecules. A summary of the assignment of the TR-SHG results discussed above is presented in figure 4.14.

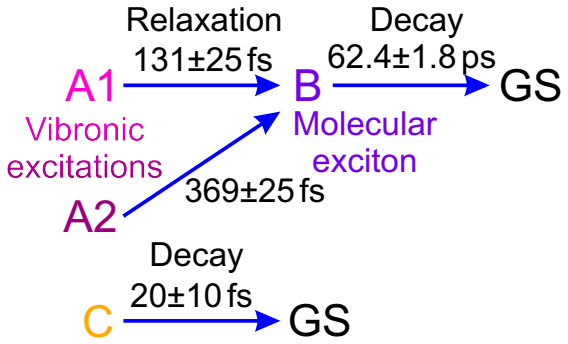

Figure 4.14: Proposed model for the excited state dynamics of PDIR-CN_2 on sapphire after excitation by 556 nm.

4.5 Bilayers

Based on the electric levels of DIP and PDIR-CN_2, the formation of CT-states is favorable [121, 161] and working solar cells based on theses molecules in combination with other molecules have already been built [122, 156]. DIP in this case, is the donor material and PDIR-CN_2 is the acceptor material due to its high electron affinity of roughly 4.3 eV [121]. This chapter discussed the TR-SHG results from three different bilayer configurations of DIP and PDIR-CN_2 on sapphire. The three samples are PDIR-CN_2 evaporated on DIP (PIDR-CN_2/DIP), DIP evaporated on PDIR-CN_2 (DIP/PDIR-CN_2), and PDIR-CN_2 evaporated on DIP (LT) (PDIR-CN_2/DIP (LT)). From the XRD measurements done by Valentina Belova (Universität Tübingen), only a very small change for the structure of the film compared to the single layer films were found. In all cases the top layer adapted to the structure of the bottom layer increasing the order of PDIR-CN_2 on DIP compared to the pure PDIR-CN_2 layer and decreasing the order of the DIP layer on PDIR-CN_2 compared to pure DIP film. Therefore all changes in the TR-SHG signal compared to the superposition of the two single layers discussed above might be assigned to interfacial effects interaction between the two layers.

4.5.1 PDIR-CN_2 on DIP

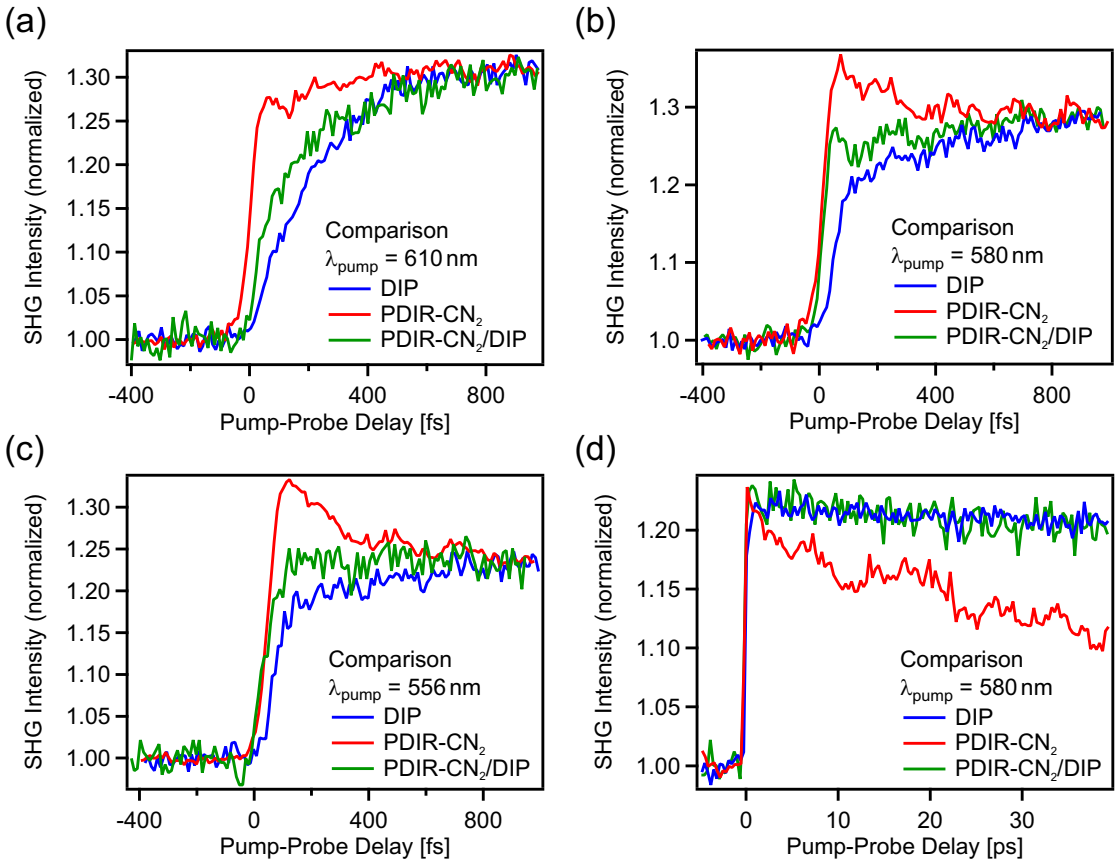

Figure 4.15: Direct comparison of the TR-SHG trace of the bilayer (PDIR-CN_2/DIP) with the single layers of DIP and PDIR-CN_2. (a)-(c) Comparison for a pump-probe delay up to 1 ps and different excitations wavelengths. (d) Comparison for 580 nm for a pump-probe delay up to 40 ps.

A direct comparison of the TR-SHG measurements for the bilayer and both single layers of DIP and PDIR-CN_2 for different excitations are shown in figure 4.15. For an excitation with 610 nm (figure 4.15a) the signal of the bilayer shows similar behavior to the signal of the single DIP film. The signal of the bilayer is a little steeper than the signal of the DIP film, but lower in intensity than the trace of the PDIR-CN_2 film. Based on these observations, the bilayer trace can be described by an superposition of the single layers, with a higher impact of the DIP layer. No new contribution to the SHG signal could be found, which could be attributed to an interaction between the two layers. For an excitation with 580 nm (figure 4.15b), the influence of the PDIR-CN_2 to the TR-SHG signal increases and the ultrafast feature C of the pure PDIR-CN_2 is clearly visible, whereas the higher vibronical excitation (A2) of PDIR-CN_2 seems to be suppressed in the bilayer trace. This suppression can be seen more clearly in the TR-SHG trace for an excitation of 556 nm (figure 4.15c), where the TR-SHG trace of the bilayer looks like

the superposition of DIP and PDIR-CN_2 without the higher vibronic excitation A2 in PDIR-CN_2.
For longer decay times (figure 4.15d), the decay of the TR-SHG trace follows the behavior of the pure DIP film and no influence of the PDIR-CN_2 could be detected, independent of the excitation energy. Here, the picture of a superposition of the two single layers used before breaks down, because in the picture of the aforementioned superposition of the signals of the two single layers, a decay of the signal somewhere in-between the decays of the single layers was expected for the bilayer. The measured decay is similar to the decay of the single layer of DIP. Therefore no influence of the PDIR-CN_2 would be the only possible explanation in the superposition model, that is contrary to the before mentioned PDIR-CN_2 features, which have been detected in the data up to 1 ps.
To get a deeper understanding of the bilayer behavior and especially look for an interaction between the two layers as it is needed for an efficient use in solar cells, further probe polarization-, pump wavelength- and pump intensity-resolved measurements were done.

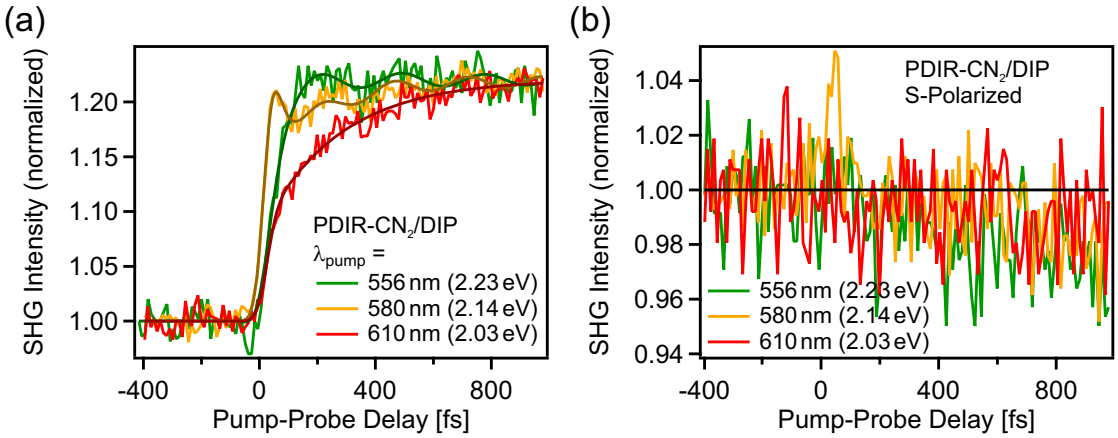

Figure 4.16: Comparison of the TR-SHG traces of the PDIR-CN_2/DIP bilayer for the different excitations and polarizations. (a) P-polarized measurements overlaid with kinetic model. (b) S-Polarized measurements.

The result of the pump wavelength-resolved measurements are shown in figure 4.16a. They are fitted by a two-step first-order kinetic model as was used for PDIR-CN_2 (see equation (4.4)), where an additional independent contribution labeled as C, was only used for an excitation by 580 nm. A more complex model (e.g. a superposition of the DIP and the PDIR-CN_2 model) was neglected, because the data can be described fully by this model. A direct comparison of fit parameters for the bilayer with the single layers is therefore not constructive. A comparison of the different bilayer curves clearly shows that the ultrafast component (C), which shows a similar behavior to the ultrafast component (C) of PDIR-CN_2, is pronounced for an excitation of 580 nm and is suppressed for 556 nm. Again, oscillations of the signal after excitation can be seen which are discussed in section 4.6. The ultrafast feature can be assigned to the pure PDIR-CN_2 layer, while the oscillations can be assigned to a superposition of both materials.

In figure 4.16b, the results of the wavelength-resolved measurements done with an s-polarized probe beam are presented. As expected from the s-polarized measurements from the single layer, only very small changes of the signal are visible. As described above, the pure DIP film did not show any signal change and the PDIR-CN_2 layer only showed a very small signal decrease and an ultrashort feature for an excitation by 580 nm. Still, a diminutive signal reduction and a very small ultrashort peak for the excitation by 580 nm can be seen, but both changes are in the range of the noise. This behavior fits the observations above that the signal of the bilayer can be described as the superposition of the two single layers.
The pump intensity-resolved measurements for an excitation wavelength of 580 nm are presented in figure 4.17. An excitation wavelength of 580 nm was chosen for the pump intensity-resolved measurements, because the ultrafast feature (C) is only visible for 580 nm. Figure 4.17a-c again gives a direct comparison of the measurements of the single layers and the bilayer for different pump intensities is given. At first glance, the bilayer could be described by a superposition of the two single layers again, but looking more into details, some interesting changes were discovered, which speaks against a pure signal superposition and led to the assumption of an interaction between the two materials. For low pump intensities the bilayer signal did not show an influence of the PDIR-CN_2 layer. With increasing pump intensity, the influence of the PDIR-CN_2 increased and for high pump intensities the signal was dominated by the PDIR-CN_2. Especially for high intensities the aforementioned suppression of the higher vibronic excitation (A2) in PDIR-CN_2 could be seen. This suppression led to a much clearer distinction of the ultrafast species (C). To get a deeper insight into the exact changes in the dynamics of the bilayer for increasing pump intensities, the signal difference of the traces of high and low pump intensities were created. To see differences in the dynamic behavior, the intensity of the signal for the low pump intensity was scaled to match the signal intensity for the high pump intensity. Therefore only the changes on dynamics and not in excitation amplitude are presented in the difference, shown in figure 4.17d. The difference shows a steep signal increase that goes along with the pump pulse, which means that the additional feature is directly excited by the pump pulse. For higher delay times the excitation decays and a biexponential function is needed to describe the decay. From the fit, the decay times of 22±17 fs and 198±45 fs can be determined. The ultrafast component fits very well to the 20±10 fs, which was measured on pure PDIR-CN_2 and the longer time constant describes the change of the bilayer trace going from a more pronounced influence of DIP to a higher influence of PDIR-CN_2 with increasing pump intensity. All measurements were modeled by a two step kinetic model expanded by an independently decaying directly excited state (C). In figure 4.17e, the result of a measurement with an high pump power overlaid with the model and in figure 4.17f the amplitudes of all three features calculated by the model are shown. For low pump intensities, the amplitude of C has to be kept at zero to enable a clean fitting process and only for pump intensities above approximately 100 $\mu J/cm^2$ the model was fitted with all parameters kept free. As in the single layers, the signal of the main features increases linearly for low intensities and saturates afterwards. The additional feature C rises beyond the saturation value of the main feature for high pump intensities. For

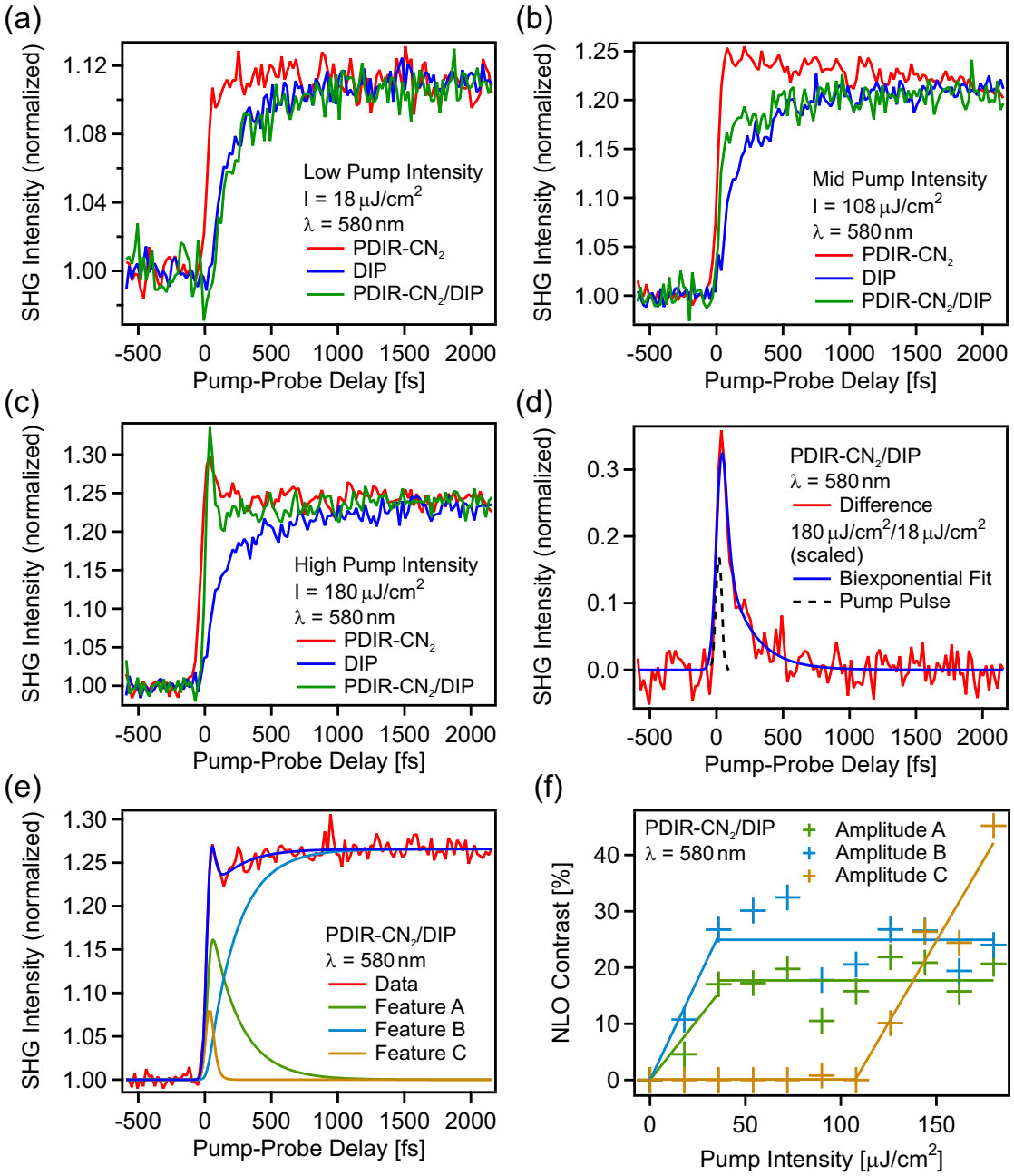

Figure 4.17: Pump intensity-resolved measurements for 580 nm excitation. (a)-(c) Direct comparison of the TR-SHG trace of the bilayer with the single layer of DIP and PDIR-CN_2 for different pump intensities. (d) Change in the dynamics due to the increase in pump intensity (scaled data, see text). (e) High pump intensity TR-SHG trace overlaid with a fit model. (f) Amplitudes of the different features of the fits (see (e)) for the different pump intensities

lower pump intensities, it is not distinguishable in the measurements and therefore the power dependence for lower pump intensities could not be evaluated.
Merging together all results described above, some conclusions can be drawn about the interactions in the bilayer. At first sight, the results of the bilayer seem to only show a superposition of the signals of the two single layers, which would mean that no detectable interaction takes place between the two materials. A closer look shows a few signal variations, which do not fit into the picture of no interaction between the two molecular layers. First of all, the signal decrease for long timescales is far too low for the bilayer compared to the single layer of PDIR-CN_2. For the case of no interaction and the assumption that the signal is composed of the signals of the non-interacting single layer, the decay of the signal for large timescales should lie between the decays for the single layers and not mirror the decay curve of the pure DIP layer. This can be interpreted either by an energy transfer from PDIR-CN_2 to DIP or a charge trapping at the interface in interfacial states. Secondly, the higher vibronic feature of the PDIR-CN_2 is suppressed in the bilayer, while the ultrafast excitations are still seen. This suppression can be interpreted as ultrafast energy transfer to the interface, which would fit to an ultrafast build-up of a charge transfer state between DIP and PDIR-CN_2 molecules. Furthermore, it would suggest an activation energy for the charge transfer generation. Finally, it was observed that the composition of the signal of the bilayer depends on the pump intensity. With increasing pump intensity the signal part coming from the PDIR-CN_2 increases in comparison to the signal from the DIP layer. Additionally, for high pump intensities, the ultrafast feature of the PDIR-CN_2 (labeled C) gets enhanced. Especially the direct excitation in PDIR-CN_2 is not visible for low pump intensities. This excitation should be clearly visible, because DIP does not give a noteworthy signal contribution for ultrashort excitation times, due to the non-detectable initial state. For higher pump intensities this feature gets visible in the bilayer measurements. This transfer, from similar to DIP, to similar to PDIR-CN_2 with increasing pump intensity is characterized by the longer decay time (198 ± 45 fs), which was calculated above from the difference between the TR-SHG trace for high and low pump intensities. A possible interpretation could be a resonant energy transfer from the PDIR-CN_2 layer to the DIP layer, which is partly suppressed for higher pump intensities, because of the charge saturation in DIP. In the saturation regime of the DIP layer, the signal of the bilayer shifts towards the behavior of PDIR-CN_2, because the excitation partly stays in the PDIR-CN_2 layer. A possible explanation for the low interaction between the two films could be the low overlap between the delocalized π-systems in the configuration used here, where the molecules in both layers have an upright orientation [48].
All these changes are attributed to changes in the excited state dynamics due to the interface between DIP and PDIR-CN_2, because XRD measurements by Valentina Belova have not shown a change in the crystal structure of the films due to the formation of the bilayer. Furthermore, the s-polarized measurements have shown a superposition of the single layers and no new effects from for example tilted molecules.
Two more interesting observations from the bilayer could help understanding the pure PDIR-CN_2 film better. First, the oscillations of the bilayer have a higher amplitude than the oscillations of the pure DIP film and their frequency can not be clearly assigned to

one of the single layers. Therefore it is assumed that there is a contribution of the PDIR-CN_2 film on DIP. Thus, their origin has to be an intrinsic property of the organic thin films and not an interface effect between the organic film and the sapphire. They can also be taken as further proof that the PDIR-CN_2 film has not changed fundamentally going from sapphire to DIP as underlying material. Secondly, the ultrafast feature can still be resolved and behaves the way it does in PDIR-CN_2, while for example the higher vibronic excitation is suppressed.

4.5.2 DIP on PDIR-CN_2

An overview of the results from the bilayer with reversed stacking direction (DIP evaporated on PDIR-CN_2 on sapphire) is given below.
Figure 4.18 compares the results of the TR-SHG measurements with an excitation wavelength of 610 nm of the bilayer to the results from the single layers of DIP and PDIR-CN_2. For both, the ultrafast timescale of 1 ps as well as for the longer time scale of 40 ps, the signal of the bilayer behaves exactly like the superposition of the two single materials and therefore no interfacial effects between the two films are assumed for the excitation with 610 nm. In comparison to the bilayer of PDIR-CN_2/DIP discussed in section 4.5.1, here the decay of the TR-SHG signal fits the "non-interacting" picture and lies in-between the decays of DIP and PDIR-CN_2. This was not the case for the PDIR-CN_2/DIP bilayer, where the signal decay was missing the PDIR-CN_2 part of the decay.

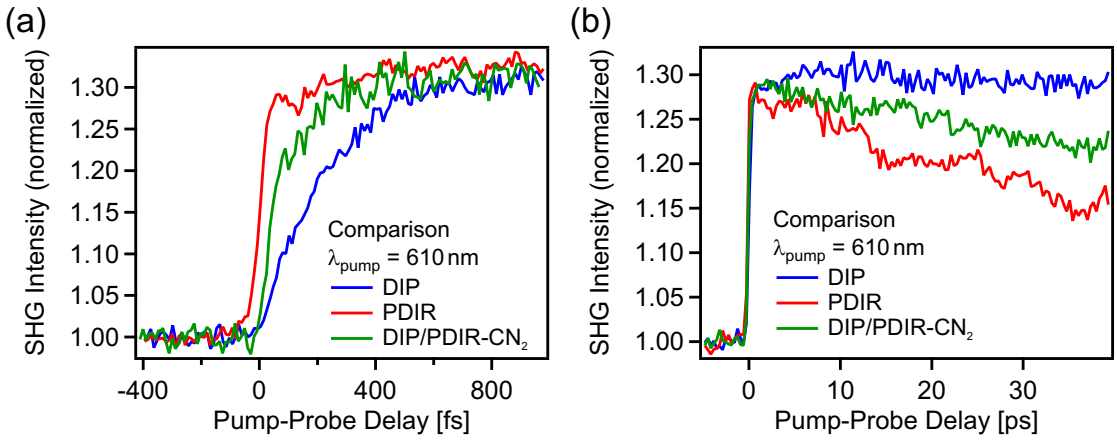

Figure 4.18: Comparison of the TR-SHG measurement of the bilayer DIP/PDIR-CN_2 with the traces of the single layer. (a) Results for a pump-probe delay of up to 1 ps. (b) Results for a pump-probe delay of up to 40 ps.

For higher excitation energies, a new feature arises in the bilayer measurements, which can not be explained by the single layers. Figure 4.19a shows the dependence of the bilayer signal to the pump wavelength. The rise of a feature with an NLO contrast of more than 150 % for the excitation at 550 nm was detected. For decreasing excitation energies, the intensity of the feature decreases. From the direct comparison of the three TR-SHG curves of the three excitation wavelengths, it can also be seen that the feature

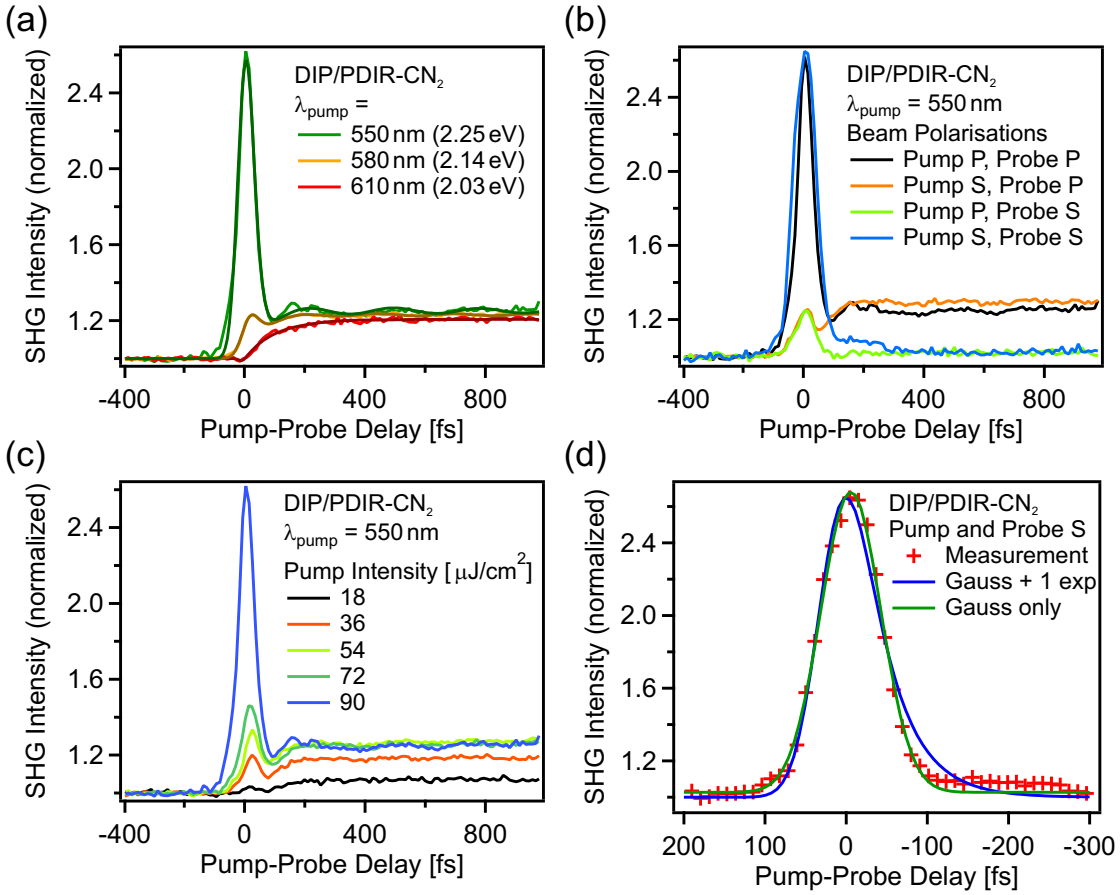

Figure 4.19: Detailed measurements of the bilayer DIP on PDIR-CN_2. (a) Rise of the resonant feature dependent on the excitation wavelength. (b) Pump and probe dependence of the TR-SHG trace. (c) Rise of the resonant feature with increasing pump intensity. (d) Comparison between two fit models for the resonant feature.

shifts the signal rise to lower pump/probe delay times. To investigate the behavior of this new feature, further pump and probe polarization-resolved, as well as pump intensity-resolved measurements were conducted (see figure 4.19b+c). The polarization-resolved measurements show a strong dependence of the feature on the combination of the two polarizations of pump and probe beam. Only when they have the same polarization the new feature has a high amplitude, whereas its amplitude is much lower for the combination of p- and s-polarized light. The intensity seems to depend solely on the combination of the polarizations of the pump and probe pulse and not on the respective single pulse polarizations. As before, the excited state dynamics except for the new feature are only visible for p-polarized probe light. Therefore a fundamental change of the film morphology is not expected. The pump power dependent measurement shows a strong dependence of the new feature on the pump intensity. The signal increase is non-linear and does not show a saturation for a pump intensity of up to 90 μJ/cm^2, while

the other signal part already saturates at $54\,\mu J/cm^2$. To investigate the position and structure of the new feature in detail, the TR-SHG trace for the excitation with 550 nm and both pump and probe beam s-polarized was modeled with two different models (see figure 4.19d). The first model is a single Gaussian distribution as was used for the x-correlation of probe and pump beam (compare figure 2.2b). A single Gaussian describes an excitation, which is instantaneously created by the overlap of the two pulses and only present while both pulses are overlapped on the sample. The second model includes a single exponential decay and is therefore the easiest model for an excitation by the pump pulse and the decay of the excited feature afterwards. The rise of the signal is described very well by both models, but the decay of the signal is only modeled by the pure Gaussian distribution, whereas the decay model overshots for pump-probe delays of roughly 100 fs and can not describe the highly symmetric behavior of the measured curve. Based on the results of the modeling and the results from the polarization-resolved measurements, it is assumed that the new feature is a coherent wave mixing of pump and probe beam meditated by the sample. Similar "coherent artifacts" have been seen and discussed since ultrashort light pulse were used in various pump-probe setups [162–167]. To summarize, the DIP/PDIR-CN_2 bilayer did not show a sign of a charge transfer between the two single layers. For low excitation energies, the TR-SHG trace looks exactly like a superposition of the single layers. For higher excitation energies, a coherent artifact based on the polarizations of pump and probe beam mediated by the sample was detected. Further investigations with other ultrafast time-resolved methods and morphology investigations could be used to shine light on this new interaction between the two laser pulses and the sample.

4.5.3 PDIR-CN_2 on DIP (LT)

Based on the DIP sample with DIP evaporated on a cooled sapphire substrate (compare section 4.3.3) a bilayer in the same configuration as discussed in section 4.5.1 with PDIR-CN_2 evaporated on top of the DIP layer was created and investigated. The aim of these investigations was to increase the interaction between DIP and PDIR-CN_2 by increasing the orbital overlap between the two molecular species at the interface, due to DIP molecules in a more lying configuration. Based on the results for similar systems, a CT-formation should then be possible [48].
Figure 4.20 showsthe bilayer PIDR-CN_2/DIP (LT) in comparison to the single layers. Like the bilayer of PDIR-CN_2 on DIP (see section 4.5.1), the TR-SHG trace looks for short timescales like a superposition of the two single layers, but for long delay times the decay of the PDIR-CN_2 trace is missing and therefore an interaction of the two materials has to take place. In contrast to the PDIR-CN_2/DIP bilayer, here the trace of the bilayer is much more similar to PDIR-CN_2 even for low excitation energies and low pump intensities. Furthermore, the higher vibronic feature of PDIR-CN_2 is not suppressed in the bilayer.
To get a deeper understanding of the interaction of the two materials, further investigations were conducted, by changing the pump wavelength and the pump and probe polarizations. The dependency of the bilayer trace of the pump wavelength is presented

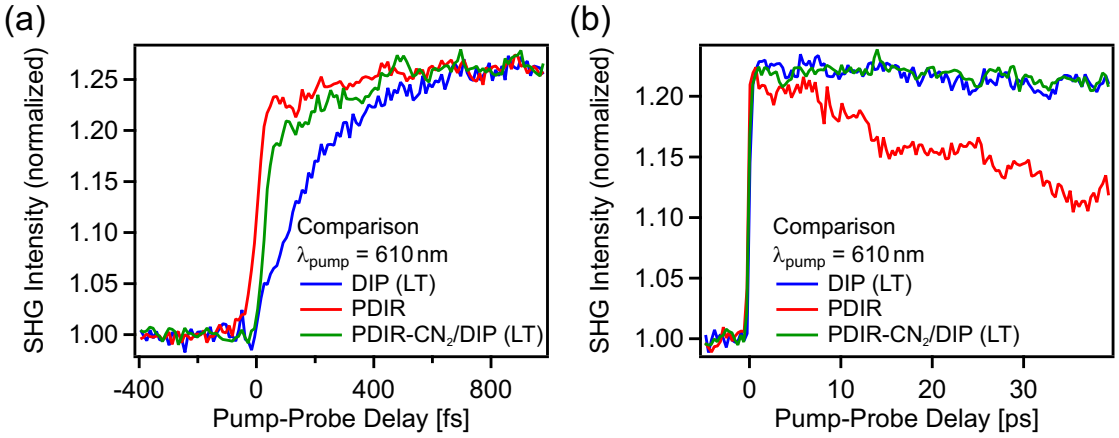

Figure 4.20: Comparison of the TR-SHG measurement of the bilayer PDIR-CN_2/DIP (LT) with the traces of the single layer for an excitation wavelength of 610 fs. (a) Results for a pump-probe delay of up to 1 ps. (b) Results for a pump-probe delay of up to 40 ps.

in figure 4.21a for short and in figure 4.21b for long timescales. A strong increase of the signal amplitude with increasing pump energy accompanied by a significant increase of the oscillations amplitude can be seen. For the 550 nm excitation wavelength, an additional shoulder can be seen in the steep signal increase. In the measurements with longer decay times, the strong increase of the initial NLO is also present and a decay of the additional part for the higher excitation energies compared to the measurement with 610 nm, which show no significant decay, could be detected. From a fit with two independent exponential decay functions convoluted with the Gaussian excitation, the following timescales were extracted: For 610 nm only one exponential function with a decay time of 700±200 ps, which is similar to the decay time of the pure DIP film of 680±110 ps, was used. For 580 nm, the additional feature starts to rise and in addition to the 700±200 ps a second decay is needed. The decay time is 7530±670 fs. For 550 nm the additional decay time becomes 5310±210 fs. The long decay time can be observed for all excitations and its amplitude stays at similar signal levels.

For the excitation with 550 nm, not only the rise of the initial NLO signal change takes place, but a new ultrashort feature was also detected with s-polarized measurements (see figure 4.21c). For the other excitations this feature is not visible and the s-polarized measurements look exactly like a superposition of the two single films. In comparison to the high intensity feature on DIP/PDIR-CN_2 discussed in section 4.5.2, it clearly shows a dependence on the polarization of the probe beam and not on the mixture of pump and probe polarization. Furthermore, it is asymmetric and has a decay time of 45±4 fs (compare figure 4.21d and figure 4.19d). Therefore it is assumed to be based on an excitation of the bilayer and not a coherent wave mixing of pump and probe beam.

Combining the results from the PDIR-CN_2/DIP (LT) bilayer, it could be possible that for this configuration, the CT-exciton formation and a decay (maybe separation) of the excitons can be seen. The high signal increase with increasing pump energy mirrors the increase of the higher vibronic feature detected in the single PDIR-CN_2 layer (compare

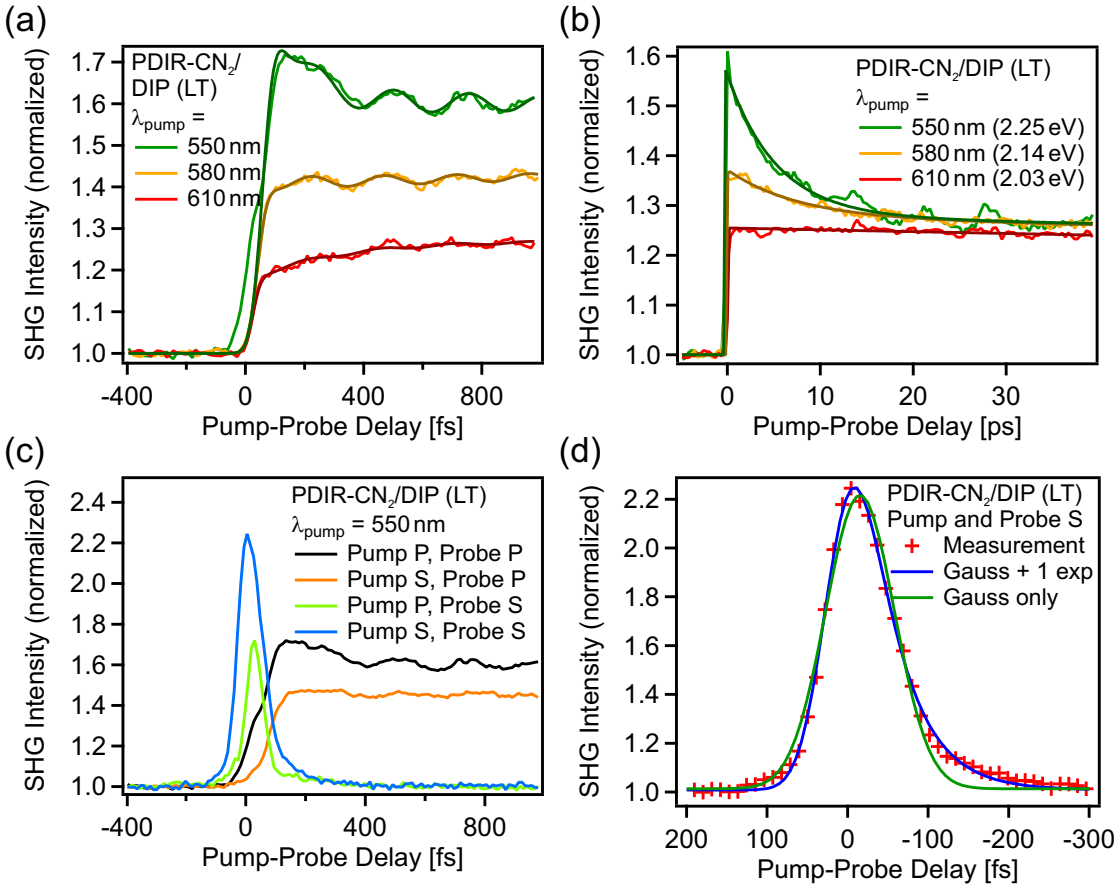

Figure 4.21: Detailed measurements of the bilayer PDIR-CN_2 on DIP (LT). (a)+(b) TR-SHG trace dependence of the pump wavelength for a pump-probe delay of up to 1 ps (a) and of up to 40 ps (b). (c) Signal dependence on pump and probe polarization. (d) Fit of the high intensity feature for both beams s-polarized and 550 nm excitation wavelength.

section 4.4), but with a much higher NLO contrast and longer decay times. The higher NLO contrast could be explained by the coherent formation of CT states at the interface, which could increase the NLO by such a large amount due to the EFISH process (see section 2.1). The decay of the signal on a picosecond timescale is attributed to the charge separation of the CT-states. A decrease of the separation time of CT-states can be explained by the higher amount of excess energy for the higher excitation energy, which supports the charge separation and therefore decreases the separation time [117]. The underlying step is attributed to the charge trapping due to excimer formation as discussed in section 4.3, which still takes place in the DIP film. The ultrafast decay, which is highly visible in the s-polarized measurements and slightly visible in the p-polarized measurements can then be attributed to initial CT-formation process. The final CT-exciton is in this case not visible in the s-polarized measurements, because the electric field, which is the basis of the high amplitude increase, is assumed to be

perpendicular to the interface, because the CT-exciton formation is between a DIP and PDIR-CN_2. To summarize, it is possible to describe the measured data with the ultrafast (45±4 fs) creation of CT-excitons at the interface between DIP and PIDR-CN_2. The CT-formation is based on the higher vibronic excitation of PDIR-CN_2. Neither an influence of the lowest optical excitation of PDIR-CN_2 nor an influence of the excitations in the DIP film could be detected.
In addition to the excited state dynamics and CT-formation, the coherent molecular vibrations are clearly visible for the bilayer (see figure 4.21a) discussed here. Especially the increase with increasing excitation energy as discussed in section 4.6 is very prominent here.

4.6 Oscillations

In the measurements of the PDIR-CN_2 films, an oscillating part of the signal was detected (see figure 4.12). Additionally, a deeper investigation in regard of an oscillating behavior of the measurements of DIP showed a very small oscillating part, which is in the order of magnitude of the noise and therefore not significant. Nevertheless the fit with the three-step model expanded by an oscillation was successful and an oscillation frequency could be extracted. In contrast to the DIP film, a significant oscillations amplitude could be observed on DIP (LT). An important side note for the interpretation of the oscillations given later is that during the measurements of the DIP (LT) film, the laser pulses were shorter compared to the pulses used for investigating the DIP film. The FWHM of a single pulse was 55±3 fs for the measurements on DIP and 39±2 fs for the measurements on DIP (LT). In addition to the single layer, the oscillations were measured on all three bilayer configurations. The bilayer PDIR-CN_2/DIP is discussed here as a representative for the bilayer films. Figure 4.22 shows the oscillations on PDIR-CN_2, on the bilayer, and on the two DIP films for all excitation energies. The resulting oscillation periods and corresponding frequencies and energies are summarized in table 4.1.
For PDIR-CN_2 the oscillations have a period of 271±2 fs, which corresponds to an oscillation frequency of 123±1 cm^{-1} and for DIP (independent of the preparation) the period is 247±3 fs, which corresponds to an oscillation frequency of 135±2 cm^{-1}. For the bilayer a separation of the two different oscillation periods coming from PDIR-CN_2 and DIP could not be done, because of the low amplitude of oscillations, the low signal to noise ratio and the low difference between the two oscillation periods of the two single materi-

Table 4.1: Measured oscillation periods and corresponding frequencies and energies of the molecular vibrations determined by fitting the TR-SHG data.

Sample	Period [fs]	Frequency [cm^{-1}]	Energy [meV]
DIP	247±3	135±2	16.7±0.2
PDIR-CN_2	271±2	123±1	15.3±0.1
PDIR-CN_2/DIP	263±15	127±8	15.7±1

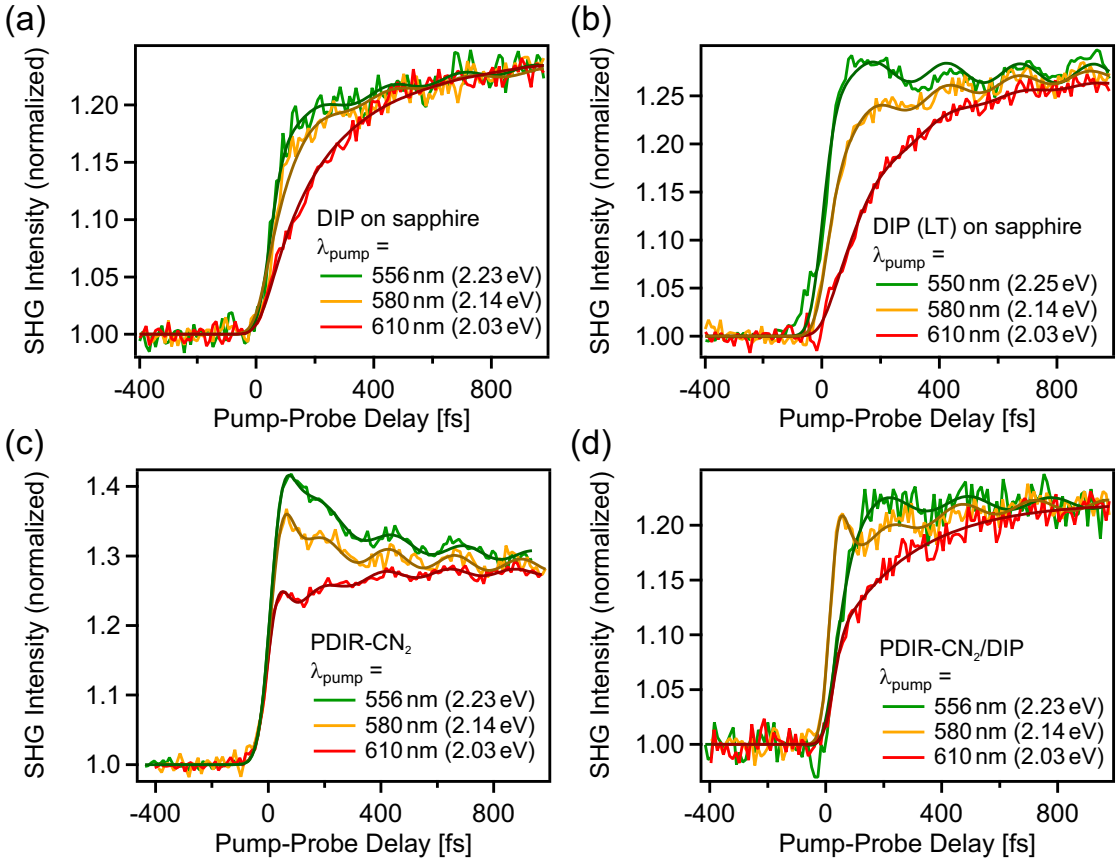

Figure 4.22: Overview over all spectroscopic TR-SHG measurements overlaid with the corresponding models including oscillations for the four systems: (a) DIP, (b) DIP (LT), (c) PDIR-CN_2, and (d) PDIR-CN_2/DIP bilayer

als. A fit with one oscillating component led to an oscillation period of 263±15 fs and an oscillation frequency of 127±8 cm^{-1}. This value can be interpreted as the superposition of the two values from the single layers, which is created by modeling the results with only one oscillation.

To get deeper insights into the physical nature of the oscillations, the dependence of the oscillations on the pump energy and the pump intensity was investigated. For the single materials, no significant dependence on the oscillation period by the pump wavelength could be detected. Therefore, it is assumed that the oscillations period is independent of the pump energies used here. For the bilayer, a high deviation is created by the different excitation energies. The oscillation period shifts from 246±3 fs for the excitation at 610 nm to 269±3 fs for the excitation at 550 nm. This shift can be explained by the shift from a dominant DIP-like behavior for low excitation energies to a PDIR-CN_2-like behavior for high excitation energies as discussed in section 4.5.1. An assignment to the period of the oscillations measured on the bilayer is therefore not reasonable. Furthermore, no change of the period of the oscillations dependent on the

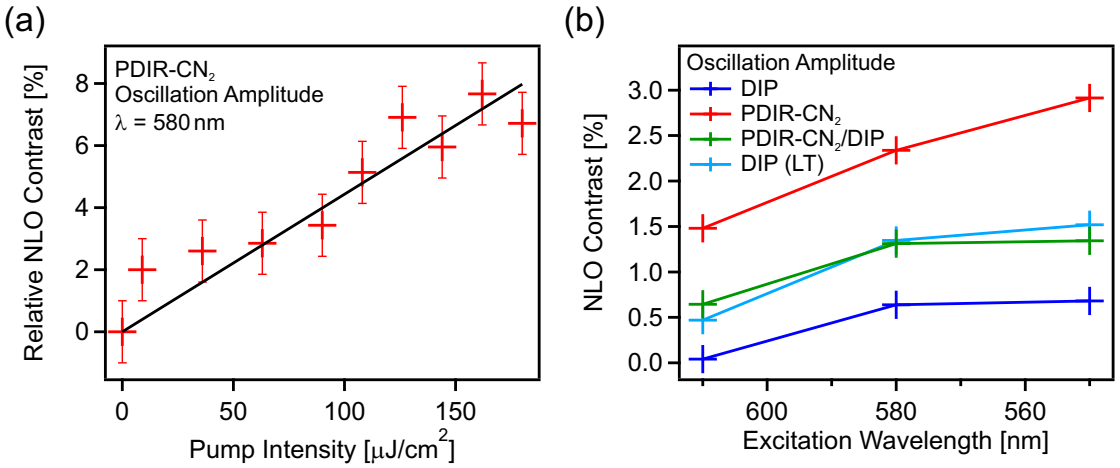

Figure 4.23: Dependence of the amplitude of the oscillations on pump intensity and pump wavelength. (a) Pump intensity dependence for the example of PDIR-CN_2 pumped with 580 nm. (b) Excitation wavelength dependence for the four systems

pump intensity was detected for any of the samples.

In contrast to the period of the oscillations, the amplitude shows a strong dependence on the excitation energy and on the pump intensity. Figure 4.23 depicts the dependence of the oscillation amplitude on PDIR-CN_2 on the pump intensity at 580 nm and the connection between the excitation wavelength and the oscillation amplitude for all four samples. First of all, the amplitude of the oscillations scales linearly with increasing pump intensity. Here, the amplitudes were calculated from the normalized TR-SHG measurements and set in correlation to the signal amplitudes. Therefore the shown linear increase is independent of the amplitude behavior of the signal amplitude of the different feature discussed in section 4.4. For the electronic excitations, a saturation of the signal amplitude was detected, this is not the case for the oscillation amplitude of the TR-SHG signal of PDIR-CN_2. Increasing the excitation energy and thereby the absorption cross-section of the samples (see figure 4.11b) investigated here has also led to an increase of the oscillation amplitudes (see figure 4.23b). Because of the non-existent change in the oscillation period, the amplitude increase due to the higher excitation energies is assigned to the higher absorption cross-section and therefore interpreted as the same effect as the increase due to the higher pump intensity.

One more important information is the damping of the oscillations with pump-probe delay. In the time-resolved measurements for a time window of 1 ps, no significant damping could be detected. For longer time windows the resolution of the measurements is not ideal to resolve the oscillations. For PDIR-CN_2 the measurements for higher pump intensities and pump-probe delays of 2.2 ps were summed up and fitted. From this fit a damping of 1200±600 fs was calculated. For the other samples, fits with similar damping times describe the measured TR-SHG curves very well. Therefore a damping of roughly 1200 fs is reasonable for all samples and was used in the models to calculate the oscillation periods and amplitudes above.

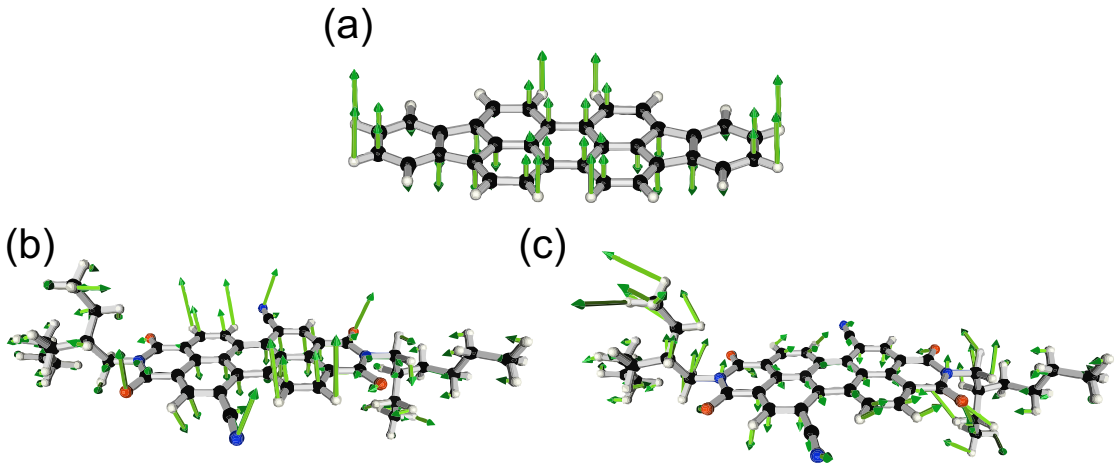

Figure 4.24: Visualization of the low-frequency vibrational modes calculated with DFT using the B3LYP functionals and the 6-311G basis set of DIP and PDIR-CN_2. (a) Short axis buckling mode of DIP at 137 cm^{-1}. (b) Long axis buckling mode of PDIR-CN_2 at 113 cm^{-1}. (c) Twisting motion around molecular center of PDIR-CN_2 at 121 cm^{-1}.

Based on the observations above, the oscillations can be explained by an coherent excited-state wave packet motion of the molecular core of the molecules [168–171]. There are two limitations to the spectral range of the measured coherent oscillations. The first one is that it is in principle only possible to excite an oscillation coherently with a pulse, which is shorter than the period of the oscillation [170]. Secondly, the oscillation amplitudes of high frequency oscillations are attenuated significantly by the limited time resolution [171], which reduces the measured amplitudes. Therefore it is not possible to measure oscillations with high frequencies with the setup used here with a pump and probe time limitation of roughly 40 fs. As mentioned before, the DIP (LT) sample was investigated with a higher time resolution than the DIP sample and it is assumed that the film structure of the two films is very similar, but on DIP (LT) much higher oscillation amplitudes were measured. For a coherent molecular oscillation, this difference in amplitude could be explained by the higher time resolution reducing the signal attenuation and leading to higher coherence during the excitation. The higher amplitudes on PDIR-CN_2 could be explained by the higher extinction coefficient of PDIR-CN_2 compared to DIP in the investigated excitation regime and by a different cross-section to excite the oscillation as well as a different sensibility of the second order susceptibility to the oscillations.

Gas phase density functional calculations (DFT) of energetically relaxed single molecules of DIP and PDIR-CN_2 were done with the Gaussian 09 program package [172]. For the calculations, the functional B3LYP and the 6-311G basis set were used. Based on these calculations, a rudimentary attribution of the oscillations to vibrational modes of single molecules were done. The oscillation of the TR-SHG signal of DIP with the frequency of 135±2 cm^{-1} is attributed to the short axis buckling mode (DFT: 137 cm^{-1}), which is the dominant mode in that frequency domain. For PDIR-CN_2 two major oscillations were found by the calculations in the range of the signal oscillation of 123±1 cm^{-1}: The

first one is the long axis buckling mode (DFT: 113 cm^{-1}) which is mostly generated by the perylene core. The second one is a kind of twisting motion around the molecular center (DFT: 121 cm^{-1}) which corresponds very well to the measured oscillation, but involves a large displacement of the side chains, which could be a hindrances in the crystal structure. Figure 4.24 visualizes all mentioned vibrational modes based on the results of the DFT calculations. For a more precise attribution, further calculations incorporating the crystal structure and neighboring molecules are necessary. For similar molecules it has been shown that it is possible to resolve such low-lying stretching motions of the C-C bonds with ultrafast time-resolved broadband pump/probe spectroscopy [170].

4.7 Discussion

In summary, the high sensitivity to electronic excitations and the femtosecond time resolution of TR-SHG were used to investigate the optically induced electronically excited state dynamics of the two organic semiconductors, namely DIP and PDIR-CN_2, as well as the interactions between DIP and silicon oxide. Furthermore, the interactions at the interface between DIP and PDIR-CN_2 in three different bilayer configurations were analyzed. Polarization-resolved measurements were utilized to separate different signal contributions and enabled the assignment of different processes, especially in DIP on silicon oxide compared to intrinsic processes in DIP. A clear separation of an ultrafast feature in PDIR-CN_2 was achieved by pump intensity-resolved measurements. In addition, spectroscopic measurements were used to identify different excited species in both materials.

For the investigations of DIP two different substrates were used: sapphire and silicon oxide. It is assumed that DIP exhibits very similar films on both substrates [120]. On sapphire, the intrinsic excited state dynamics after optical excitation were investigated, whereas on silicon oxide the focus of the investigations lay on the interaction between DIP and the substrate. Especially the influence of trap states in the silicon oxide, which lie in the energetic range of the first electronically excited state of DIP [133, 142], were of significance. The ultrafast excited state dynamics on a sub picosecond timescale for DIP had not been investigated before. The conclusion drawn based on the investigations is that in DIP the initial excitation is highly delocalized and can only be detected indirectly by the TR-SHG measurements because it leads to no detectable change in the second-order susceptibility. Afterwards the relaxation of the initial excitation into molecular excitons in the vibronical ground state takes place on a timescale of 140±60 fs for off-resonant excitations. The relaxation time can be largely reduced to 19±30 fs using a resonant excitation energy. On a timescale of 471±100 fs, excimer states are formed and dimers are created in the DIP film. This result very well-matches those of earlier investigations with time-resolved transient absorption measurements, which have set an upper limit of 1 ps for the excimer formation [125]. However, a slightly different assignment based on recent simulations with a different approach in the calculations has to be considered. In these the initial relaxation (A to B) is already into a CT-state,

delocalized over a dimer of DIP molecules, and the second transfer is into a lower-lying excited dimer state with Frenkel character. A clear attribution to one of the two models can not be given based on the TR-SHG results. After the initial relaxation, the excimer states (independent of CT or Frenkel character) decay in a few hundred picoseconds back to non-excited single molecules. Both effects, the reduction of the relaxation time and the excimer build up time are important, as both effects could limit the CT-state formation at the interface to acceptor molecules. Cooling the sample during evaporation and therefore introducing more disorder into the DIP thin film, does not fundamentally change the ultrafast dynamics. The excimer formation time is even slightly reduced compared to the more ordered film. Introducing trap states through a silicon oxide interface leads to a suppression of the excimer formation, by trapping the excited electrons on a timescale of 207±95 fs which is even faster than the excimer formation. Afterwards, no decay of the trapped species could be detected. Furthermore, an additional ultrafast feature was found for DIP on silicon oxide, that is probably due to an excitation in the silicon film, which undergoes momentum relaxation on a timescale of roughly 30 fs [152] and is therefore independent of the excited state dynamics in the DIP layer.
For the application of DIP in organic electronics, two important conclusions can be drawn from the results discussed above. First, the influence of silicon oxide to the DIP layer in particular and organic thin films in general has to be taken into account for the excited state dynamics, even if silicon oxide is treated as a non-interacting substrate for the non-excited molecules. This thesis showed that the charge transfer to trap states in silicon oxide takes place on a timescale of 200 fs, which is on the timescale of charge transport processes in organic semi-conducting films. This can explain the efficient suppression of charge transport in organic field effect transistors with silicon oxide as the gate dielectric [133]. Second, the ultrafast formation of excimer species in the DIP film on a timescale of 500 fs has to be considered in the application of DIP as an active material in solar cells, because the excimer formation can act as charge trapping and therefore reduce the efficiency. It also reduces the energy stored in the excitation and thus lowers the overall efficiency of the device. Because of this, it is possible that, due to the excimer formation, the CT-exciton generation becomes energetically unfavorable. The excimer formation is intrinsic to the organic thin film and depends on the morphology of the film. Therefore any introduced change in the morphology, which hinders the dimer formation, could suppress the excimer formation and improve the functionality of DIP as an active material in a photovoltaic device.

The intrinsic properties of a PDIR-CN_2 film were examined. In contrast to DIP, on PDIR-CN_2, the initial excitation could be measured with TR-SHG. For higher excitation energies, a second higher vibronic excitation of S1 was excited and the dynamics were measured. Both vibronic excitations decay to the relaxed molecular exciton, the lower one on a timescale of 131±25 fs and the higher one in 369±25 fs. Afterwards a decay back to the non-excited state on a timescale of 62.4±1.8 ps was detected. Furthermore, an ultrafast component, which showed the largest signal contribution for the resonant excitation with 580 nm and a decay time of 20±10 fs, was measured. This excitation is

attributed to a polarization of the molecules due to the resonant excitation at 580 nm. Despite having the same molecular perylene core, the excited state differs completely from that of DIP. No excimer formation takes place due to the large side groups, which changes the structure of the thin films and hinders a rearrangement of the molecules to dimers. In contrast to DIP the deexcitation is one order of magnitude faster.
In regard to the application in organic devices the deexcitation time is still reasonably long compared to the ultrafast process of charge transfer at the donor/acceptor interface. The relaxation times of the initial vibronic excitations are more important because based on recent experiments [173] a high influence on the CT-exciton formation at the donor/acceptor interface is attributed to the vibronically excited states. It is even discussed that an efficient charge separation depends largely on the excess energy of the hot excitonic states [117]. Here, the relaxation times of 131±25 fs and 369±25 fs have to be considered in the efficiency discussion using PDIR-CN_2 as active material in photovoltaic devices. Except for the initial relaxation of the vibronical excitations, no further relaxations were detected. The work for the present thesis observed the timescales of these relaxation pathways for the first time.

The aim of the investigations of the bilayer systems was to investigate the dynamics of the CT-excimer generation and separation at the interface between DIP and PDIR-CN_2 by exploiting the high interface sensitivity of the SHG signal. Unfortunately, no clear sign of a CT-formation was detected for the PDIR-CN_2/DIP bilayer, but based on deeper investigations, some conclusions about possible interactions between DIP and PDIR-CN_2 after optical excitation can be drawn. First of all, the prominent decay of the TR-SHG signal of the PDIR-CN_2 film is missing in the signal of the bilayer, only the decay behavior of the TR-SHG signal of the DIP film could be detected, which can be taken as a hint of a charge transfer to the DIP layer. Furthermore, the signal of the higher vibronic excitation of PDIR-CN_2 for higher excitation energies is suppressed, while the signal of the ultrafast polarization effect of PDIR-CN_2 is still detected. This could be taken as a hint of a resonant charge transfer from PDIR-CN_2 to DIP for high enough excitation energies, which is not possible for lower excitation energies. Finally, the behavior of the bilayer signal looks like DIP for low pump intensities and like PDIR-CN_2 for high pump intensities, which can again be explained by a charge transfer to the DIP layer until saturation for high pump intensities is reached and then the excitations partly stay in the PDIR-CN_2 layer. Taking these observations into account and assuming a charge transfer from PDIR-CN_2 to the DIP layer or a CT-state at the interface, the new time constant of 198±45 fs, arising from the difference between low and high pump intensities of the TR-SHG traces of the bilayer, can be interpreted as the transfer time for the non-resonant case. The full picture would then be that a energy transfer from PDIR-CN_2 to DIP takes place on 198±45 fs and gets resonant for the higher vibronic excitation. What argues against this interpretation is that usually a large influence to the SHG signal of CT-states at an interface is expected, which was not detected. An explanation could be that due to the standing configuration of both layers, the creation of CT-states is suppressed, because the overlap of the delocalized π-electron systems at the interface is diminutive [48]. Nevertheless an interaction of the excited states of DIP

and PDIR-CN_2 is needed to describe the measured data.

Taking into account the results from the PDIR-CN_2/DIP (LT) bilayer, where a large signal increase was measured for high enough excitation energies, a CT-state generation leading to the build-up of an electric field at the interface becomes a reasonable explanation. In both bilayer films with PDIR-CN_2 on top of DIP, the long decay constant of the excimer species formed in the pure DIP film is present and is not influenced by the bilayer formation, while there was no relaxation of PDIR-CN_2 to be detected. Increasing the excitation energy to the second vibronic feature in PDIR-CN_2 leads to additional effects in both bilayers. On the one hand for the PDIR-CN_2/DIP bilayer an excitation of the second vibronic feature of PDIR-CN_2 is suppressed and for high pump intensities, compared to lower ones, a new time constant of 198±45 fs arises, which is attributed to the transfer of the exciton energy of PDIR-CN_2 to the interface or the DIP film. One the other hand for the PDIR-CN_2/DIP (LT) bilayer the initial signal change increases to more than the doubled amplitude of the expected signal with a decay time of 5310±210 fs accompanied by an intense (up to 130 % NLO contrast) ultrafast decay in the s-polarized measurements on a timescale of 45±4 fs. An explanation for the high signal amplitudes in PDIR-CN_2/DIP (LT) could be the EFISH signal generation by a static electric field at the interface between DIP and PDIR-CN_2, due to CT-state formation. The timescale of 45±4 fs very well fits the CT-state build-up times of 30-45 fs measured on various systems [4, 174–176]. The decay of the signal back to the signal level of pure DIP on a timescale of 5310±210 fs could then be interpreted as the CT-state separation, which became faster for higher excitation energies. In this case, the formation of the CT-states would depend on the excess energy of the higher vibronic excitation in PDIR-CN_2, because the effect is only accomplished for excitation energies where the second excitation is visible in the pure PDIR-CN_2 film. In addition to the excitation energy, the full CT-generation process only takes place on the sample cooled during evaporation, which means that somehow the more lying configuration induced by this procedure is necessary for the CT-state build up. This could for example be due to an increased overlap of the delocalized π-electron system of lying DIP molecules with the PDIR-CN_2 molecules [48]. For the PDIR-CN_2/DIP film this component seems to be missing and instead only a trapping of the excitations of the PDIR-CN_2 at the interface or a transfer to the DIP takes place.

Changing the stacking order of DIP and PDIR-CN_2 results in a full suppression of any interactions between the two films in regard to the excited state dynamics. All spectra could be explained by a superposition of the two single layers. Only as long as both pump and probe pulses overlap in the material system, an additional SHG response was detected, which perfectly mirrors the cross-correlation of the two pulses. The intensity of the additional SHG response strongly depends on the polarization relation between the two pulses. It is therefore assumed that for an unexplained reason, the two waves mediated by the bilayer interact with each other creating a coherent artifact.

For all three systems, the trace of the pure DIP layer seems to be the basis of the bilayer trace, and for long decay times in all systems, the step introduced by the long decay time of the excimer species in DIP remains. Based on this observation, it is assumed that the excitation of DIP does not take part (or at least only to a diminishing degree) in the CT-state formation at the interface to PDIR-CN_2. This effect can be explained one the one hand by the measurements of the pure DIP layer, which showed ultrafast relaxation times for the vibronical excited state, and on the other hand by the excimer formation in DIP. Especially the excimer formation could act as highly efficient charge trapping in regard to the CT-state formation. Figure 4.25 summarizes all proposed excited state dynamics discussed in this thesis.

In regard of an application in solar cells, the system DIP and PDIR-CN_2 empathizes the importance of the interface geometry for efficient solar cells, because a build-up of CT-states at the interface could be only detected in one case. The measurements even showed no influence at all of the interface to the excited state dynamics in the case of DIP on PDIR-CN_2, which could be explained by unfortunate alignment of the side groups of PDIR-CN_2 in this configuration. In addition to the strong geometric influence, the excitation energy seems to play an important role, too. In both films of PDIR-CN_2 on top of DIP, significant interface mediated effects only took place for high enough excitation energies leading to the excitation of a second higher vibronic excitation. Therefore the influence of excess energy on the efficient CT build-up and charge separation has to be kept in mind when choosing donor and acceptor materials.

Independent of the excited electronic state dynamics and interfacial effects oscillations of the TR-SHG signal were detected. Based on the dependence on the pump-pulse intensity and energy of the amplitude and period of these oscillations, an assignment to coherent excited-state wave packet motion of the molecular cores could be done. Furthermore, the measured oscillations could be correlated with vibrational modes of the corresponding molecules calculated by DFT simulations. For DIP an oscillation frequency of $135\pm2\,\mathrm{cm}^{-1}$ was measured and attributed to the short axis buckling mode (DFT: $137\,\mathrm{cm}^{-1}$). For PDIR-CN_2 a oscillation frequency of $123\pm1\,\mathrm{cm}^{-1}$ was measured. DFT simulations identified two different modes: the long axis buckling mode (DFT: $113\,\mathrm{cm}^{-1}$) and a twisting motion around the molecular center (DFT: $121\,\mathrm{cm}^{-1}$). Concerning the bilayers, no clear separation of the oscillations of the single layers could be done.

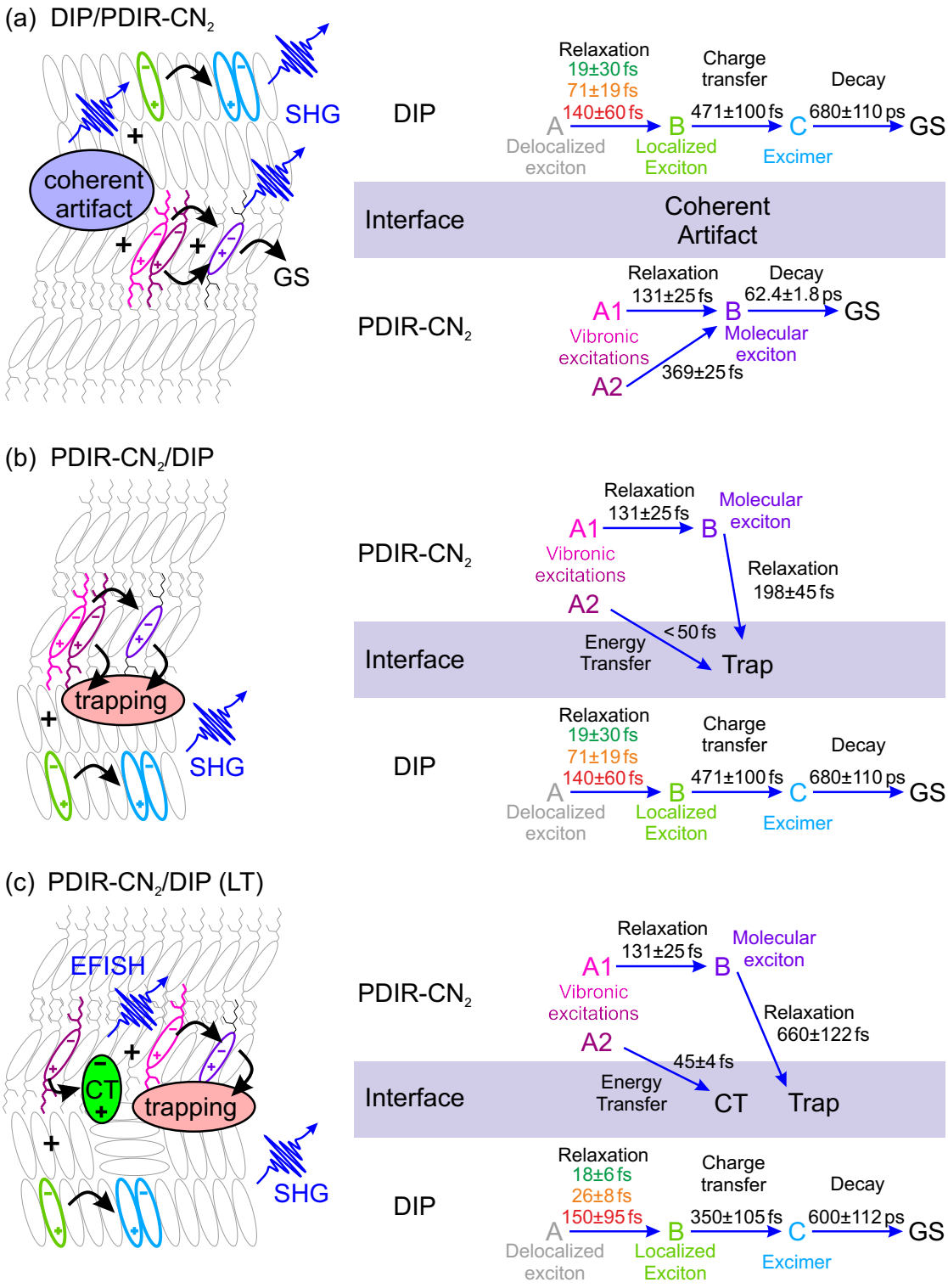

Figure 4.25: Summary of the proposed ultrafast excited state dynamics at the interfaces of the three DIP and PDIR-CN_2 bilayers as discussed in the text

5 Conclusion and Outlook

In the framework of this thesis, two major topics were of interest. The first topic was to evaluate the quality of a new immobilization approach of molecular switches on silicon and the optimization of the non-linear contrast created by the switching process. The other topic was getting a deeper understanding of the ultrafast excited state dynamics of optically excited organic semiconductors. Especially understanding the influence of the excitation energy, the substrate, and interfacial effects at the donor/acceptor interface were of great importance. SHG measurements were used to cover all of these topics. The inherent surface/interface sensitivity of the SHG process and the high influence of delocalized π-electron systems to the SHG process was used to investigate the light-driven ring-opening/ring-closure reaction of a sub-monolayer of fulgimide molecules immobilized on a silicon surface. Furthermore the femtosecond time resolution of the setup combined with the high surface/interface sensitivity was used to investigate the excited state dynamics in organic semiconductors and at donor/acceptor interfaces.

The first topic of the thesis was the investigation of the photochromism of different fulgimide derivatives immobilized by an alkyne linker on the Si(111) surface. This showed the reversible switching between the open- and closed-form for all samples with NLO contrasts of 20-25 %. It even achieved a 33 % NLO contrast for the sample with CH_2 spacer and p-polarized light. Here, the approach of using SHG to distinguish the different molecular states has proven to be very effective. In addition to the closed- and open-form, a third thermally metastable state induced by the high intensity IR-light of the probe beam was observed. All three states could be switched reversibly into each other without any significant signal losses. Based on the polarization resolved measurements and the structures of the different samples, the third state could be assigned to the interaction between the electron donating phenyl ring attached to the fulgimide and the fulgimide itself. This process is independent of the fulgimide derivative and can be suppressed by a CH_2 spacer between the two groups. Furthermore, the thermal stability of the closed-form is decreased by the interaction. Without the CH_2 spacer, the cross-sections of the ring opening/closure reactions are lowered by one order magnitude to 10^{-19}-$10^{-20}\,cm^2$ compared to the molecules in solution or in fully decoupled configurations. In this case, the switching processes into the IR-state have a cross-section of $10^{-23}\,cm^2$. Using the CH_2 spacer regains the thermal stability of the closed-form and increases the cross-sections of the ring-opening/ring-closure reaction by one order of magnitude to $10^{-18}\,cm^2$, corresponding to the level of the decoupled fulgimide molecules. Additionally, the cross-sections for the IR-state are reduced by to two orders of magnitude. A possible assignment of the IR-state is the dipole-form of the molecules, which is stabilized by the electron-donating nature of the phenyl ring directly attached to the

fulgimides. Looking at the thermal decay times of the IR-state supports this interpretation. For the 2-Indolylfulgimide a decay time of 424 s at room temperature was observed. With the CH_2 spacer, the decay time is reduced to 192 s. In the final step, the polarization-dependent NLO contrasts were measured and compared with DFT calculations of the hyperpolarizability of the fulgimides. Based on these comparisons the orientation of the fulgimides on the surface could be determined. Without the CH_2 spacer the long axis of the fulgimides is mostly oriented perpendicular to the surface. Introducing the CH_2 spacer leads to a higher degree of freedom of the orientation of the fulgimides and they rotate to a nearly parallel configuration.

Applying these results to the further development of new photonic devices leads to several conclusions. First of all, SHG has proven to be a method which can deliver high contrast between the photochromic states, especially when the electronic structure is changed by the switching process like it is in fulgimides. A further increase of the NLO contrast might be achieved by reducing the background signal coming from the linker group and the substrate. An alternative coupling unit for the phenyl ring without a delocalized electron system could be helpful for increasing the NLO contrast significantly. Secondly, the thesis at hand showed that an electron-donating linker group is unfavorable for the immobilization of the fulgimides. Based on that observation, there needs to be caution in designing the linker group in a way that the functionality of the fulgimides is not influenced. Another possibility could be that the third state is used to increase the range of applications of the fulgimides. For this a three level storage with added functionality is imaginable, if all three states could be made thermally stable by the molecular design.

The second major topic of this thesis was the investigation of the ultrafast dynamics of optical excited electronic states in organic semiconductors and at donor/acceptor interfaces. This made use of the time resolution of the setup of better than 50 fs and the high sensitivity to surfaces/interfaces.
The organic semiconductor diindenoperylene (DIP) was investigated on two substrates: sapphire and silicon oxide. On sapphire, two DIP films prepared with different substrate temperatures during evaporation were examined. In the DIP films on sapphire, an ultrafast localization of the initially delocalized excited states on a timescale of 20-140 fs, depending on the excitation energy, were observed. For more resonant excitation energies the localization time gets shorter. After localization, dimer generation accompanied by a charge transfer into a excimer like state was discovered. From a theoretical point of view, the nature of this dimer-induced state is presently under lively discussion. Therefore both cases of charge-transfer or Frenkel-like behaviour were considered. Finally, the excited molecules relax into their non-excited form on a timescale of roughly 700 ps. The general process is independent of the substrate temperature during evaporation of the DIP, only the charge transfer time into the dimer state is reduced due to the increased disorder in the film evaporated on a cold substrate. Using silicon with a native oxide layer as a substrate significantly changes the excited state dynamics. The silicon oxide has a high amount of trap states at the surface, which energetically lie below the excited states in

DIP, which leads to an ultrafast charge trapping on a timescale of 200 fs. This process suppresses the dimer formation observed in DIP on sapphire. Furthermore, there was an additional substrate-mediated ultrafast decaying excitation, which is accredited to momentum relaxation in the substrate.
The case of the perylene derivative n,n'-bis-(2-ethylhexyl)-1,7-dicyanoperylene-3,4:9,10-bis(dicarboximide) (PDIR-CN_2) dependent on the excitation energy showed the excitation of two different vibrational sub-levels of the first electronic excitation and their relaxation times into the vibronic ground state. According to the measurements, the lower excitation led to a relaxation time of 130 fs, and the higher excitation to one of 370 fs. Afterwards the molecules relax into the ground state in 62 ps. Furthermore, a polarization of the PDIR-CN_2 could be observed. The polarization is resonantly excited with 580 nm and decays on a timescale of 20 fs.
Combining DIP and PDIR-CN_2 in different bilayer configurations with the aim to investigate the CT formation at the interface in regard to possible applications in organic solar cells led to the observation of additional effects. For the stack DIP/PDIR-CN_2, no interaction of the excited states of DIP and PDIR-CN_2 was noticeable. Changing the stacking order and thereby increasing the disorder of the system led to a trapping of the excited states of PDIR-CN_2 at the interface. A dependence of the process on the excitation energy could be observed. For the higher excitation energy, the process is nearly coherent with the excitation and directly driven from the hot excited state, while for the lower excitation the relaxation into the vibronic ground state takes place first, followed by the transfer into the surface-induced state on a timescale of 200 fs takes place. Finally by increasing the disorder at the interface even more due to evaporation of DIP on a cold substrate and then evaporating PDIR-CN_2 on top, the build-up of CT-states at the interface could be achieved. The CT-generation is in this context depends on a high enough excitation energy, driven by the PDIR-CN_2 and takes place on a timescale of 45 fs. Lower excitation energies still showed a trapping at the interface. All bilayer systems exhibited no interaction of the excitation of the DIP film with the PDIR-CN_2 layer. Here, the ultrafast relaxation combined with the trapping into dimer states could be a reason for the suppression of any interaction with PDIR-CN_2.
In all systems, independent of single materials or bilayer systems, the coherent excitation of vibrational modes of the molecular cores could be achieved. In DIP the short axis buckling mode (137 cm^{-1}) could be observed and PDIR-CN_2 probably showed a mixture of the long axis buckling mode (113 cm^{-1}) and a twisting motion around the molecular center (121 cm^{-1}). It was determined that the amplitude of the oscillations of the TR-SHG signal depends on the excitation energy and on the time resolution of the pump-pulse. Higher excitation energies and shorter pump-pulses lead to higher oscillation signals.

Regarding future applications the results allow for a few conclusions to be drawn. Based on the results of the DIP films, the possibility of dimer formation as a relaxation channel was experimentally shown on ultrafast timescales. The dimer formation can act as trapping of the charge carriers in this and suppress further processes like charge transport or CT-formation. For applications in organic devices with DIP as a functional layer, a

suppression of the dimer formation by side groups could lead to a significant increase in efficiency and dimer formation has to be considered in general for similar molecules. The ultrafast excited state trapping in the silicon oxide is of significant importance in organic field effect transistors, where silicon oxide is usually used as gate electrode. For this, an isolation between the excited DIP layer and the silicon oxide is needed. The results of the bilayer systems show the importance of the molecular orientation at the interface. It is not enough to align the energetic level of the two materials, because the overlap of the delocalized π-electron systems at the interface is of high importance, too. It was shown in this context that for the simple case of stacking DIP and PDIR-CN_2 onto each other no CT-generation could be achieved, due to the inappropriate molecular orientation of the molecules in regard to CT-formation. The necessity of creating lying areas of molecules in order to allow a measurable amount of CT-generation was proven. Furthermore, the thesis led to the observation of a dependence of the CT-generation on the excess energy of the excited states in PDIR-CN_2, which has to be considered when designing solar cells.

Bibliography

[1] Browne, W. R.; Feringa, B. L. Light Switching of Molecules on Surfaces. *Annu. Rev. Phys. Chem.* **2009**, *60*, 407–428.

[2] Zhang, J.; Zou, Q.; Tian, H. Photocromic Materials: More Than Meets The Eye. *Adv. Mater* **2013**, *25*, 378–399.

[3] Gust, D.; Andréasson, J.; Pischel, U.; Moore, T. A.; Moore, A. L. Data and signal processing using photochromic molecules. *Chem. Commun.* **2012**, *48*, 1947–1957.

[4] Brabec, C. J.; Sariciftci, N. S.; Hummelen, J. C. Plastic Solar Cells. *Adv. Funct. Mater.* **2001**, *11*, 15–26.

[5] Gregg, B. A. Excitonic Solar Cells. *J. Phys. Chem. B* **2003**, *107*, 4688–4698.

[6] Hoppe, H.; Sariciftci, N. S. Organic solar cells: An overview. *J. Mater. Res.* **2004**, *19*, 1924–1945.

[7] Clarke, T. M.; Durrant, J. R. Charge Photogeneration in Organic Solar Cells. *Chem. Rev.* **2010**, *110*, 6736–6767.

[8] Chan, W.-L.; Ligges, M.; Jailaubekov, A.; Kaake, L.; Miaja-Avila, L.; Zhu, X.-Y. Observing the Multiexciton State in Singlet Fission and Ensuing Ultrafast Multi-electron Transfer. *Science* **2011**, *334*, 1541–1545.

[9] Jailaubekov, A. E.; Willard, A. P.; Tritsch, J. R.; Chan, W.-L.; Sai, N.; Gearba, R.; Kaake, L. G.; Williams, K. J.; Leung, K.; Rossky, P. J.; Zhu, X.-Y. Hot charge-transfer excitons set the time limit for charge separation at donor/acceptor interfaces in organic photovoltaics. *Nat. Mater.* **2013**, *12*, 66–73.

[10] Wu, X.; Park, H.; Zhu, X.-Y. Probing Transient Electric Fields in Photoexcited Organic Semiconductor Thin Films and Interface by Time-Resolved Second Harmonic Generation. *J. Phys. Chem. C* **2014**, *118*, 10670–10676.

[11] Shen, Y. R. Surface studies by optical second harmonic generation: An overview. *J. Vac. Sci. Technol. B* **1985**, *3*, 1464–1466.

[12] Guyot-Sionnest, P.; Chen, W.; Shen, Y. R. General considerations on optical second-harmonic generation from surfaces and interfaces. *Phys. Rev. B* **1986**, *33*, 8254–8263.

[13] Shen, Y. R. Surface properties probed by second -harmonic and sum-frequency generation. *Nature* **1989**, *337*, 519–525.

[14] Shen, Y. R. Surface probed by nonlinear optics. *Surf. Sci.* **1993**, *299/300*, 551–562.

[15] McGilp, J. F. A review of optical second-harmonic and sum-frequency generation at surfaces and interfaces. *J. Phys. D: Appl. Phys.* **1996**, *29*, 1812–1821.

[16] Wang, J.-P. Magnetic Data Storage Tilting for the top. *Nat. Mater.* **2005**, *4*, 191–192.

[17] Kawata, S.; Kawata, Y. Three-Dimensional Optical Data Storage Using Photochromic Materials. *Chem. Rev.* **2000**, *100*, 1777–1788.

[18] Liang, Y.; Dvornikov, A. S.; Rentzepis, P. M. A novel non-destructible readout molecular memory. *Opt. Commun.* **2003**, *223*, 61–66.

[19] Dvornikov, A. S.; Liang, Y.; Cruse, C. S.; Rentzepis, P. M. Spectroscopy and Kinetics of a Molecular Memory with Nondestructive Readout for Use in 2D and 3D Storage Systems. *J. Phys. Chem. B* **2004**, *108*, 8652–8658.

[20] Walz, J.; Ulrich, K.; Port, H.; Wolf, H. C.; Wonner, J.; Effenberger, F. Fulgides as switches for intramolecular energy transfer. *Chem. Phys. Lett.* **1993**, *213*, 321–324.

[21] Straight, S. D.; Liddell, P. A.; Terazono, Y.; Moore, T. A.; Moore, A. L.; Gust, D. All-Photonic Molecular XOR and NOR Logic Gates Based on Photochemical Control of Fluorescence in a Fulgimide-Porphyrin-Dithienylethene Triad. *Adv. Funct. Mater.* **2007**, *17*, 777–785.

[22] Stobbe, H. Die farbigen Anhydride der Butadiën-β, γ-dicarbonsäuren; ihr Verhalten gegen Licht und Wärme. (II. Abhandlung ber Butadiënverbindungen.). *Ber. Dtsch. Chem. Ges.* **1904**, *37*, 2236–2240.

[23] Hartley, G. S. The *Cis*-form of Azobenzene. *Nature* **1937**, *140*, 281.

[24] Cordes, T.; Herzog, T. T.; Malkmus, S.; Draxler, S.; Brust, T.; DiGirolamo, J. A.; Lees, W. J.; Braun, M. Wavelength and solvent independent photochemistry: the electrocyclic ring-closure of indolylfulgides. *Photochem. Photobiol. Sci.* **2009**, *8*, 528–534.

[25] Liang, Y.; Dvornikov, A. S.; Rentzepis, P. M. Solvent and ring substitution effect on the photochromic behavior of fluorescent 2-indolylfulgide derivates. *J. Photochem. Photobio.* **1999**, *125*, 79–84.

[26] Comstock, M. J.; Levy, N.; Kirakosian, A.; Cho, J.; Lauterwasser, F.; Harvey, J. H.; Strubbe, D. A.; Fréchet, J. M. J.; Trauner, D.; Louie, S. G.; Crommie, M. F. Reversible Photomechanical Switching of Individual Engineered Molecules at a Metallic Surface. *Phys. Rev. Lett.* **2007**, *99*, 038301.

[27] Zhuang, X.; Lackritz, H. S.; Shen, Y. R. Photo-isomerization of polymer monolayers and multi-layers on water. *Chem. Phys. Lett.* **1995**, *246*, 279–284.

[28] Manzo, C.; Savoia, A.; Paparo, D.; Marrucci, L. Photoinduced Dynamics of Azobenzene Dyes in Langmuir Films Investigated by Optical Second Harmonic Generation. *Mol. Cryst. Liq. Cryst.* **2006**, *454*, 91/[493]–100/[502].

[29] Seki, T.; Sakuragi, M.; Kawanishi, Y.; Suzuki, Y.; Tamaki, T. Command Surfaces of Langmuir-Blodgett Films. Photoregulations of Liquid Crystal Alignment by Molecularly Tailored Surface Azobenzene Layers. *Langmuir* **1993**, *9*, 211–218.

[30] Rück-Braun, K.; Petersen, M. A.; Michalik, F.; Hebert, A.; Przyrembel, D.; Weber, C.; Ahmed, S. A.; Kowarik, S.; Weinelt, M. Formation of Carboxy- and Amide-Terminated Alkyl Monolayers on Silicon(111) Investigated by ATR-FTIR, XPS, and X-ray Scattering: Construction of Photoswitchable Surfaces. *Langmuir* **2013**, *29*, 11758–11769.

[31] Maurer, R. J.; Reuter, K. Bistability Loss as a Key Feature in Azobenzene (Non-)Switching on Metal Surfaces. *Angew. Chem. Int. Ed.* **2012**, *51*, 12009–12011.

[32] Dulić, D.; van der Molen, S. J.; Kudernac, T.; Jonkman, H. T.; de Jong, J. J. D.; Bowden, T. N.; van Esch, J.; Feringa, B. L.; van Wees, B. J. One-Way Optoelectronic Switching of Photochromic Molecules on Gold. *Phys. Rev. Lett.* **2003**, *91*, 207402.

[33] Piantek, M.; Schulze, G.; Koch, M.; Franke, K. J.; Leyssner, F.; Krüger, A.; Navó, C.; Miguel, J.; Bernien, M.; Wolf, M.; Kuch, W.; Tegeder, P.; Pascual, J. I. Reversing the Thermal Stability of a Molecular Switch on a Gold Surface: Ring-Opening Reaction of Nitrospiropyran. *J. Am. Chem. Soc.* **2009**, *131*, 12729–12735.

[34] Hagen, S.; Leyssner, F.; Nandi, D.; Wolf, M.; Tegeder, P. Reversible switching of tetra-*tert*-butyl-azobenzene on a Au(111) surface induced by light and thermal activation. *Chem. Phys. Lett.* **2007**, *444*, 85–90.

[35] Rau, H. In *Photochromism: Molecules and Systems*; Dürr, H., Bouas-Laurent, H., Eds.; Elsevier, Amsterdam, 1990.

[36] Goldschmidt, S.; Riedle, R.; Reichardt, A. Über die Bisdiphenylenfulgide und die Spaltung der Bisdiphenylenfulgensäure in Optisch Aktive Komponenten. *Liebigs Ann. Chem.* **1957**, *604*, 121–132.

[37] Liang, Y.; Dvornikov, A. S.; Rentzepis, P. M. Synthesis of novel photochromic fluorescing 2-indolylfulgimides. *Tetrahedron Lett.* **1999**, *40*, 8067–8069.

[38] Liang, Y.; Dvornikov, A. S.; Rentzepis, P. M. Synthesis and photochemistry of photochromic fluorescing indol-2-ylfulgimides. *J. Mater. Chem.* **2000**, *10*, 2477–2482.

[39] Dirk, C. W.; Twieg, R. J.; Wagniére, G. The Contribution of π Electrons to Second Harmonic Generation in Organic Molecules. *J. Am. Chem. Soc.* **1986**, *108*, 5387–5395.

[40] Kippelen, B.; Brédas, J.-L. Organic photovolatics. *Energy Envir. Sci.* **2008**, *2*, 251–261.

[41] Bakulin, A. A.; Rao, A.; Pavelyev, V. G.; van Loosdecht, P. H. M.; Pshenichnikov, M. S.; Niedzialek, D.; Cornil, J.; Beljonne, D.; Friend, R. H. The Role of Driving Energy and Delocalized States for Charge Separation in Organic Semiconductors. *Science* **2012**, *16*, 1340–1344.

[42] Cros, S.; de Bettignies, R.; Berson, S.; Bailly, S.; Maisse, P.; Lemaitre, N.; Guillerez, S. Definition of encapsulation barrier requirements: A method applied to organic solar cells. *Sol. Energy Mater. Sol. Cells* **2011**, *95*, S65–S69.

[43] Nunzi, J.-M. Organic photovoltaic materials and devices. *C. R. Phys.* **2002**, *3*, 523–542.

[44] Kozma, E.; Catellani, M. Perylene diimides based materials for organic solar cells. *Dyes Pigm.* **2013**, *98*, 160–179.

[45] Tripathi, A. K.; Pflaum, J. Correlation between ambipolar transport and structural phase transition in diindenoperylene single crystals. *Appl. Phys. Lett.* **2006**, *89*, 082103.

[46] Sellner, S.; Gerlach, A.; Schreiber, F.; Kelsch, M.; Kasper, N.; Dosch, H.; Meyer, S.; Pflaum, J.; Fischer, M.; Gompf, B. Strong Enhanced Thermal Stability of Crystalline Organic Thin Films Induced by Aluminium Oxide Capping Layers. *Adv. Mater.* **2004**, *16*, 1750–1753.

[47] Würthner, F. Perylene bismide dyes as versatile building blocks for functional supramolecular architectures. *Chem. Commun.* **2004**, 1564–1579.

[48] Aghamohammadi, M.; Fernández, A.; Schmidt, M.; Pérez-Rodríguez, A.; Goñi, A. R.; Fraxedas, J.; Sauthier, G.; Paradinas, M.; Ocal, C.; Barrena, E. Influence of the Relative Molecular Orientation on Interfacial Charge-Transfer Excitons at Donor/Acceptor Nanoscale Heterojunctions. *J. Phys. Chem. C* **2014**, *118*, 14833–14839.

[49] Nelson, C. A.; Monahan, N. R.; Zhu, X.-Y. Exceeding the Shockley-Queisser limit in solar energy conversation. *Energy Environ. Sci.* **2013**, *6*, 3508–3519.

[50] Balzani, V.; Ceroni, P.; Juris, A. *Photochemistry and Photophysics*; Wiley-VCH: Weinheim, 2014.

[51] Settels, V.; Schuber, A.; Tafipolski, M.; Liu, W.; Stehr, V.; Topczak, A. K.; Pflaum, J.; Deibel, C.; Fink, R. F.; Engel, V.; Engels, B. Identification of Ultrafast Relaxation Processes As a Major Reason for Inefficient Exciton Diffusion in Perylene-Based Organic Semiconductors. *J. Am. Chem. Soc.* **2014**, *136*, 9327–9337.

[52] Schubert, A.; Settels, V.; Liu, W.; Würthner, F.; Meier, C.; Fink, R. F.; Schindlbeck, S.; Lochbrunner, S.; Engels, B.; Engel, V. Ultrafast Exciton Self-Trapping upon Geometry Deformation in Perylene-Based Molecular Aggregates. *J. Phys. Chem. Lett.* **2013**, *4*, 792–796.

[53] Maiman, T. H. Stimulated Optical Radiation in Ruby. *Nature* **1960**, *187*, 493–494.

[54] Franken, P. A.; Hill, A. E.; Peters, C. W.; Weinreich, G. Generation of Optical Harmonics. *Phys. Rev. Lett.* **1961**, *7*, 118–119.

[55] Lee, C. H.; Chang, R. K.; Bloembergen, N. Nonlinear Electroreflectance in Silicon and Silver. *Phys. Rev. Lett.* **1967**, *18*, 167–170.

[56] Dadap, J. I.; Wilson, P. T.; Anderson, M. H.; Downer, M. C.; ter Beek, M. Femtosecond carrier-induced screening of dc electric-field-induced second-harmonic generation at the Si(001)-SiO_2 interface. *Opt. Lett.* **1997**, *22*, 901–903.

[57] Nahata, A.; Heinz, T. F.; Misewich, A. High-speed elelectric sampling using optical second-harmonic generation. *Appl. Phys. Lett.* **1996**, *69*, 746–748.

[58] J. Bloch, H. M. v. D., J. G. Mihaychuk Electron Photoinjection from Silicon to Ultrathin SiO_2 Films via Ambient Oxygen. *Phys. Rev. Lett.* **1996**, *77*, 920–923.

[59] Bjorkman, C. H.; Yasuda, T.; Shearon, C. E.; Ma, Y.; Lucovsky, G.; Emmerichs, U.; Meyer, C.; Leo, K.; Kurz, H. Influence of surface roughness on the elelectric properties of Si-SiO_2 interfaces and on second-harmonic generation at these interfaces. *J. Vac. Sci. Technol. B* **1993**, *11*, 1521–1527.

[60] Dadap, J. I.; Doris, B.; Deng, Q.; Lowell, J. K.; Diebold, A. C.; Downer, M. C. Randomly oriented Angstrom-scale microroughness at the Si(100)/SiO_2 interface probed by optical second harmonic generation. *Appl. Phys. Lett.* **1994**, *64*, 2139–2141.

[61] Daum, W.; Krause, H.-J.; Reichel, U.; Ibach, H. Identification of Strained Silicon Layers at Si-SiO_2 Interfaces and Clean Si Surfaces by Nonlinear Optical Spectroscopy. *Phys. Rev. Lett.* **1993**, *71*, 1234–1237.

[62] Pedersen, K.; Morgen, P. Dispersion of optical second-harmonic generation from Si(111)7×7. *Phys. Rev. B* **1995**, *52*, R2277–R2280.

[63] Heinz, T. F.; Loy, M. M. T.; Thompson, W. A. Study of Si(111) Surface by Optical Second-Harmonic Generation: Reconstruction and Surface Phase Transformation. *Phys. Rev. Lett.* **1985**, *54*, 63–66.

[64] Bratu, P.; Höfer, U. Phonon-Assisted Sticking of Molecular Hydrogen on Si(111) -(7×7). *Phys. Rev. Lett.* **1995**, *74*, 1625–1628.

[65] Dadap, J. I.; Xu, Z.; Hu, X. F.; Downer, M. C.; Russell, N. M.; Ekerdt, J. G.; Aktsipetrov, O. A. Second-harmonic spectroscopy of a Si(001) surface during calibrated variations in temperature and hydrogen coverage. *Phys. Rev. B* **1997**, *56*, 13367–13379.

[66] Qi, J.; Yeganeh, M. S.; Koltover, I.; Yodh, A. G.; Theis, W. M. Depletion-Electric-Field-induced Changes in Second-Harmonic Generation from GaAs. *Phys. Rev. Lett.* **1993**, *71*, 633–636.

[67] Dadap, J. I.; Hu, X. F.; Anderson, M. H.; Downer, M. C.; Lowell, J. K.; Aktsipetrov, O. A. Optical second-harmonic electroreflectance spectroscopy of a Si(001) metal-oxide-semiconductor structure. *Phys. Rev. B* **1996**, *53*, R7607–R7609.

[68] Stehlin, T.; Feller, M.; Guyot-Sionnest, P.; Shen, Y. R. Optical second-harmonic generation as a surface probe for noncentrosymmetric media. *Opt. Lett.* **1988**, *13*, 389–391.

[69] Yamada, C.; Kimura, T. Anisotropy in Second-Harmonic Generation from Reconstructed Surfaces of GaAs. *Phys. Rev. Lett.* **1993**, *70*, 2344–2347.

[70] Scheidt, T.; Rohwer, E. G.; von Bergmann, H. M.; Stafast, H. Optical second harmonic imaging: a versatile tool to investigate semiconductor surfaces and interfaces. *Eur. Phys. J. Appl. Phys.* **2004**, *27*, 393–397.

[71] Boyd, R. W. *Nonlinear Optics*; Academic Press: New York, 2008.

[72] Sutherland, R. L. *Handbook of Nonlinear Optics*; Marcel Dekker, Inc., 2003.

[73] Schulze, M. Second Harmonic Generation: Probing Photochromic Interface and Ultrafast Charge Transfer Processes. Ph.D. thesis, Freie Universität Berlin, 2014.

[74] Schulze, M.; Utecht, M.; Hebert, A.; Rück-Braun, K.; Saalfrank, P.; Tegeder, P. Reversible Photoswitching of the Interfacial Nonlinear Optical Response. *J. Phys. Chem. Lett.* **2014**, *6*, 505–509.

[75] Bouas-Laurent, H.; Dürr, H. Organic Photochromism. *Pure Appl. Chem.* **2001**, *73*, 639–665.

[76] Stobbe, H. Die Farbe der "Fulgensäure" und "Fulgide". (7. Abhandlung ber Butadiënverbindungen.). *Ber. Dtsch. Chem. Ges.* **1905**, *38*, 3673–3682.

[77] Brust, T.; Malkmus, S.; Draxler, S.; Ahmed, S. A.; Rück-Braun, K.; Zinth, W.; Braun, M. Photochemistry with thermal versus optical excess energy: Ultrafast cycloreversion of indolylfulgides and indolylfulgimides. *J. Photochem. Photobiol.* **2009**, *207*, 209–216.

[78] Heller, H. G.; Koh, K.; Elliot, C.; Whittall, J. Fulgides and Fulgimides for Practical Applications. *Mol. Cryst. Liq. Cryst.* **1994**, *246*, 79–86.

[79] Klajn, R. Spiropyran-based dynamic materials. *Chem. Soc. Rev.* **2014**, *43*, 148–184.

[80] Matsuda, K.; Irie, M. Diarylethene as a photoswitching unit. *J. Photochem. Photobiol.* **2014**, *5*, 169–182.

[81] Tian, H.; Yang, S. Recent progresses on diarylethen based photochromic switches. *Chem. Soc. Rev.* **2004**, *33*, 85–97.

[82] Kumar, G. S.; Neckers, D. C. Photochemistry of Azobenzene-Containing Polymers. *Chem. Rev.* **1989**, *89*, 1915–1925.

[83] Cembran, A.; Bernardi, F.; Garavelli, M.; Gagliardi, L.; Orlandi, G. On the Mechanism of the cis-trans Isomerization in the Lowest Electronic States of Azobenzene: S_0, S_1, T_1. *J. Am. Chem. Soc.* **2004**, *126*, 3234–3243.

[84] Schmidt, R.; Hagen, S.; Brete, D.; Carley, R.; Gahl, C.; Dokić, J.; Saalfrank, P.; Hecht, S.; Tegeder, P.; Weinelt, M. On the electronic and geometrical structure of the *trans*- and *Cis*-isomer of tetra-*tert*-butyl-azobenzene on Au(111). *Phys. Chem. Chem. Phys.* **2010**, *12*, 4488–4497.

[85] Brete, D.; Przyrembel, D.; Eickhoff, C.; Carley, R.; Freyer, W.; Reuter, K.; Weinelt, C. G. Mixed self-assembled monolayers of azobenzene photoswitches with trifuoromethyl and cyano end groups. *J. Phys.: Condens. Matter* **2012**, *24*, 394015.

[86] Malkmus, S.; Koller, F. O.; Heinz, B.; Schreier, W. J.; Schrader, T. E.; Zinth, W.; Schulz, C.; Dietrich, S.; Rück-Braun, K.; Braun, M. Ultrafast ring opening reaction of a photochromic indolyl-fulgimide. *Chem. Phys. Lett.* **2006**, *417*, 266–271.

[87] Koller, F. O.; Schreier, W. J.; Schrader, T. E.; Malkmus, S.; Schulz, C.; Dietrich, S.; Rück-Braun, K.; Braun, M. Ultrafast Ring-Closure Reaction of Photochromic Indolylfulgimides Studied with UV-Pump - IR-Probe Spectroscopy. *J. Phys. Chem. A* **2008**, *112*, 210–214.

[88] Woodward, R. B.; Hoffmann, R. Stereochemistry of Electocyclic Reactions. *J. Am. Chem. Soc.* **1965**, *87*, 395–397.

[89] Hoffmann, R.; Woodward, R. B. The Conservation of Orbital Symmetry. *Acc. Chem. Res.* **1968**, *1*, 17–22.

[90] Hoffmann, R.; Woodward, R. B. *The Conservation of Orbital Symmetry*; Academic Press: New York, 1970.

[91] Yokoyama, Y. Fulgides for Memories and Switches. *Chem. Rev.* **2000**, *100*, 1717–1739.

[92] Uchida, S.; Yamada, S.; Yokoyama, Y.; Kurita, Y. Steric Effects of Substituents on the Photochromism of Indolylfulgides. *Bull. Chem. Soc. Jpn.* **1995**, *68*, 1677–1682.

[93] Uchida, S.; Yokoyama, Y.; Kiji, J.; Okano, T.; Kitamura, H. Electronic Effects of Substituents on Indole Nitrogen on the Photochromic Properties of Indolylfulgides. *Bull. Chem. Soc. Jpn.* **1995**, *68*, 2961–2967.

[94] Islamova, N. I.; Chen, X.; DiGirolamo, J. A.; Silva, Y.; Lees, W. J. Thermal stability and photochromic properties of a fluorinated indolylfulgimide in a protic and aprotic solvent. *J. Photochem. Photobiol. A* **2008**, *199*, 85–91.

[95] Seibold, M.; Port, H. Mid-infrared recognition of the reversible photoswichting of fulgides. *Chem. Phys. Lett.* **1996**, *252*, 135–140.

[96] Chen, Y.; Wang, C.; Fan, M.; Yao, B.; Menke, N. Photochromic fulgide for holographic recording. *Opt. Mat.* **2004**, *26*, 75–77.

[97] Sun, Q.; Zhang, C.; Wang, L.; Li, Z.; Hu, A.; Tan, Q.; Xu, W. Surface-assisted *cis-trans* Isomerization of an alkene molecule on Cu(110). *Chem. Commun.* **2014**, *50*, 1728–1730.

[98] Bazarnik, M.; Henzl, J.; Czajka, R.; Morgenstern, K. Light driven reactions of single physisorbed azobenzenes. *Chem. Commun.* **2011**, *47*, 7764–7766.

[99] Liljeroth, P.; Repp, J.; Meyer, G. Current-Induced Hydrogen Tautomerization and Conductance Switching of Naphthalocyanine Molecules. *Science* **2007**, *317*, 1203–1206.

[100] Schulze, M.; Utecht, M.; Moldt, T.; Przyrembel, D.; Gahl, C.; Weinelt, M.; Saalfrank, P.; Tegeder, P. Nonlinear optical response of photochromic azobenzene-functionalized self-assembled monolayers. *Phys. Chem. Chem. Phys.* **2015**, *17*, 18079–18086.

[101] Caldwell, W.; Campbell, D. J.; Chen, K.; Herr, B. R.; Mirkin, C. A.; Malik, A.; Durbin, M. K.; Dutta, P.; Huang, K. G. A Highly Ordered Self-Assembled Monolayer Film of an Azobenzenealkanethiol on Au(1 1 1): Electrochemical Properties and Structural Characterization by Synchrotron in-Plane X-ray Diffraction, Atomic Force Microscopy, and Surface-Enhanced Raman Spectroscopy. *J. Am. Chem. Soc.* **1995**, *117*, 6071–6082.

[102] Valley, D. T.; Onstott, M.; Malyk, S.; Benderskii, A. V. Steric Hindrance of Photoswitching in Self-Assembled Monolayers of Azobenzene and Alkane Thiols. *Langmuir* **2013**, *29*, 11623–11631.

[103] Gahl, C.; Schmidt, R.; Brete, D.; McNellis, E. R.; Freyer, W.; Carley, R.; Reuter, K.; Weinelt, M. Structure and Excitonic Coupling in Self-Assembled Monolayers of Azobenzene-Functionalized Alkanethiols. *J. Am. Chem. Soc.* **2010**, *132*, 1831–1838.

[104] Schulze, M.; Hänsel, M.; Tegeder, P. Hot Excitons Increase the Donor/Acceptor Charge Transfer Yield. *J. Phys. Chem. C* **2014**, *118*, 28527–28534.

[105] Matsushima, R.; Sakaguchi, H. Comparison of the photochromic properties of fulgides and fulgimides. *J. Photochem. Photobio.* **1997**, *108*, 239–245.

[106] Wolak, M. A.; Thomas, C. J.; Gillespie, N. B.; Birge, R. R.; Lees, W. J. Tuning the Optical Properties of Fluorinated Indolylfulgimides. *J. Org. Chem.* **2003**, *68*, 319–326.

[107] Wagner, S.; Leyssner, F.; Kördel, C.; Zarwell, S.; Schmidt, R.; Weinelt, M.; Rück-Braun, K.; Wolfad, M.; Tegeder, P. Reversible photoisomerization of an azobenzene-functionalized self-assembled monolayer probed by sum-frequency generation vibrational spectroscopy. *Phys. Chem. Chem. Phys.* **2009**, *11*, 6242–6248.

[108] Schulze, G.; Franke, J.; Pascual, J. I. Induction of a Photostationary Ring-Opening Ring-Closing State of Spiropyran Monolayers on the Semimetallic Bi(110) Surface. *Phys. Rev. Lett.* **2012**, *109*, 026102.

[109] Utecht, M. M. Zur Optimierung und dem Auslesen molekularer Schalter: Quantenmechanische Untersuchungen an vier Beispielen. Ph.D. thesis, Universität Potsdam, 2015.

[110] Frisch, M. J. et al. Gaussian 09 Revision D. 01. 2013; Gaussian Inc. Wallingford CT.

[111] Plaquet, A.; Guillaume, M.; Champagne, B.; Castet, F.; Ducasse, L.; Pozzo, J.-L.; Rodriguez, V. *In silico* optimization of merocyanine-spiropyran compounds as second-order nonlinear optical molecular switches. *Phys. Chem. Chem. Phys.* **2008**, *10*, 6223–6232.

[112] Suponitsky, K. Y.; Tafur, S.; Masunov, A. E. Applicability of hybrid density functional theory methods to calculation of molecular hyperpolarizability. *J. Chem. Phys.* **2008**, *129*, 044109.

[113] Hansch, C.; Leo, A.; Taft, R. W. A Survey of Hemmett Substituent Constants and Resonance and Field Parameters. *Chem. Rev.* **1991**, *91*, 165–195.

[114] Horie, K.; Ushiki, H.; Winnik, F. M. *Molecular Photonics*; Wiley-VCH: Weinheim, 2000.

[115] Evans, R. C., Douglas, P., Burrows, H. D., Eds. *Applied Photochemistry*; Springer, 2013.

[116] Schwoerer, M.; Wolf, H. C. *Organic Molecular Solids*; Wiley-VCH: Weinheim, 2007.

[117] Grancini, G.; Maiuri, M.; Fazzi, D.; Petrozza, A.; Egelhaaf, H.-J.; Brida, D.; Cerullo, G.; Lanzani, G. Hot exciton dissociation in polymer solar cells. *Nat. Mater.* **2012**, *12*, 29–33.

[118] Schreiber, F. Organic molecular beam deposition: Growth studies beyond the first monolayer. *Phys. Status Solidi A* **2004**, *201*, 1037–1054.

[119] Hinderhofer, A.; Schreiber, F. Organic-Organic Heterostructures: Concepts and Applications. *ChemPhysChem* **2012**, *13*, 628–643.

[120] Kowarik, S.; Gerlach, A.; Sellner, S.; Cavalcanti, L.; Konovalov, O.; Schreiber, F. Real-time X-ray diffraction measurements of structural dynamics and polymorphism in diiendenoperylene growth. *Appl. Phys. A* **2008**, *95*, 233–239.

[121] Jones, B. A.; Facchetti, A.; Wasielewski, M. R.; Marks, T. J. Tuning Orbital Energetics in Arylene Diimide Semiconductors. Material Design for Ambient Stability of n-Type Charge Transport. *J. Am. Chem. Soc.* **2007**, *129*, 15259–15278.

[122] Wagner, J.; Gruber, M.; Hinderhofer, A.; Wilke, A.; Bröker, B.; Frisch, J.; Amsalem, P.; Vollmer, A.; Opitz, A.; Koch, N.; Schreiber, F.; Brütting, W. High Fill Factor and Open Circuit Voltage in Organic Photovoltaic Cells with Diindenoperylene as Donor Material. *Adv. Funct. Mater.* **2010**, *20*, 4295–4303.

[123] Heinemeyer, U.; Scholz, R.; Gisslén, L.; Alonso, M. I.; Ossó, J. O.; Garriga, M.; Hinderhofer, A.; Kytka, M.; Kowarik, S.; Gerlach, A.; Schreiber, F. Exciton-phonon coupling in diindenoperylene thin films. *Phys. Rev. B* **2008**, *78*, 085210.

[124] Heinemeyer, U.; Broch, K.; Hinderhofer, A.; Kytka, M.; Scholz, R.; Gerlach, A.; Schreiber, F. Real-Time Changes in the Optical Spectrum of Organic Semiconducting Films and Their Thickness Regimes during Growth. *Phys. Rev. Lett.* **2010**, *104*, 257401–1 – 257401–4.

[125] Nichols, V. M.; Broch, K.; Schreiber, F.; Bardeen, C. J. Excited-State Dynamics of Diindenoperylene in Liquid Solution and Solid Films. *J. Phys. Chem. C* **2015**, *119*, 12856–12864.

[126] Kowarik, S.; Gerlach, A.; Sellner, S.; Schreiber, F.; Cavalcanti, L.; Konovalov, O. Real-Time Observation of Structural and Orientational Transitions during Growth of Organic Thin Films. *Phys. Rev. Lett.* **2006**, *96*, 125504.

[127] Huang, Y. L.; Chen, W.; Huang, H.; Qi, D. C.; Chen, S.; Gao, X. Y.; Pflaum, J.; Wee, A. T. S. Ultrathin Films of Diindenoperylene on Graphite and SiO_2. *J. Phys. Chem. C* **2009**, *113*, 9251–9255.

[128] Dürr, A. C.; Schreiber, F.; Ritley, K. A.; Kruppa, V.; Krug, J.; Dosch, H.; Struth, B. Rapid Roughening in Thin Film Growth of an Organic Semiconductor (Diindenoperylene). *Phys. Rev. Lett.* **2003**, *90*, 016104.

[129] Kurrle, D.; Pflaum, J. Exciton diffusion lenght in the organic semiconductor diindenoperylene. *Appl. Phys. Lett.* **2008**, *92*, 133306.

[130] Gruber, M.; Rawolle, M.; Wagner, J.; Magerl, D.; Hörmann, U.; Perlich, J.; Roth, S. V.; Opitz, A.; Schreiber, F.; Müller-Buschbaum, P.; Brütting, W. Correlating Structure and Morphology to Device Performance of Molecular Organic Donor-Acceptor Photovoltaic Cells Based on Diindenoperylene (DIP) and C_{60}. *Adv. Energy Mater.* **2013**, *3*, 1075–1083.

[131] Banerjee, R.; Novak, J.; Frank, C.; Lorch, C.; Hinderhofer, A.; Gerlach, A.; Schreiber, F. Evidence for kinetically limited thickness dependent phase separation in organic thin film blends. *Phys. Rev. Lett.* **2013**, *110*, 185506.

[132] Horlet, M.; Kraus, M.; Brütting, W.; Opitz, A. Diindenoperylene as ambipolar semiconductor: Influence of electrode materials and mobility asymmetry in organic field-effect transistors. *Appl. Phys. Lett.* **2011**, *98*, 233304.

[133] Opitz, A.; Horlet, M.; Kiwull, M.; Wagner, J.; Kraus, M.; Brütting, W. Bipolar charge transport in organic field-effect transistors: Enabling high mobilities and transport of photo-generated charge carriers by a molecular passivation layer. *Org. Electronics* **2012**, *13*, 1614–1622.

[134] Ahn, T. S.; Müller, A. M.; Al-Kaysi, R. O.; Spano, F. C.; Norton, J. E.; Beljonne, D.; Brédas, J. L.; Bardeen, C. J. Experimental and theoretical study of temperature dependent exciton delocalization and relaxation in anthracene thin films. *J. Chem. Phys.* **2008**, *128*, 054505.

[135] Katoh, R.; Suzuki, K.; Furube, A.; Kotani, M.; Tokumaru, K. Fluorescence Quantum Yield of Aromatic Hydrocarbon Crystals. *J. Phys. Chem. C* **2009**, *113*, 2961–2965.

[136] Albrecht, W. G.; Coufal, H.; Haberkorn, R.; Michel-Beyerle, M. E. Excitation Spectra of Exciton Fission in Organic Crystals. *Phys. Status Solidi B* **1978**, *89*, 261–265.

[137] Eaton, S. W.; Shoer, L. E.; D.Karlen, S.; Dyar, S. M.; Margulies, E. A.; Veldkamp, B. S.; Ramanan, C.; Hartzler, D. A.; Savikhin, S.; Marks, T. J.; et al., Singlet Exciton Fission in Polycrystalline Thin Films of a Slip-Stacked Perylenediimide. *J. Am. Chem. Soc.* **2013**, *135*, 14701–14712.

[138] Burdett, J. J.; Bardeen, C. J. The Dynamics of Singlet Fission in Crystalline Tetracene and Covalent Analogs. *Acc. Chem. Res.* **2013**, *46*, 1312–1320.

[139] Jundt, C.; Klein, G.; Sipp, B.; Moigne, J. L.; Joucla, M.; Villaeys, A. A. Exciton Dynamics in Pentacene Thin Films Studied by Pump- Probe Spectroscopy. *Chem. Phys. Lett.* **1995**, *241*, 84–88.

[140] Rao, A.; Wilson, M. W. B.; Hodgkiss, J. M.; Albert-Seifried, S.; Bassler, H.; Friend, R. H. Exciton Fission and Charge Generation Via Triplet Excitons in Pentacene/C_60 bilayers. *J. Am. Chem. Soc.* **2010**, *132*, 12698–12703.

[141] Wilson, M. W. B.; Rao, A.; Clark, J.; Kumar, R. S. S.; Brida, D.; Cerullo, G.; Friend, R. H. Ultrafast Dynamics of Exciton Fission in Polycrystalline Pentacene. *J. Am. Chem. Soc.* **2011**, *133*, 11830–11833.

[142] Chua, L.-L.; Zaumseil, J.; Chang, J.-F.; Ou, E. C.-W.; Ho, P. K.-H.; Sirringhaus, H.; Friend, R. H. General observation of n-type field-effect behaviour in organic semiconductors. *Nature* **2005**, *434*, 194–199.

[143] Engel, E.; Koschorreck, M.; Leo, K.; Hoffmann, M. Ultrafast Relaxation in Quasi-One-Dimensional Organic Molecular Crystals. *Phys. Rev. Lett.* **2005**, *95*, 157403.

[144] Gisslén, L.; Scholz, R. Crytallochromy of perylene pigments: Interference between Frenkel excitons and charge-transfer states. *Phys. Rev. B* **2009**, *80*, 115309.

[145] Heilig, M.; Domhan, M.; Port, H. Optical properties and morphology of thin diindenoperylene films. *J. Lumin.* **2004**, *110*, 290–295.

[146] Settels, V.; Liu, W.; Pflaum, J.; Fink, R. F.; Engels, B. Comparison of the Electronic Structure of Different Perylene-Based Dye-Aggregates. *J. Comput. Chem.* **2012**, *33*, 1544–1553.

[147] Bellinger, D.; Settels, V.; Liu, W.; Fink, R.; Engels, B. Influence of a Polarizable Surrounding on the Electronically Excited States of Aggregated Perylene Materials. *J. Comput. Chem.* **2016**, *37*, 1601–1610.

[148] Bellinger, D.; Pflaum, J.; Brüning, C.; Engel, V.; Engels, B. The electronic character of PTCDA thin films in comparison to other perylene-based organic semiconductors: ***ab initio-***, TD-DFT and semi-empirical computations of the optoelectronic properties of large aggregates. *Phys. Chem. Chem. Phys.* **2017**, *19*, 2434–2448.

[149] Engels, B.; Engel, V. The dimer-approach to characterize opto-electronic properties of and exciton trapping and diffusion in organic semiconductor aggregates and crystals. *Phys. Chem. Chem. Phys.* **2017**, *19*, 12604–12619.

[150] Saeta, P. N.; Greene, B. I. Primary Relaxation Processes at the Band Edge of SIO_2. *Phys. Rev. Lett.* **1993**, *70*, 3588–3591.

[151] Mao, S. S.; Quéré, F.; Guizard, S.; Mao, X.; Russo, R. E.; Petite, G.; Martin, P. Dynamics of femtosecond laser interaction with dielectrics. *Appl. Phys. A* **2004**, *79*, 1695–1709.

[152] Sabbah, A. J.; Riffe, D. M. Femtosecond pump-probe reflectivity study of silicon carrier dynamics. *Phys. Rev. B* **2002**, *66*, 165217.

[153] Herbst, W.; Hunger, K. *Industrial Organic Pigments*; Wiley-VCH: Weinheim, 1997.

[154] Huang, C.; Barlow, S.; Marder, S. R. Perylene-3,4,9,10-tetracarboxylic Acid Diimides: Synthesis, Physical Properties, and Use in Organic Electronics. *J. Org. Chem.* **2011**, *76*, 2386–2407.

[155] Chen, Z.; Baumeister, U.; Tschierske, C.; Würthner, F. Effect of Core Twisting on Self-Assembly and Optical Properties of Perylene Bisimide Dyes in Solution and Columnar Liquid Crystalline Phases. *Chem. Eur. J.* **2007**, *13*, 450–465.

[156] Li, C.; Wonneberger, H. Perylene Imides for Organic Photovoltaics: Yesterday, Today, and Tomorrow. *Adv. Mater.* **2012**, *24*, 613–636.

[157] Segura, J. L.; Herrera, H.; Bäuerle, P. Oligothiophene-functionalized naphthalimides and perylene iimide: design, synthesis and applications. *J. Mater. Chem.* **2012**, *22*, 8717–8733.

[158] Kamm, V.; Battagliarin, G.; Howard, I. A.; Pisula, W.; Mavrinskiy, A.; Li, C.; Müllen, K.; Laquai, F. Polythiophene:Perylene Diimide Solar Cells - the Impact of Alkyl-Substitutuion on the Photovoltaic Performance. *Adv. Energy Mater.* **2011**, *1*, 297–302.

[159] Zhong, Y. et al. Efficient Organic Solar Cells with Helical Perylene Diimide Electron Acceptors. *J. Am. Chem. Soc.* **2014**, *136*, 15215–15221.

[160] Piliego, C.; Jarzab, D.; Gigli, G.; Chen, Z.; Facchetto, A.; Loi, M. A. High Electron Mobility and Ambient Stability in Solution-Porcessed Perylene-Based Organic Field-Effect Transistors. *Adv. Mater.* **2009**, *21*, 1573–1576.

[161] Han, W. N.; Yonezawa, K.; Makino, R.; Kato, K.; Hinderhofer, A.; Murdey, R.; Shiraishi, R.; Yoshida, H.; Sato, N.; Ueno, N.; Kera, S. Quantitatively identical orientation-dependent ionization Energy and electron affinity of diindenoperylene. *Appl. Phys. Lett.* **2013**, *103*, 253301.

[162] von Jena, A.; Lessing, H. E. Coherent Coupling Effects in Picosecond Absorption Experiments. *Appl. Phys.* **1979**, *19*, 131–144.

[163] Heinz, T. F.; Palfrey, S. L.; Eisenthal, K. B. Coherent coupling effects in pump-probe measurements with collinear, copropagating beams. *Opt. Lett.* **1984**, *9*, 359–361.

[164] Joo, T.; Albrecht, A. C. Femtosecond time-resolved coherent anti-Stokes Raman spectroscopy of liquid benzene: A Kubo relaxation function analysis. *Chem. Phys.* **1993**, *99*, 3244–3251.

[165] Harris, A. L.; Rothberg, L. Surface vibrational energy relaxation by sum frequency generation: Five-wave mixing and coherent transients. *Chem. Phys.* **1991**, *94*, 2449–2457.

[166] Wong, K. S.; Han, S. G.; Vardeny, Z. V. Studies of resonant and preresonant femtosecond degenerate four-wave mixing in unoriented conducting polymers. *Appl. Phys.* **1991**, *70*, 1896–1898.

[167] Lebedev, M. V.; Misochko, O. V.; Dekorsy, T.; Georgiev, N. On the Nature of "Coherent Artifact". *J. Exp. Theor. Phys.* **2005**, *100*, 272–282.

[168] Rosker, M. J.; Wise, F. W.; Tang, C. L. Femtosecond Relaxation Dynamics of Large Molecules. *Phys. Rev. Lett.* **1986**, *57*, 321–324.

[169] Nelson, K. A.; Williams, L. R. Femtosecond Time-Resolved Observation of Coherent Molecular Vibrational Motion. *Phys. Rev. Lett.* **1987**, *58*, 745.

[170] Son, M.; Park, K. H.; Yoon, M.-C.; Kim, P.; Kim, D. Excited-State Vibrational Coherence in Perylene Bisimide PProbe by Femtosecond Broadband Pump-Probe Spectroscopy. *J. Phys. Chem. A* **2015**, *119*, 6275–6282.

[171] Lee, G.; Kim, J.; Kim, S. Y.; Kim, D. E.; Joo, T. Vibrational Sepectrum of an Excited State and Huang-Rhys Factor by Coherent Wave Packets in Time-Resolved Fluoresence Spectroscopy. *ChemPhysChem* **2017**, *18*, 670–676.

[172] Frisch, M. J. et al. Gaussian 09 Revision A. 02. 2009; Gaussian Inc. Wallingford CT.

[173] Chen, K.; Barker, A. J.; Reish, M. E.; Gordon, K. C.; Hodgkiss, J. M. Broadband Ultrafast Photoluminescence Spectroscopy Resolves Charge Photogeneration via Delocalized Hot Excitons in Polymer:Fullerene Photovoltaic Blends. *J. Am. Chem. Soc.* **2013**, *135*, 18502–18512.

[174] Brabec, C. J.; Zerza, G.; Cerullo, G.; Silvestri, S. D.; Hummelen, J. C.; Sariciftci, S. Tracing photoinduced electron transfer process in conjugated polymer/fullerene bulk heterjunctions in real time. *Chem. Phys. Lett.* **2001**, *340*, 232–236.

[175] Bakulin, A. A.; Hummelen, J. C.; Pshenichnikov, M. S.; van Loosdrecht, P. H. M. Ultrafast Hole-Transfer Dynamics in Polymer/PCBM Bulk Heterojunctions. *Adv. Funct. Mater.* **2010**, *20*, 1653–1660.

[176] Gélinas, S.; Rao, A.; Kumar, A.; Smith, S. L.; Chin, A. W.; Clark, J.; van der Poll, T. S.; Bazan, G. C.; Friend, R. H. Ultrafast Long-Range Charge Separation in Organic Semiconductor Photovoltaic Diodes. *Science* **2014**, *343*, 512–516.

List of Publications, Conference Contributions and Supervised Theses

List of Publications

Publications Related to this Thesis

Excited State Dynamics in Diindenoperylene Films
Marc Hänsel, Valentina Belova, Alexander Hinderhofer, Frank Schreiber, Katharina Broch and Petra Tegeder
J. Phys. Chem. C, in press (2017)
DOI: 10.1021/acs.jpcc.7b04380

Excited State Dynamics at the Diindenoperylene/PDIR-CN_2 Interface
Marc Hänsel, Valentina Belova, Alexander Hinderhofer, Frank Schreiber, Katharina Broch and Petra Tegeder
In Preparation (2017)

Nonlinear Optical Response of Switchable Interfaces: Molecular Engineering Towards High Nonlinear Optical Contrast
Marc Hänsel, Clemens Rietze, Christoph Barta, Karola Rück-Braun, Peter Saalfrank and Petra Tegeder
In Preparation (2017)

Nonlinear Optical Response of Fulgimide Functionalized Silicon Surfaces
Marc Hänsel, Clemens Rietze, Christoph Barta, Karola Rück-Braun, Peter Saalfrank and Petra Tegeder
In Preparation (2017)

Publications Not Related to this Thesis

Hot Excitons Increase the Donor/Acceptor Charge Transfer Yield
Michael Schulze, Marc Hänsel and Petra Tegeder
J. Phys. Chem. C, **2014**, *118*, 28527-28534

Processing Follows Function: Pushing the Formation of Self-Assembled Monolayers to High-Throughput Compatible Time Scales
Milan Alt, Janusz Schinke, Sabina Hillebrandt, Marc Hänsel, Gerardo Hernández-Sosa, Norman Mechau, Tobias Glaser, Eric Mankel, Manuel Hamburger, Kaja Deing, Wolfram Jaegermann, Annemarie Pucci, Wolfgang Kowalsky, Uli Lemmer and Robert Lovrinčić
ACS Appl. Mater. Interfaces, **2014**, *6*, 20234-20241

List of Conference Contributions

Ultrafast Exciton Dynamics in Diindenoperylene Films
Marc Hänsel, Valentina Belova, Katharina Broch, Frank Schreiber and Petra Tegeder
Presentation
DPG Spring Meeting, Dresden, Germany, 2017

Ultrafast Excited State Dynamics in Diindenoperylene Films
Marc Hänsel, Valentina Belova, Katharina Broch, Alexander Hinderhofer, Frank Schreiber and Petra Tegeder
Poster
10. HGSFP Winterschool, Obergurgl, Austria, 2017

Photo Switching the Optical Nonlinear Response of a Fulgimide Functionalized Silicon Surface
Marc Hänsel, Christoph Barta, Karola Rück-Braun and Petra Tegeder
Presentation
DPG, Spring Meeting, Regensburg, Germany, 2016

Charge separation at C_60/P3HT and P3HT/ZnO interfaces probed by femtosecond time-reolved second harmonic generation measurements
Marc Hänsel, Michael Schulze, Yunus Sevinchan, Yana Vaynzof and Petra Tegeder
Presentation
DPG Spring Meeting, Berlin, Germany, 2015

Tuning the work function of metal substrates by defined cleaning procedures and self assembling monolayers
Marc Hänsel, Eric Mankel, Janusz Schinke, Wolfgang Kowalsky, Thomas Mayer and Wolfram Jaegermann Poster
DPG Spring Meeting, Regensburg, Germany, 2013

List of Supervised Theses

Untersuchung einer geordneten Diindenoperylene-Dünnschicht auf einem Siliziumwafer mittels Frequenzverdopplung
Jochen Lauer, Ruprecht-Karls-Universität Heidelberg, July 2016
Scientific Internship

Untersuchung einer selbstorganisierten, photochromen 3-Indolylfulgimid Monolage auf einer Silizium(111)-Oberfläche mittels Frequenzverdopplung
Tobias Wesp, Ruprecht-Karls-Universität Heidelberg, October 2015
Scientific Internship

Untersuchung der Photochemie einer Fulgimidschicht auf Silizium mittels Frequenzverdopplung
Michael Hofmeister, Ruprecht-Karls-Universität Heidelberg, July 2015
Bachelor Thesis

Untersuchung des Photoschaltens von Fulgimiden durch zeitaufgelöste Frequenzverdopplung
Sebastian Intorp, Ruprecht-Karls-Universität Heidelberg, April 2014
Scientific Internship

Acknowledgments

An dieser Stelle möchte ich mich bei allen bedanken, die mich im Laufe meiner Promotion unterstüzt und begleitet haben. Insbesondere danke ich:

Frau Prof. Dr. Petra Tegeder für die Möglichkeit in ihrer Gruppe in Heidelberg am Physikalisch-Chemischen Institut zu promovieren und die hervorragende Betreuung während der Promotion. Außerdem möchte ich mich besonders für die Unterstüzung der Teilnahme an zahlreichen Tagungen und dem Forschungsaufenthalt an der Columbia State University in New York City bedanken.

Frau Prof. Dr. Annemarie Pucci für die freundliche Übernahme der offiziellen Erstbetreuung und für die Erstellung des Erstgutachten.

Herrn Prof. Dr. Wolfgang Kowalsky für die freundliche Übernahme des Zweitgutachtens.

Valentina Belova für die Bereitstellung der Dynamik Proben und zusammen mit Dr. Katharina Broch, Dr. Alexander Hinderhofer und Prof. Dr. Frank Schreiber für die fruchtvolle Zusammenarbeit und konstruktiven Diskussionen.

Christoph Barta für die Fertigung der funktionalisierten Oberflächen und zusammen mit Prof. Dr. Karola-Rück Braun für die produktive Zusammenarbeit und weiterbringenden Diskussionen.

Clemenz Rietze für die Anfertigung der Simulationen und zusammen mit Prof. Dr. Peter Saalfrank für die Unterstüzung meiner Ergebnisse mit Rechungen.

meinen Kollegen David Gerbert, Friedrich Maaß, Arnulf Stein, Vipilan Sivanesan, Michael Schulze, Stephan Stremlau und Christoph Bronner für die tolle Arbeitsumgebung, die immerwährende Hilfsbereitschaft und die ausführlichen Diskussionen. Besonders gilt mein Dank Michael Schulze für die Einführung in den experimentellen Aufbau und David Gerbert für die super Zeit in NYC, die Zeit im Labor und die Unterstüzung in schwierigen Zeiten.

allen Studenten die ich betreuen durfte und die mich im Labor und bei der Interpretation der Messungen begleitet haben und neue Ideen eingebracht haben.

meinen Freunden Michael Huy, Sebastian Hüttel, Markus Wiesner, Richard Haas, Simone Wälde, Sebastian Lorek, Sabina Hillebrandt und Katja Bigge die mich zum Teil

seit der Schulzeit begleiten und immer für mich da waren.

meinen beiden Mitbewohnerinnen für die vielen lustigen und teilweise nachdenklichen Küchengespräche.

dem kompletten UWH Team Heidelberg für den sportlichen Ausgleich und ganz viele super Turniere und Trainingslager in Deutschland und Europa. Insbesondere gilt mein Dank Sabina Hillebrandt und Conrad Wagner für die Gründung des Heidelberger Teams und den fortdauernden Einsatz im UWH.

der Ladenburger Origami Gruppe für viele enspannte Abenden und super Jahrestreffen, sowie der Frankfurter Origami Gruppe für neue Impulse und viele spannende Gespräche.

ein ganz besonderer Dank gilt meinen Eltern, Großeltern und Geschwistern, die mich immer unterstützt haben und für mich da waren.

DANKE!